

CHARACTERIZING THE MODULATION OF STRESS GRANULE RESPONSES
BY CORONAVIRUSES

by

Stacia M. Dolliver

Submitted in partial fulfillment of the requirements
for the degree of Master of Science

at

Dalhousie University

Halifax, Nova Scotia

July 2022

TABLE OF CONTENTS

LIST OF FIGURES	v
ABSTRACT	vi
LIST OF ABBREVIATIONS USED	vii
ACKNOWLEDGEMENTS	x
CHAPTER 1: INTRODUCTION	1
1.1 Coronaviruses	1
1.2 Coronavirus genome and host detection	1
1.3 Stress granule formation and eIF2 α phosphorylation	6
1.4 Stress granule nucleation	7
1.5 SG function	8
1.6 SG dissolution	9
1.7 Dephosphorylation of eIF2 α	9
1.8 Stress granule formation independent of eIF2 α phosphorylation	10
1.9 Stress granules and the antiviral response	10
1.10 Coronaviruses and stress granules	12
1.11 Rationale and objectives	13
CHAPTER 2: MATERIAL & METHODS	14
2.1 Cells	14
2.2 Viruses	14
2.3 Plasmids and lentivirus stocks	15
2.4 Generation of stably transduced cells	15
2.5 Cell treatments	16
2.6 Virus infections	16
2.7 Transfection	17
2.8 siRNA knockdown	17
2.9 Immunofluorescence staining	17
2.10 Western blotting	18

2.11 RNA isolation and RT-QPCR	19
2.12 Statistical analyses	19
CHAPTER 3: RESULTS	20
3.1 Coronavirus OC43 inhibits stress granule formation	20
3.2 Coronavirus OC43 limits eIF2 α phosphorylation	24
3.3 Coronavirus OC43 limits eIF2 α phosphorylation irrespective of the activated eIF2 α kinase	28
3.4 Coronavirus OC43 upregulates GADD34 RNA levels	30
3.5 Coronavirus OC43 upregulates GADD34 independently from downstream activation of the integrated stress response	32
3.6 Upregulation of GADD34 by OC43 is not required for dephosphorylation of eIF2 α	36
3.7 OC43 inhibits stress granule formation in the presence of 6-Thioguanine ...	39
3.8 Coronavirus OC43 inhibits stress granules independently of eIF2 α phosphorylation	42
3.9 Coronavirus OC43 inhibits canonical stress granule formation	44
3.10 Coronavirus N proteins inhibit stress granule formation downstream of eIF2 α phosphorylation	47
3.11 Coronavirus OC43 Nsp15 does not inhibit stress granule formation	50
3.12 Coronavirus Nsp1 inhibits stress granules and limits eIF2 α phosphorylation	52
3.13 The RNA degradation function of CoV2-Nsp1 is required for TIAR redistribution and G3BP1 depletion from stress granules	56
3.14 Nsp1 of OC43 primarily inhibits stress granules through limiting eIF2 α phosphorylation	60
3.15 G3BP1 overexpression inhibits OC43 infection	62
CHAPTER 4: DISCUSSION	65
4.1 Overview	65
4.2 Inhibition of eIF2 α phosphorylation by OC43	65
4.3 Nsp1-mediated inhibition of eIF2 α phosphorylation	67
4.4 Stress granule inhibition by Nsp1	69
4.5 Stress granule inhibition by N	71

4.6 The antiviral role of G3BP1 during OC43 infection	72
4.7 Limitations	73
4.8 Future directions	74
4.9 Implications.....	75
4.10 Conclusions and models	75
BIBLIOGRAPHY	79
APPENDIX: ISRIB INHIBITS GADD34 INDUCTION AND DEPHOSPHORYLATION OF EIF2 α	92

LIST OF FIGURES

Figure 1.1. Model of the integrated stress response and stress granule formation	4
Figure 3.1: Coronavirus OC43 inhibits stress granule formation	22
Figure 3.2: Coronavirus OC43 limits eIF2 α phosphorylation	26
Figure 3.3: Coronavirus OC43 limits eIF2 α phosphorylation irrespective of the activated eIF2 α kinase	29
Figure 3.4: Coronavirus OC43 upregulates GADD34 RNA levels	31
Figure 3.5: Coronavirus OC43 upregulates GADD34 independently from downstream activation of the integrated stress response	34
Figure 3.6: Upregulation of GADD34 by OC43 is not required for dephosphorylation of eIF2 α	37
Figure 3.7: OC43 inhibits stress granule formation in the presence of 6-Thioguanine ...	40
Figure 3.8: Coronavirus OC43 inhibits stress granules independently of eIF2 α phosphorylation	43
Figure 3.9: Coronavirus OC43 inhibits canonical stress granule formation	45
Figure 3.10: Coronavirus N proteins inhibit stress granule formation downstream of eIF2 α phosphorylation	48
Figure 3.11: Coronavirus OC43 Nsp15 does not inhibit stress granule formation	51
Figure 3.12: Coronavirus Nsp1 inhibits stress granules and limits eIF2 α phosphorylation	54
Figure 3.13: The RNA degradation function of CoV2-Nsp1 is required for TIAR redistribution and G3BP1 depletion from stress granules	58
Figure 3.14: Nsp1 of OC43 primarily inhibits stress granules through limiting eIF2 α phosphorylation	61
Figure 3.15: G3BP1 overexpression inhibits OC43 infection	63
Figure 4.1: Coronavirus OC43 inhibits stress granule formation through multiple mechanisms	77
Figure 4.2: Coronavirus SARS-CoV2 inhibits SG formation through multiple mechanisms	78

ABSTRACT

Coronaviruses (CoVs) are a family of viruses that circulate in human populations causing mild common colds as well as severe and fatal respiratory disease. Stress granules (SGs) are cytoplasmic condensates that often form as part of the cellular antiviral response. Despite growing interest in SGs and other biological condensates, the role of SG formation during CoV infection is poorly understood. In this work, I analyzed SG formation during infection of the human common cold CoV OC43. Little SG formation was observed in infected cells and OC43 inhibited SG formation induced by exogenous stress (e.g. sodium arsenite or silvestrol treatment). Furthermore, OC43 inhibited phosphorylation of eukaryotic initiation factor 2 α (eIF2 α) – the hallmark of translation inhibition induced by integrated stress response (ISR). Inhibition of eIF2 α phosphorylation by OC43 was unaffected by treatment with the integrated stress response inhibitor (ISRIB) or knockdown of GADD34, suggesting that OC43 can limit eIF2 α phosphorylation independently from activation of the ISR or upregulation of GADD34. Further, GADD34 knockdown decreased OC43 replication. Upon ectopic overexpression, the nucleocapsid (N) and non-structural protein 1 (Nsp1) from both OC43 and the severe acute respiratory syndrome coronavirus 2 (SARS-CoV-2) inhibited SG formation. Furthermore, SARS-CoV2 Nsp1 expression resulted in depletion of G3BP1 protein – the master regulator of SG formation. This phenotype was dependent on Nsp1-mediated depletion of cytoplasmic mRNAs, which was also associated with nuclear retention of TIAR, another SG-nucleating protein. To test the role of G3BP1 in CoV replication, we infected cells overexpressing EGFP-tagged G3BP1 with OC43 and observed a significant decrease in infection compared to parental or control cells expressing EGFP. The antiviral role of G3BP1 and the existence of multiple SG suppression mechanisms that are conserved between the common cold OC43 and the pandemic SARS-CoV2 suggests that SG formation may represent an important antiviral host defense that CoVs target to ensure efficient replication.

LIST OF ABBREVIATIONS USED

3CLpro	3C-like proteinase
6-TG	6-Thioguanine
ACE2	Angiotensin converting enzyme 2
ALS	Amyotrophic lateral sclerosis
As	Arsenite
ATCC	American Type Culture Collection
ATF4	Activating transcription factor 4
ATG7	Autophagy related protein 7
BEBM	Basal Epithelial Cell Growth Medium
BEGM	Bronchial Epithelial Cell Growth Medium
BSA	Bovine serum albumin
C	Celsius
Caprin 1	Cell cycle associated protein 1
CHOP	C/EBP homologous protein
CNBP	Cellular nucleic acid binding protein
CoV	Coronavirus
CoV2	Severe acute respiratory syndrome coronavirus 2
COVID-19	Coronavirus disease 2019
CPE	Cytopathic effects
CReP	Constitutive repressor of eIF2 α phosphorylation
d	Day
DDX3	DEAD-box helicase 3
DMEM	Dulbecco's modified Eagle's medium
dsRNA	double-stranded RNA
DTT	Dithiothreitol
DYRK3	Dual specificity tyrosine phosphorylation regulated kinase 3
E	Envelope
EGFP	Eukaryotic green fluorescent protein (tag)
eIF	eukaryotic initiation factor
ER	Endoplasmic reticulum
FBS	Fetal bovine serum
FTD	Frontotemporal dementia
g	Gravity
G3BP1/2	Ras-GTPase-activating protein SH3 domain-binding protein 1/2
GADD34	Growth arrest and DNA damage-inducible protein 34
GCN2	General control nonderepressible 2
GDP	Guanosine diphosphate
GTP	Guanosine triphosphate
HA	Hemagglutinin (tag)
HCl	Hydrogen chloride
HCoV	Human coronavirus
HCT-8	Human colon adenocarcinoma
HEK	Human embryonic kidney
hpi	hours post infection
hpt	hours post transfection

HRI	Heme-regulated inhibitor
Hsp90	Heat shock protein 90
HSV	Herpes simplex virus
IAV	Influenza A virus
IBV	Infectious bronchitis virus
ID/LC	Intrinsically disordered/ low complexity
IFN	Interferon
IRF	Interferon regulatory factor
ISR	Integrated stress response
LARP1	La related protein 1
M	Membrane
MDA5	Melanoma differentiation-associated gene 5
MERS	Middle Eastern respiratory syndrome
Min	Minutes
ml	Milliliter
mm	Millimeter
MOI	Multiplicity of infection
mRNP	Messenger ribonucleoprotein
mTORC1	Mammalian target of rapamycin complex 1
N	Nucleocapsid
NF- κ B	Nuclear factor kappa light chain enhancer of activated B cells
ng	Nanogram
Nsp	Non-structural protein
NTF2	Nuclear transport factor 2
OAS	2'-5' oligoadenylate synthetase
OC43	Human coronavirus OC43
ORF	Open reading frame
PABP	Poly(A)-binding protein
PAGE	Polyacrylamide gel electrophoresis
PCR	Polymerase chain reaction
PEI	Polyethylenimine
PERK	PKR-like endoplasmic reticulum kinase
PKR	dsRNA-activated protein kinase
PLpro	Papain-like proteinase
Poly I:C	Polyinosinic:polycytidylic acid
PP1	Protein phosphatase 1
PPP1R15	Protein phosphatase 1 regulatory subunit 15
PRAS40	Proline-rich AKT substrate of 40 kDa
PRMT1	Protein arginine methyltransferase 1
PRV	Pseudorabies virus
PVDF	Polyvinylidene fluoride
RGG	Arginine glycine glycine
RIG-I	Retinoic acid-inducible gene I
RNA	Ribonucleic acid
ROS	Reactive oxygen species
RRM	RNA recognition motif

RT-qPCR	Reverse transcription quantitative PCR
S	Spike
SARS	Severe acute respiratory syndrome
SDS	Sodium dodecyl sulphate
SG	Stress granule
Sil.	Silvestrol
siRNA	Small interfering RNA
SL1	Stem loop 1
SR	Serine arginine
SRPK1	Serine arginine protein kinase 1
ssRNA	Single stranded RNA
TDP-43	TAR DNA-binding protein 43
TFEB	Transcription factor EB
Tg	Thapsigargin
TGEV	Transmissible gastroenteritis virus
TIA-1	T-cell intracellular antigen 1
TIAR	TIA-1-related protein
TRIM25	Tripartite motif containing 25
µg	Microgram
µl	Microliter
µM	Micrometer
uORF	Upstream open reading frame
USP10	Ubiquitin specific peptidase 10
UTR	Untranslated region
UV	Ultraviolet
VCP	Valosin-containing protein
Vhs	Virion host shutoff

ACKNOWLEDGMENTS

There are a number of individuals who I am incredibly grateful to and who have supported me throughout the completion of this degree. First and foremost, I would like to thank my supervisor, Denys. His enthusiasm for science and his support for his students genuinely helped make this project and the time in his lab an enjoyable experience. I would also like to thank all of my lab mates who were always willing to help me work through a problem. In particular, Eileigh, Shan, Juliette, and Kathleen, thank you for your helpful advice and for making the lab a happy environment to come to every day. I am also grateful to my committee members, Dr. Roy Duncan, Dr. Craig McCormick, and Dr. Paola Marcato, for their support and encouragement over the last two years. Thank you to the McCormick lab for always willing to let us borrow reagents and thank you to the funding agencies that supported this project: NSERC, CIHR, Research NS, Infection, Immunity, Inflammation & Vaccinology (I3V) – Dalhousie Medical Research Foundation (DMRF) Graduate Studentship, Dalhousie Faculty of Medicine Graduate Studentship, and Mitacs. Lastly, I am grateful for my friends and family who were always willing to listen when I had trouble with an experiment and who were always happy to cheer me on when experiments were a success. Thank you all.

CHAPTER 1: INTRODUCTION

1.1 Coronaviruses

Coronaviruses (CoVs) are a family of enveloped single-stranded positive-sense RNA viruses (V'kovski et al., 2021). There are seven CoVs known to circulate in human populations, presenting as common colds to more severe, and sometimes fatal, respiratory disease (V'kovski et al., 2021). Common cold human coronaviruses (HCoVs) include HCoV-OC43 (OC43) and HCoV-229E, which have been reported to circulate in human populations for decades, as well as more recently identified HCoV-NL63 and HCoV-HKU1 (V'kovski et al., 2021). More pathogenic CoVs have entered human populations due to spillover from zoonotic sources. This group includes severe acute respiratory syndrome coronavirus (SARS-CoV) which emerged in 2002 as well as Middle Eastern respiratory syndrome coronavirus (MERS-CoV) which emerged in 2011 (Hartenian et al., 2020). The most recent pathogenic CoV is SARS-CoV2 (CoV2); this virus emerged in 2019 from Wuhan, China and is the cause of the devastating pandemic of coronavirus disease 2019 (COVID-19). To date, there are over 550 million cases of COVID-19 worldwide, accounting for 6.3 million deaths globally (July 5th, 2022) (*COVID-19 Map*, 2022).

1.2 Coronavirus genome and host detection

Within the *Coronaviridae* family lies the subfamily *Coronavirinae* which houses four genera: *Alphacoronavirus*, *Betacoronavirus*, *Gammacoronavirus*, and *Deltacoronavirus* (V'kovski et al., 2021). The three recently emerged severe CoVs as well as OC43 and HCoV-HKU1 belong to the *Betacoronavirus* genera (Hartenian et al., 2020). *Betacoronaviruses* have a 30 kilobase RNA genome with a large open reading frame (ORF), ORF1ab (Hartenian et al., 2020). ORF1ab encodes a polyprotein which is proteolytically processed by viral enzymes Nsp3 papain-like proteinase (PLpro) and Nsp5 3C-like proteinase (3CLpro) (Hartenian et al., 2020; Ziebuhr et al., 2000). Viral processing of the polyprotein releases the remaining non-structural proteins (Nsps) which function in viral replication and transcription as well as evasion of host antiviral responses (Hartenian et al., 2020; V'kovski et al., 2021). Assembly of the viral RNA-dependent RNA polymerase then generates subgenomic mRNAs which encode accessory

ORFs and the structural proteins (Brian & Baric, 2005; Hartenian et al., 2020). These accessory ORFs have been shown to vary greatly between CoV groups and some accessory proteins have been reported to limit interferon (IFN) responses (V'kovski et al., 2021). The structural proteins include membrane (M) and envelope (E) which are responsible for viral particle formation, nucleocapsid (N) which is an RNA-binding protein that coats the viral genome, and spike (S) that is a receptor glycoprotein that binds the host cell receptor to mediate viral entry (Hartenian et al., 2020; V'kovski et al., 2021). OC43 S binds sialic acid that is abundant on the surface of most cell types (Künkel & Herrler, 1993), while SARS-CoV and CoV2 S bind angiotensin converting enzyme 2 (ACE2) on the surface of the host cell (Hoffmann et al., 2020; W. Li et al., 2003).

After entry into the host cell, CoVs uncoat and deliver their genome to the cytoplasm. Like many RNA viruses, CoVs must utilize host translation machinery to facilitate viral protein production. To shift translation to viral mRNAs instead of host mRNAs, CoVs utilize host shutoff protein Nsp1 (Narayanan et al., 2015). Nsp1 is able to inhibit host translation by outcompeting host mRNAs for the 40S ribosome; cryogenic electron microscopy analysis of Nsp1 in complex with the 40S ribosome revealed that Nsp1 binds the mRNA entry channel, blocking host mRNAs from entering the ribosome, and preventing translation initiation (Borišek et al., 2021; Narayanan et al., 2015). Nsp1 of some CoVs, like SARS and CoV2, are also able to induce mRNA degradation, depleting the level of host mRNAs that could compete for the ribosome (Narayanan et al., 2015; Schubert et al., 2020). Importantly, Nsp1 does not block translation of viral mRNAs. The 5' untranslated region (UTR) of CoV mRNA contains secondary structures including stem loops (SL). The first SL, SL1 specifically, has been shown to confer protection to mRNAs from Nsp1 induced degradation and translation block (Banerjee et al., 2020; Vora et al., 2022).

Upon successful translation of viral mRNAs, Nsp1s involved in viral replication and transcription are expressed. Multiple Nsp1s will remodel the endoplasmic reticulum (ER), creating convoluted membranes and double membrane vesicles (Hartenian et al., 2020). CoV replication occurs in these highly modified membranes and replication of the viral genome can generate double-stranded RNA (dsRNA) intermediates (Hartenian et

al., 2020). Leakage of these dsRNA products into the cytoplasm can then activate cytoplasmic immune sensors, including retinoic acid-inducible gene I (RIG-I), melanoma differentiation-associated gene 5 (MDA5), and dsRNA-activated protein kinase (PKR) (Rehwinkel & Gack, 2020). RIG-1 is activated by 5'-triphosphate groups of single-stranded RNA (ssRNA) while MDA5 and PKR are activated by dsRNA (Rehwinkel & Gack, 2020). These cytosolic sensors activate a downstream signalling cascade resulting in the activation of transcription factors interferon regulatory factor 3 (IRF3), IRF7, and nuclear factor kappa light chain enhancer of activated B cells (NF- κ B), promoting induction of type I and type III IFNs (Rehwinkel & Gack, 2020). Further, detection of dsRNA by PKR also activates the integrated stress response (ISR) which halts host translation and results in the formation of stress granules (SGs). The ISR and SG formation are illustrated in Figure 1.1.

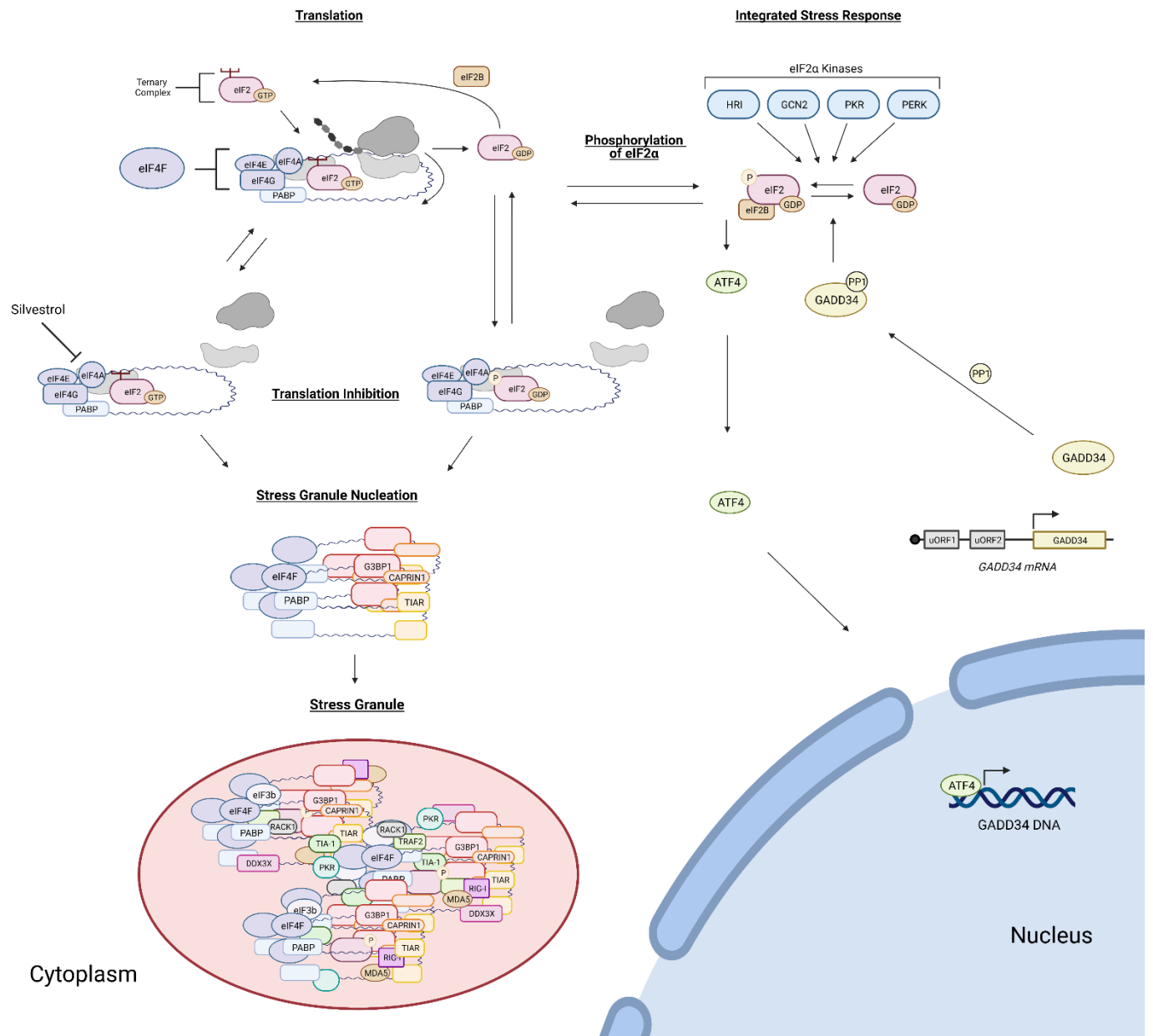


Figure 1.1. Model of the integrated stress response and stress granule formation.

Translation: During initiation of host translation, the 43S small ribosomal subunit complex is recruited to mRNA. This complex includes the eIF2–GTP–Met-tRNA^{Met}_i ternary complex and upon recognition of the initiation codon, eIF2-GTP is hydrolysed to eIF2-GDP and is released. The guanine exchange factor activity of eIF2B promotes the conversion of eIF2-GDP for eIF2-GTP, which can be used for the translation of additional mRNAs. Recycling of the ternary complex is inhibited when eIF2 α is phosphorylated, because phosphorylated eIF2 α binds tightly with eIF2B preventing the exchange of eIF2-GDP for eIF2-GTP. **Phosphorylation of eIF2 α :** The translation factor eIF2 α can be phosphorylated in response to various types of stress by four different kinases: haeme-regulated inhibitor (HRI), general control non-derepressible protein 2 (GCN2), double-stranded RNA (dsRNA)-activated protein kinase (PKR) and PKR-like endoplasmic reticulum (ER) kinase (PERK). Following phosphorylation of eIF2 α , eIF2 is unable to exchange GDP for GTP, halting host translation and resulting in polysome disassembly. **Translation inhibition:** Translation inhibition can occur through phosphorylation of eIF2 α or interference with the eIF4F complex. The eIF4F complex is composed of the RNA helicase eIF4A, cap-binding protein eIF4E, and scaffold protein eIF4G which bridges poly(A)-binding protein (PABP) to eIF4E and eIF4A. Silvestrol treatment interferes with eIF4A function, leaving eIF4A attached to the mRNA and preventing mRNA scanning. This mechanism also halts host translation and results in the release of polysomes. **Stress granule nucleation:** Many translation factors are then bound by SG-nucleating proteins like Ras-GTPase-activating protein SH3 domain-binding protein 1 (G3BP1) and T-cell intracellular antigen 1-related protein (TIAR), which promotes the aggregation of additional RNA-binding proteins. This SG nucleation seeds the formation of larger dynamic SGs. **Stress granules:** Stress granule nucleation promotes the formation of SGs composed of various RNA molecules, translation factors, and immune signalling proteins. **The integrated stress response:** The phosphorylation of eIF2 α is also an important step in the ISR. The decrease in active eIF2–GTP–Met-tRNA^{Met}_i ternary complexes increases uORF skipping which promotes expression of transcription factor activating transcription factor 4 (ATF4). ATF4 translocates to the nucleus to promote transcription of target genes, including growth arrest and DNA damage-

inducible protein 34 (GADD34). *GADD34* mRNA is released to the cytoplasm, where because of the increase in uORF skipping, there is an increase in translation of the downstream GADD34 ORF and GADD34 protein production. GADD34 can complex with protein phosphatase 1 (PP1) to dephosphorylate eIF2 α . The dephosphorylation of eIF2 α allows eIF2-GDP to be exchanged for eIF2-GTP and translation resumes. Adapted from (McCormick & Khapersky, 2017).

1.3 Stress granule formation and eIF2 α phosphorylation

SGs are aggregates of messenger ribonucleoproteins (mRNPs), RNA, and translation factors, among other proteins (N. Kedersha et al., 2002; N. L. Kedersha et al., 1999). SGs primarily form through the phosphorylation of translation initiation factor eIF2 α (N. Kedersha et al., 2002; Tourrière et al., 2003) which is the integration point of the ISR (Jousse et al., 2003). There are four kinases which phosphorylate eIF2 α that are activated by their respective activators (N. Kedersha et al., 2002, 2013): dsRNA-activated protein kinase (PKR) is activated by dsRNA (García et al., 2007a); PKR-like endoplasmic reticulum kinase (PERK) is activated by ER stress (Harding et al., 1999; Harding, Zhang, et al., 2000); heme-regulated inhibitor (HRI) kinase is activated by oxidative stress and heat shock (Han et al., 2001); and general control nonderepressible 2 (GCN2) kinase is activated by UV light and amino acid starvation (P. Zhang et al., 2002). Following kinase activation, eIF2 α is phosphorylated and translation initiation is inhibited (Jackson et al., 2010; McCormick & Khapersky, 2017). During translation initiation, the eIF2-GTP-Met-tRNA^{Met} ternary complex is formed, which is a part of the 43S pre-initiation complex (Jackson et al., 2010). Recycling of the ternary complex requires the exchange of GDP for GTP on eIF2 (Jackson et al., 2010); eIF2B is a guanine exchange factor responsible for this exchange (Jackson et al., 2010). However, when eIF2 α is phosphorylated, it binds tightly with eIF2B, preventing the recycling of GDP for GTP and stalling translation (Jackson et al., 2010). This halt on host translation creates an accumulation of untranslated mRNPs which are key components of SGs and involved in the initial nucleation of SGs (N. Kedersha et al., 2002; McCormick & Khapersky, 2017). This nucleation is mediated primarily by Ras-GTPase-activating protein SH3 domain-binding protein 1 (G3BP1), G3BP2, T-cell intracellular antigen 1 (TIA-1), and

TIA-1-related protein (TIAR), with participation of other factors (N. Kedersha et al., 2013; Protter & Parker, 2016).

1.4 Stress granule nucleation

G3BP1 is recruited to SGs and promotes recruitment of other proteins and RNAs (N. Kedersha et al., 2013; Tourrière et al., 2003). In addition, G3BP1 can mediate SG formation; overexpression of G3BP1 has been reported to induce SG formation in the absence of exogenous stressors (Tourrière et al., 2003). G3BP2, an isoform of G3BP1, has also been shown to promote SG formation (Matsuki et al., 2013). Both G3BP1 and G3BP2 contain N-terminal nuclear transport factor 2 (NTF2) domains which can interact with other proteins to regulate SG formation; for example, binding to cell cycle associated protein 1 (Caprin1) promotes SG formation while binding to ubiquitin specific peptidase 10 (USP10) suppresses SG formation (N. Kedersha et al., 2016a; Matsuki et al., 2013). In addition, G3BP1 and G3BP2 contain C-terminal arginine-glycine-glycine (RGG) domains, important for interaction with the 40S ribosomal subunit, which is crucial for SG formation (N. Kedersha et al., 2016a). In addition to G3BP1 and G3BP2, there are other nucleators of SGs. TIAR and TIA-1, two closely related proteins, were two of the first RNA-binding proteins identified to initiate formation of and localize to SGs (N. L. Kedersha et al., 1999). These proteins were first reported to cause DNA damage in thymocytes, but have since been shown to act as major regulators of SGs, containing multiple RNA recognition motifs (RRMs) which promote the recruitment of RNA and proteins to SGs (N. L. Kedersha et al., 1999).

After the initial nucleation of SGs, SGs begin to grow because of many protein-protein and protein-RNA interactions (Jain et al., 2016; Protter & Parker, 2016). These interactions are largely mediated through intrinsically disordered and low complexity (ID/LC) domains (Protter & Parker, 2016); SG nucleating proteins like G3BP1 and TIA-1 contain ID/LC domains which contribute to the maturation of SGs (Gilks et al., 2004; P. Yang et al., 2020). Once the level of accumulated RNA and proteins reaches a critical threshold, they phase separate to form SGs (Jain et al., 2016). Phase separation is an event when a group of molecules, like RNA and proteins, forms a network of multiple

weak multivalent interactions to a point where these molecules concentrate into a separate phase (Protter & Parker, 2016).

Following phase separation, SGs are thought to exist as a stable core surrounded by a fluid outer shell (Jain et al., 2016). Exchange of proteins into the outer shell as well as between the outer shell and the inner core illustrates the dynamic nature of SGs (Jain et al., 2016). This dynamic nature of SGs also greatly influences SG composition. While multiple core SG proteins have been identified, the composition of SGs is varied and accounts for many different proteins involved in many cellular pathways. In fact, the composition of SGs was found to depend upon the stressor that induced its formation (Aulas et al., 2017). Thus, these foci act as a cytoplasmic hub in which proteins and RNA molecules can enter, exit, and interact with one another.

1.5 SG function

Given the highly dynamic nature and varied composition of SGs, the precise function of SGs has been difficult to determine and remains unknown. Our current understanding is that SGs function as areas of mRNA triage during cellular stress, where SGs help determine the fate of certain mRNAs (Protter & Parker, 2016). SG-localized mRNAs may be stored and protected in SGs until the cellular stress is absent and these mRNAs can be released to the cytoplasm and translated. In addition, these mRNAs may be directed from SGs to P-bodies, another biological condensate independent from SGs, where mRNA decay machinery in P-bodies can promote degradation of mRNAs (Protter & Parker, 2016). SG formation has also been tied to cell survival; cells that do not form SGs are more sensitive to stress, suggesting that SG formation is cytoprotective (N. Kedersha et al., 2013). Conversely, prolonged SG formation can have negative impacts as well. Mutations in SG RNA-binding proteins, like TIA-1 or TAR DNA-binding protein 43 (TDP-43), and persistent aggregate formation in neurons is thought to contribute to neuronal cell death in neurodegenerative and muscular degenerative diseases, like amyotrophic lateral sclerosis (ALS) or frontotemporal dementia (FTD) (Protter & Parker, 2016). Thus, a possible model for SG function suggests that SGs balance the fate of mRNAs; SGs can protect mRNAs during cellular stress but during long periods of stress where the cell is unlikely to recover, SGs promote cell death.

1.6 SG dissolution

As a cytoplasmic hub for proteins and RNA, SGs can store these molecules during cellular stress. However, it is important for SGs to dissolve following the removal of stress so mRNAs can resume translation and SG-localized proteins can return to their SG-independent functions. The primary method of SG dissolution is through the autophagy pathway, sometimes termed granulophagy (Buchan et al., 2013). Mutations in autophagy proteins valosin-containing protein (VCP) or autophagy related protein 7 (ATG7) have been shown to result in sustained SG formation despite the removal of the exogenous stressor, suggesting that intact autophagy machinery is crucial for SG clearance (Buchan et al., 2013). Regulation of SG clearance by autophagy was also linked to the dual specificity tyrosine phosphorylation regulated kinase 3 (DYRK3) and heat shock protein 90 (Hsp90) (Mediani et al., 2021; Wippich et al., 2013). Hsp90 can bind and stabilize DYRK3, and active DYRK3 can phosphorylate and inactivate proline-rich AKT substrate of 40 kDa (PRAS40) (Mediani et al., 2021); PRAS40 is an inhibitor of mammalian target of rapamycin complex 1 (mTORC1) and inactivation of PRAS40 restores mTORC1 signalling (Wippich et al., 2013). The mTORC1 complex is a major regulator of cellular metabolism and it promotes the translation of mRNAs encoding proteins involved in many different cellular processes. Activation of mTORC1, through DYRK3-mediated inactivation of mTORC1 inhibitor PRAS40, promotes SG disassembly and resumes translation (Mediani et al., 2021; Wippich et al., 2013).

1.7 Dephosphorylation of eIF2 α

Following sustained phosphorylation of eIF2 α and translation arrest, there is induction of downstream genes involved in the ISR. The lack of active ternary complexes increases leaky scanning, or upstream open reading frame (uORF) bypass by the 48S preinitiation complex which in turn promotes translation of downstream ORFs (Jackson et al., 2010). One of these downstream ORFs encodes activating transcription factor 4 (ATF4) (Jackson et al., 2010); this transcription factor can promote expression of additional downstream ORFs, such as C/EBP homologous protein (CHOP) and growth arrest and DNA damage-inducible protein 34 (GADD34) (Harding, Novoa, et al., 2000; Jackson et al., 2010). Expression of GADD34 (a.k.a. protein phosphatase 1 regulatory

subunit 15A, PPP1R15A) has been linked to dephosphorylation of eIF2 α and it was later shown that GADD34 binds both eIF2 α and protein phosphatase 1 (PP1), bridging these two proteins and facilitating the dephosphorylation of eIF2 α (Choy et al., 2015; Rojas et al., 2015). Shortly after, another protein capable of decreasing levels of eIF2 α phosphorylation was identified (Jousse et al., 2003). The PP1-binding domain of GADD34 was highly conserved in the C-terminus of this protein and it was named constitutive repressor of eIF2 α phosphorylation (CReP) (Jousse et al., 2003). CReP (a.k.a. protein phosphatase 1 regulatory subunit 15B, PPP1R15B) is consistently expressed within the cell to maintain basal levels of dephosphorylated eIF2 α (Jousse et al., 2003; Kastan et al., 2020).

1.8 Stress granule formation independent of eIF2 α phosphorylation

Independently from the phosphorylation of eIF2 α , SGs can also form when translation is inhibited through interference with the eIF4F complex. The eIF4F complex comprises eIF4E which binds the 5' methyl-cap, eIF4A which is an RNA helicase responsible for unwinding secondary RNA structures to promote scanning of the mRNA, and eIF4G which connects eIF4E, eIF4A, and poly(A)-binding protein (PABP) bound to the poly-adenylated tail of the mRNA (Jackson et al., 2010). Silvestrol (Sil.) is a roscaglate derived from the *Aglaia* plant, previously shown to interfere with the function of eIF4A (Chu et al., 2016). Treatment with Sil. results in translation inhibition, without the phosphorylation of eIF2 α , and subsequent SG formation (Slaine et al., 2017).

1.9 Stress granules and the antiviral response

Regardless of how SGs form, they have been shown to recruit antiviral signalling molecules and it is speculated that SGs can act as a platform to facilitate the activation of antiviral responses. Innate immune sensors like RIG-I, MDA5, PKR, tripartite motif containing 25 (TRIM25), RNase L, and 2'-5' oligoadenylate synthetases (OAS) have all been shown to localize to SGs (Langereis et al., 2013; Manivannan et al., 2020; Onomoto et al., 2012; Sánchez-Aparicio et al., 2017). In addition, SG-nucleating proteins have been linked to antiviral signalling responses. G3BP1 can recruit inactive PKR to SGs, where PKR is subsequently activated and released into the cytosol to induce IFN production (Reineke et al., 2015; Reineke & Lloyd, 2015). In addition, overexpression of

G3BP1 and increasing formation of SGs has been correlated with increasing activation of NF- κ B (Reineke & Lloyd, 2015). Further, G3BP1 has been shown to interact with RIG-I and antagonize its degradation as well as promote RIG-I-mediated IFN β production (Kim et al., 2019; W. Yang et al., 2019). Additionally, DEAD-box helicase 3 (DDX3), a core SG protein, has been shown to limit influenza A virus (IAV) infection. Knock down of this protein prevented SG formation in virus-infected cells and increased viral titers (Thulasi Raman et al., 2016), but in DDX3-expressing cells, SG induction and IFN β production were both increased in response to IAV infection (Kesavardhana et al., 2021).

The idea that SGs are antiviral is further supported by the fact that many viruses have evolved to suppress SG formation. Viruses, including Chikungunya virus, Zika virus, Japanese encephalitis virus, and Semliki Forest virus, have been reported to sequester SG proteins, like G3BP1 and Caprin1, to replication complexes, thereby limiting SG formation and promoting viral replication (Fros et al., 2012; Hou et al., 2017b; Katoh et al., 2013; Panas et al., 2012). Sequestration of SG proteins is often mediated by viral proteins, but binding of SG proteins to viral RNA, like the viral RNA of Tick-borne encephalitis virus, West Nile virus, or Dengue virus, has also been reported to re-localize SG proteins and limit SG formation (Albornoz et al., 2014; Emara & Brinton, 2007). In addition, some viruses will cleave SG proteins to inhibit SGs (Visser et al., 2019; White et al., 2007); for example, the 3C protease of polio virus cleaves G3BP1 and eIF4G, limiting SG formation (White et al., 2007). Viruses have also been reported to antagonize SG formation and maintain translation through interference with eIF2 α kinases. Both the NS1 protein of IAV and the virion host shutoff (vhs) protein of herpes simplex virus (HSV) will inactivate PKR, limiting eIF2 α phosphorylation in response to viral infection, and preventing SG formation (Dauber et al., 2016; Khapersky et al., 2014). Viruses also encode multiple strategies to prevent SG formation, like IAV (Khapersky et al., 2012, 2014), HSV (Dauber et al., 2016; Y. Li et al., 2011), and Zika virus (Hou et al., 2017a) to name a few. Given the limited coding capacity of viral genomes and the redundant functions of these viral proteins, it suggests that limited SG formation is crucial for efficient viral replication.

1.10 Coronaviruses and stress granules

For CoVs, the relationship between SG formation and viral infection remains unclear. Some CoVs inhibit SG formation: both MERS and *Gammacoronavirus* infectious bronchitis virus (IBV) attenuate PKR activation to limit eIF2 α phosphorylation and SG formation (Brownsword et al., 2020; Gao et al., 2021; Nakagawa et al., 2018; Rabouw et al., 2016). While other CoVs induce SG formation: SGs form during transmissible gastroenteritis virus (TGEV) infection and are thought to play a role in post-transcriptional regulation of the viral genome (Sola et al., 2011).

With the resurgence of CoV research due to the COVID-19 pandemic, novel roles of CoVs proteins have been proposed in relation to SG formation. The N protein of CoV2 has been proposed to interfere with SG formation (Cascarina & Ross, 2020) and this idea has been strengthened by recent publications showing CoV2 binds to SG proteins G3BP1 and G3BP2 in multiple proteomics studies (Gordon et al., 2020; J. Li et al., 2021; Nabeel-Shah et al., 2022). For the virus, N is important for coating and protecting the viral mRNA. Because of this intrinsic function of N, it is built to self-oligomerize and to bind mRNA, and it has been shown to phase separate in the presence of RNA (Savastano et al., 2020; J. Wang et al., 2021). These are all similar characteristics as common SG proteins. Thus, it is possible that N can sequester key SG proteins away from SGs and interfere with SG formation.

Furthermore, previous publications have investigated the role of Nsp15 in limiting SG formation (Gao et al., 2021). Nsp15 is a conserved endoribonuclease that targets polyuridine stretches and is thought to promote viral evasion of host immune detection (Hartenian et al., 2020). Previously, Nsp15 has also been shown to limit SG formation during IBV infection (Gao et al., 2021). Infection with recombinant IBV that encodes a catalytically inactive Nsp15 increased the level of SG formation in IBV-infected cells and resulted in a loss of the SG inhibitory function of IBV. This coincided with increased PKR activation, IRF3 signalling, and IFN- β mRNA, suggesting that Nsp15 functions to limit SG formation and antiviral immune signalling by limiting detection of viral mRNA by PKR (Gao et al., 2021). While this function of Nsp15 has proven to be important for

IBV infection, whether Nsp15 has similar functions for additional members of the CoV family has yet to be elucidated.

Additionally, CoVs encode host shutoff factor Nsp1 which has also been shown to limit IFN induction (Kumar et al., 2021; Narayanan et al., 2008). Nsp1 interferes with IFN induction by blocking host translation and inducing the degradation of cellular mRNAs (Narayanan et al., 2015; Schubert et al., 2020). In addition to binding the 40S ribosome to block host translation, Nsp1 has also been shown to bind other host proteins, including translation initiation factors as well as SG proteins G3BP1, G3BP2, and eIF4G (Gerassimovich et al., 2021). In fact, one publication found that ectopic overexpression of SARS Nsp1 resulted in localization of Nsp1 to As-induced SGs where Nsp1 disrupted SG maturation and altered SG composition (Gerassimovich et al., 2021). Whether this function of Nsp1 is conserved in other CoVs and how Nsp1 can interfere with SG formation is still unclear.

1.11 Rationale and objectives

Given the questionable role of SGs during CoV infection and the growing literature suggesting that CoV gene products can interfere with SG formation, my project has been focusing on the modulation of SG responses by CoVs. Using *Betacoronavirus* OC43 as an infection model along with overexpression of viral proteins from both OC43 and CoV2, I aim to clarify the relationship between SG formation and CoV infection. Initial results for this project revealed that OC43 infection inhibits SG formation and eIF2 α phosphorylation. Further, overexpression of viral proteins OC43-Nsp1 and CoV2-Nsp1 limited SG formation. Therefore, my objectives for this project include: 1) To identify the mechanism of OC43-mediated inhibition of eIF2 α phosphorylation; and 2) To characterize the functional differences of coronavirus Nsp1 proteins in modulating stress granule formation.

CHAPTER 2: MATERIAL AND METHODS

2.1 Cells

Human embryonic kidney (HEK) 293A and 293T cells, human colon adenocarcinoma (HCT-8) cells, and green monkey kidney (Vero) cells were cultured in Dulbecco's modified Eagle's medium (DMEM) supplemented with heat-inactivated 10% fetal bovine serum (FBS), and 2 mM L-glutamine (all purchased from Thermo Fisher Scientific (Thermo), Waltham, MA, USA). BEAS-2B cells were cultured in Bronchial Epithelial Cell Growth Medium (BEGM, Lonza, Kingston, ON, Canada) on plates prepared with coating media (0.01 mg/mL fibronectin, 0.03 mg/mL bovine collagen type I, and 0.01 mg/mL bovine serum albumin (BSA) (all from Millipore Sigma, Oakville, ON, Canada) dissolved in Basal Epithelial Cell Growth Medium (BEBM, Lonza)). The 293A, 293T, Vero, and BEAS-2B cells were purchased from American Type Culture Collection (ATCC, Manassas, VA, USA), and the HCT-8 cells were purchased from Millipore Sigma.

2.2 Viruses

OC43 was purchased from ATCC. To generate initial virus stocks, Vero cells (ATCC) were infected at multiplicity of infection (MOI) <0.1 for 1 h in serum-free DMEM at 37°C following replacement of the inoculum with DMEM supplemented with 1% FBS + 0.5% BSA and continued incubation at 33 °C. Once cytopathic effects (CPE) reached 75% at 4-5 days post-infection, the viral supernatant was harvested, centrifuged at 2,500 x g for 5 min, and then the cleared viral supernatant was aliquoted and stored at -80 °C. Stocks were titered by plaque assay on Vero cells. After initial experiments and the discovery that OC43 grows efficiently in 293A cells, 293A cells were infected with OC43 to generate later virus stocks. The 293A cells were infected at MOI <0.1 for 1 h in serum-free DMEM at 37 °C following replacement of the inoculum with DMEM supplemented with 1% FBS + 0.5% BSA and continued incubation at 37 °C. At 48 hours post infection (hpi), the viral supernatant was harvested, centrifuged at 2,500 x g for 5 min, and then the cleared viral supernatant was aliquoted and stored at -80 °C. Stocks were titered by foci-forming unit assay on 293A cells.

2.3 Plasmids and lentivirus stocks

CoV2 and OC43 N, Nsp1, and Nsp15 ORFs were amplified using polymerase chain reaction (PCR) from cDNAs generated from total RNA of infected Vero cells collected at 24 hpi using specific primers with simultaneous introduction of flanking restriction sites. Then, coding sequences were inserted between EcoRI and XhoI sites into pCR3.1-EGFP vector (Khapersky et al., 2016) to generate pCR3.1-EGFP-OC43-N, pCR3.1-EGFP-CoV2-N, pCR3.1-EGFP-OC43-Nsp1, pCR3.1-EGFP-CoV2-Nsp1, and pCR3.1-EGFP-OC43-Nsp15 plasmids. To generate N-terminally HA-tagged Nsp1 constructs, coding sequences were inserted between KpnI and XhoI sites into 3xHA-miniTurbo-NLS_pCDNA3 vector (a gift from Alice Ting, Addgene plasmid # 107172) to generate pCDNA3-HA-OC43-Nsp1 and pCDNA3-HA-CoV2-Nsp1 vectors (miniTurbo-NLS coding sequence was replaced by Nsp1 sequences). Amino acid substitutions in pCDNA3-HA-CoV2-Nsp1 vector were introduced using Phusion PCR mutagenesis (New England Biolabs) to generate pCDNA-HA-CoV2-Nsp1(R99A) and pCDNA-HA-CoV2-Nsp1(R124A,K125A) vectors. To generate lentivirus vectors pLJM1-EGFP-BSD and pLJM1-EGFP-G3BP1-BSD, the PCR-amplified EGFP and G3BP1 coding sequences were inserted into the multicloning site of pLJM1-B* vector (71). All constructs were verified by Sanger sequencing, sequences are available upon request. To generate lentivirus stocks, HEK 293T cells (ATCC) were reverse-transfected with polyethylenimine (PEI, Polysciences, Warrington, PA, USA) and the following plasmids for lentiviral generation: pLJM1-B* backbone-based constructs, pMD2.G, and psPAX2. pMD2.G and psPAX2 are gifts from Didier Trono (Addgene plasmids #12259 and #12260). At 48 h post-transfection, lentivirus containing supernatants were passed through a 0.45 μ M filter and frozen at -80 °C.

2.4 Generation of stably transduced cell lines

To generate 293A[EGFP] and 293A[EGFP-G3BP1] cells, 293A cells were transduced with lentiviruses produced from pLJM1-EGFP-BSD and pLJM1-EGFP-G3BP1-BSD vectors and at passage 3 post-transduction, EGFP-positive cells were isolated using live cell sorting on BD FACSAria III instrument, cultured, and used for experiments at passage 5 to 6.

2.5 Cell treatments

For SG induction, sodium arsenite (As; Millipore Sigma) was added to the media to a final concentration of 500 μM and cells were returned to 37 °C incubator for 50 min; or silvestrol (Sil.; MedChemExpress, Monmouth Junction, NJ, USA) was added to the media to a final concentration of 500 nM and cells were returned to 37 °C incubator for 1 h. To induce eIF2 α phosphorylation, thapsigargin (Tg; Sigma) was added to the media to a final concentration of 1 μM and cells were returned to 37 °C incubator for 1 h; cells were transfected with 1 μg Polyinosinic:polycytidylic acid (poly I:C; Thermo) and cells were returned to 37 °C incubator for 2 h; or cells were washed briefly with phosphate-buffered saline (PBS) and exposed to 20 mJ/cm^2 ultraviolet light (254 nm, UVC) in a HL-2000 Hybrilinker chamber (UVP) and cells were returned to 37 °C incubator for 2 h. To induce GADD34, Tg (Sigma) was added to the media to a final concentration of 1 μM and cells were returned to 37 °C incubator for 4 h. To inhibit the integrated stress response, integrated stress response inhibitor (ISRIB; Sigma) was added to the media to a final concentration of 200 nM and cells were returned to 37 °C incubator for 23 h. To test 6-Thioguanine (6-TG) for potential SG induction, 6-TG (Sigma) was added to the media to a final concentration of 10 μM and cells were returned to 37 °C incubator for 4 h or 20 h.

2.6 Virus infections

Cell monolayers grown in 20-mm wells of 12-well cluster dishes with or without glass coverslips were washed briefly with PBS and 300 μl of virus inoculum diluted to the calculated MOI = 1.0 in 1% FBS DMEM was added. MOI was calculated based on titering in 293A cells and this calculation was used for infection of 293A, BEAS2B, and HCT-8 cells. Cells were placed at 37 °C for 1 h, with manual horizontal shaking every 10-15 min. Then, virus inoculum was aspirated from cells, cells were washed with PBS, 1 ml of fresh 1% FBS DMEM was added to each well, and cells were returned to 37 °C until the specified time post-infection.

2.7 Transfection

The 293A cells were seeded into 20-mm wells of 12-well cluster dishes with or without glass coverslips and the next day transfected with 500 ng DNA mixes/well containing expression vectors (250 ng) and pUC19 filler DNA (250 ng) using Fugene HD (Promega, Madison, WI, USA) according to manufacturer's protocol. Where indicated, the amount of filler DNA was reduced to 150 ng and 100 ng of the pCR3.1-EGFP plasmid was co-transfected with expression vectors for Nsp1 proteins. Cells were used for experiments 23-24 h post-transfection as indicated.

2.8 siRNA knockdown

For silencing of GADD34, 293A cells were transfected with Ambion Silencer Select siRNAs (siGADD34#1 (s24269) & siGADD34#2 (s24268)) using Lipofectamine RNAiMAX (Invitrogen) according to manufacturer's protocol (reverse transfection in 12-well cluster dishes) and treated/analysed at 48 h post-transfection. For a non-targeting siRNA control, cells were transfected with Silencer Select Negative Control #2 siRNA (siNT; Ambion, #4390846).

2.9 Immunofluorescence staining

Cell fixation and immunofluorescence staining were performed according to the procedure described in (Ying & Khapersky, 2020). Briefly, cells grown on 18-mm round coverslips were fixed with 4% paraformaldehyde in PBS for 15 min at ambient temperature and permeabilized with cold methanol for 10 min. After 1 h blocking with 5% BSA (BioShop, Burlington, ON, Canada) in PBS, staining was performed overnight at +4 °C with antibodies to the following targets: eIF3B (1:400; rabbit, Bethyl Labs, A301761A); eIF4G (1:200; rabbit, Cell Signaling, #2498); G3BP1 (1:400; mouse, BD Transduction, 611126); G3BP2 (1:1000; rabbit, Millipore Sigma, HPA018304); HA tag (1:100; mouse, Cell Signalling, #2367); OC43 N (1:500; mouse, Millipore, MAB9012); TIA-1 (1:200; goat, Santa Cruz Biotechnology, sc-1751); TIAR (1:1000; rabbit, Cell Signaling, #8509). Alexa Fluor (AF)-conjugated secondary antibodies used were: donkey anti-mouse IgG AF488 (Invitrogen, A21202), donkey anti-rabbit IgG AF555 (Invitrogen, A31572), donkey anti-goat IgG AF647 (Invitrogen, A32839). Where indicated, nuclei

were stained with Hoechst 33342 dye (Invitrogen, H3570). Slides were mounted with ProLong Gold Antifade Mountant (Thermo Fisher) and imaged using Zeiss AxioImager Z2 fluorescence microscope and Zeiss ZEN 2011 software. Quantification of SG-positive cells was performed by counting the number of cells with at least two discrete cytoplasmic foci from at least 3 randomly selected fields of view, analysing >100 cells per treatment in each replicate. Analysis of SG number and size was performed on cropped images of individual cells using ImageJ software Analyze Particles function after automatic background subtraction and thresholding. For each of 3 independent biological replicates, 7 cells selected from at least 3 random fields of view were analyzed for a total of 21 cells per condition.

2.10 Western blotting

Whole-cell lysates were prepared by direct lysis of PBS-washed cell monolayers with 1× Laemmli sample buffer (50 mM Tris-HCl pH 6.8, 10% glycerol, 2% sodium dodecyl sulphate (SDS), 100 mM DTT, 0.005% Bromophenol Blue). Lysates were immediately placed on ice, homogenized by passing through a 21-gauge needle, and stored at -20°C. Aliquots of lysates thawed on ice were incubated at 95°C for 3 min, cooled on ice, separated using denaturing polyacrylamide gel electrophoresis (PAGE), transferred onto polyvinylidene fluoride (PVDF) membranes using Trans Blot Turbo Transfer System with RTA Transfer Packs (Bio-Rad Laboratories, Hercules, CA, USA) according to manufacturer's protocol and analysed by immunoblotting using antibody-specific protocols. Antibodies to the following targets were used: ATF4 (1:1000; Rabbit, Cell Signalling, #9644); β -actin (1:2000; HRP-conjugated, mouse, Santa Cruz Biotechnology, sc-47778); Bip (rabbit, Cell Signalling, #3177); eIF2 α (1:1000; rabbit, Cell Signaling, #5324); eIF4G (1:1000; rabbit, Cell Signaling, #2498); G3BP1 (1:4000; mouse, BD Transduction, 611126); G3BP2 (1:2500; rabbit, Millipore Sigma, HPA018304); GADD34 (1:1000; mouse, Proteintech, #10449-1-AP); GCN2 (1:1000; rabbit, Cell Signalling, #3302s); GFP (1:1000; rabbit, Cell Signaling, #2956); HA tag (1:1000; mouse, Cell Signalling, #2367); OC43 N (1:1,000; mouse, Millipore, MAB9012); phospho-S51-eIF2 α (1:1000; rabbit, Cell Signaling, #3398); phospho-T899-GCN2 (1:1,000; rabbit, Cell Signalling, #94668); phospho-T448-GCN2 (1:1,000; rabbit,

Cell Signalling, #3076); PKR (1:1000; rabbit, Cell Signaling, #3072); TIAR (1:1000; rabbit, Cell Signaling, #8509). For band visualization, HRP-conjugated anti-rabbit IgG (Goat, Cell Signaling, #7074) or anti-mouse IgG (Horse, Cell Signaling, #7076) were used with Clarity Western ECL Substrate on the ChemiDoc Touch Imaging System (Bio-Rad Laboratories). Where indicated, total protein was visualised post-transfer to PVDF membranes on ChemiDoc using Stain-free fluorescent dye (Bio-Rad Laboratories). For analyses of protein band intensities, western blot signals were quantified using Bio-Rad Image Lab 5.2.1 software and values normalized to the Stain-free signal for each lane.

2.11 RNA isolation and RT-QPCR

Total RNA was isolated from cells using RNeasy Plus Mini kit (Qiagen) according to manufacturer's protocol and 250 ng of RNA was used to synthesize cDNA using qScript cDNA SuperMix (Quanta) or Maxima H Minus Reverse Transcriptase (Thermo Fisher). Quantitative PCR amplification was performed using PerfeCTa SYBR Green PCR master mix (Quanta) and specific primers listed below on Cielo 3 QPCR unit (Azure). Primers used: 18S - Left: cgttcttagttggtggagcg, Right: ccggacatctaagggcatca; ACTB - Left: catccgcaaagacctgtacg, Right: cctgcttgctgatccacatc; G3BP1 - Left: ggtcttaggcgtgtaccctg, Right: tatcgggaggaccctcagtg; G3BP2 - Left: gcctgttaatgctgggaacac, Right: tgttgctcctctgttcagat; GADD34 - Left: ctcaagcggcccagaaac, Right: ggaaatggacagtaccttc; GAPDH - Left: gagtcaacggatttggtcgt, Right: ttgattttggagggatctcg; OC43-N - Left: ggaccaagtagcgatgagg, Right: gtgcgcgaagtagatctgga; TIAR - Left: tggaaatgcagaagaccgag, Right: tgcactccctagctctgaca. Relative target levels were determined using $\Delta\Delta C_t$ method with normalization to 18S.

2.12 Statistical analyses

All numerical values are plotted as means (bar graphs) and display individual datapoints representing independent biological replicates (separate experiments performed on different days); the error bars represent standard deviations. Statistical analyses for each data set are described in figure legends and were performed using GraphPad Prism 8 software.

CHAPTER 3: RESULTS

3.1 Coronavirus OC43 inhibits stress granule formation.

To begin, I infected HEK293A (293A) cells with OC43 at an MOI of 1 and analyzed SG formation using SG marker TIAR. At various hpi, little to no SG formation was observed in infected cells (Figure 3.1A). In fact, the only timepoint where SG formation was observed in response to viral infection was at 24 hpi and SG formation occurred in less than 5% of cells (Figure 3.1A). Because so few SGs were observed in infected cells, I analyzed if OC43 actively inhibited SG formation. To test this, I used sodium arsenite (As) treatment; As is a potent SG-inducing agent which causes SG formation through activation of HRI and subsequent phosphorylation of eIF2 α (N. Kedersha et al., 2002; N. L. Kedersha et al., 1999). The 293A cells were infected with OC43 and treated with As for 50 m prior to fixation at 24 hpi. At 24 hpi and 50 m-post As treatment, cells were stained for N, to analyze the level of viral infection, and TIAR, to observe SG formation. Approximately 100% of mock cells treated with As formed SGs as expected (Figure 3.1B,C); however, only 30% of infected cells treated with As formed SGs (Figure 3.1B,C). In fact, OC43-infected cells had increased TIAR localization to the nucleus, away from the cytoplasm where SGs form (Figure 3.1B). This observation suggests that OC43 infection limits the formation of SGs, not only induced through viral infection but also SGs induced through exogenous stressors like As.

To verify that this phenotype was not only limited to 293A cells, I tested the level of SG formation in OC43-infected cells in two additional cell lines: BEAS-2B cells and HCT-8 cells. BEAS-2B cells are immortalized primary human upper airway epithelial cells which closely represent a cell type infected by CoVs *in vivo*. HCT-8 cells are a human colon cell line which are commonly used to grow OC43 virus, therefore they would be permissive to OC43 infection. Similar to 293A cells, BEAS-2B and HCT-8 cells were infected with OC43, treated with As, and SG formation was analyzed at 24 hpi. For BEAS-2B cells, nearly 100% of mock-As treated cells formed SGs while only 45% of infected cells formed SGs (Figure 3.1D,E), indicating that OC43 limits SG formation in BEAS-2B cells as well. In contrast, there was little SG inhibition by OC43 in HCT-8 cells at 24 hpi, where infected cells treated with As formed SGs to a similar

level as mock cells treated with As (Figure 3.1F,G). However, I also observed a lower level of infection in HCT-8 cells at 24 hpi compared to 293A cells or BEAS-2B cells at this timepoint (Figure 3.1B,D,F - OC43 only). Fewer infected HCT-8 cells at 24 hpi may be due to differential replication kinetics in this cell line compared to 293A or BEAS-2B cells. Thus, I questioned if SG formation would be inhibited by OC43 at later timepoints in HCT-8 cells. At 48 hpi, the level of OC43 infected HCT-8 cells was similar to that of infected 293A or BEAS-2B cells at 24 hpi. Additionally, at 48 hpi, OC43 also significantly limited SG formation (Figure 3.1H,I). Therefore, OC43 suppresses As-induced SG formation and this phenotype is not limited to a specific cell type.

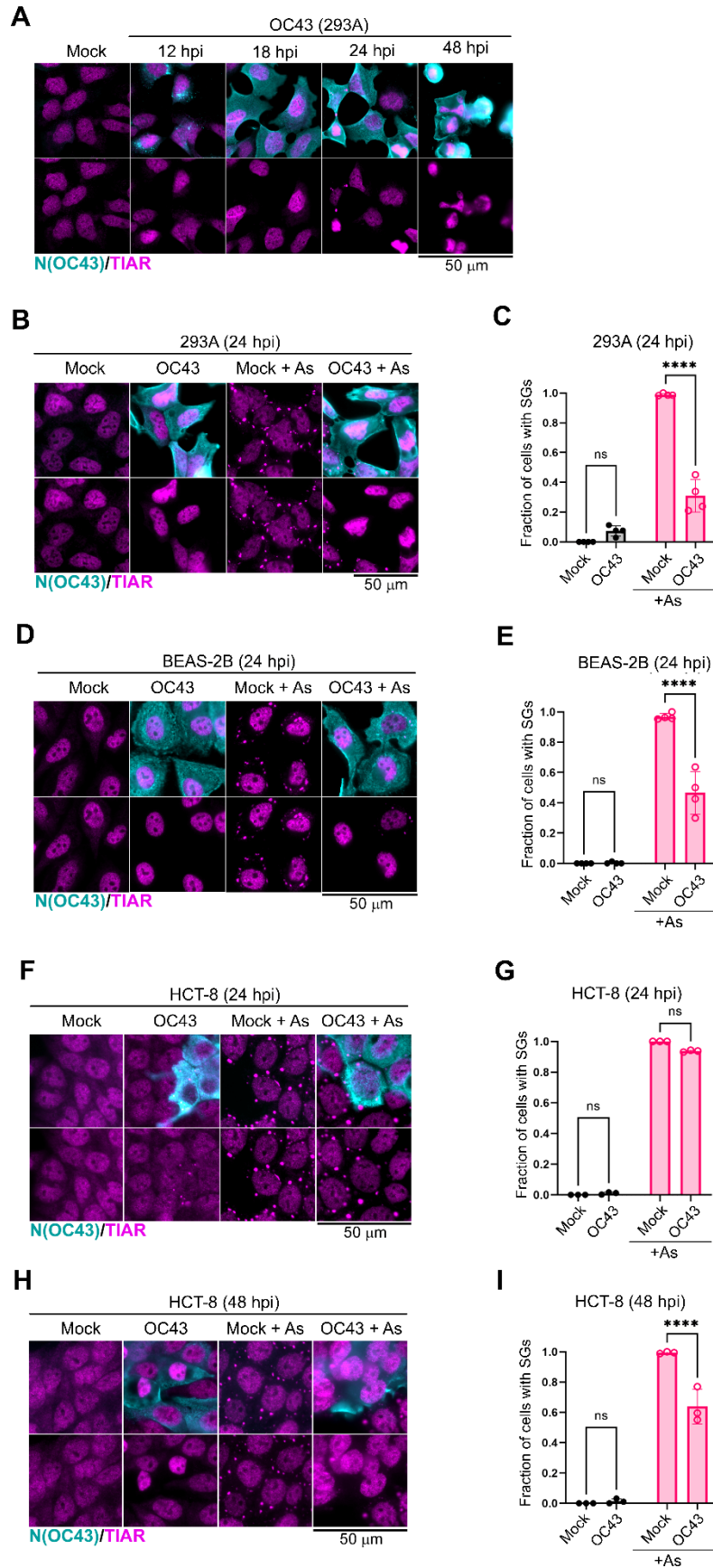


Figure 3.1 Coronavirus OC43 inhibits stress granule formation. Cells were infected with OC43 at multiplicity of infection (MOI) = 1.0 and SG formation in infected cells was analyzed at the indicated times post-infection using immunofluorescence staining for nucleoprotein (N(OC43), teal) and SG marker TIAR (magenta). hpi = hours post-infection. Scale bars = 50 μ m. (A) Immunofluorescence analysis of infected 293A cells at different times post-infection. (B,D,F,H) Immunofluorescence analysis of SG formation in mock infected and OC43-infected 293A (B), BEAS-2B (D), and HCT-8 (F,H) cells treated with sodium arsenite (+ As) or untreated infected cells at indicated times post-infection. (C,E,G,I) Fraction of cells with SGs was quantified in mock and OC43-infected cells at the indicated times post-infection. Two-way ANOVA and Tukey multiple comparisons tests were done to determine statistical significance (****, p -value < 0.0001, ns = non-significant). On all plots each data point represents independent biological replicate ($N \geq 3$). Error bars = standard deviation.

3.2 Coronavirus OC43 limits eIF2 α phosphorylation.

Because OC43 could limit SG formation induced through As treatment, I next examined the levels of eIF2 α phosphorylation during infection. As treatment induces the production of reactive oxygen species (ROS) which causes oxidative stress, activating the eIF2 α kinase HRI and resulting in the phosphorylation of eIF2 α and subsequent SG formation (N. Kedersha et al., 2002; N. L. Kedersha et al., 1999). Thus, I infected 293A cells with OC43 at an MOI of 1 and treated with As for 50 m prior to lysis at 24 hpi to analyze eIF2 α phosphorylation by western blot. As expected, As treatment increased the level of phosphorylated eIF2 α (Figure 3.2A Lane 2). Interestingly, OC43 infection decreased the level of eIF2 α phosphorylation in As-treated infected cells at 12 hpi, with further decreases in the level of eIF2 α phosphorylation at later timepoints (Figure 3.2A). Quantification of eIF2 α phosphorylation at 24 hpi in infected cells, showed a significant reduction when compared to mock cells treated with As (Figure 3.2B). In addition, there was a reduction in G3BP1 protein levels at later times post-infection (Figure 3.2A); G3BP1 is a SG-nucleating protein and significantly influences SG formation (N. Kedersha et al., 2016b; Tourrière et al., 2003).

Because I observed similar levels of SG inhibition by OC43 in 293A, BEAS-2B, and HCT-8 cells, I wondered if OC43 could limit eIF2 α phosphorylation in these additional cell lines as well. Thus, I examined eIF2 α phosphorylation in BEAS-2B and HCT-8 cells infected with OC43 and treated with As. For BEAS-2B cells, western blot analysis showed little eIF2 α phosphorylation in OC43-infected and As-treated cells (Figure 3.2C), and quantification of the level of eIF2 α phosphorylation at 24 hpi showed a significant decrease of phosphorylated eIF2 α in infected cells (Figure 3.2D). For HCT-8 cells, there was little difference to the level of eIF2 α phosphorylation in mock cells or infected cells treated with As at 24 hpi (Figure 3.2F). However, analysis of the level of phosphorylated eIF2 α at 48 hpi in HCT-8 cells showed a significant decrease in infected cells treated with As compared to mock-As treated cells (Figure 3.2G). Thus, not only does OC43 limit SG formation in various cells lines, this inhibition of SG formation coincides with significant decreases in the level of eIF2 α phosphorylation in infected cells. These results

suggest that OC43 may limit eIF2 α phosphorylation which results in the decreased level of SG formation observed during OC43 infection.

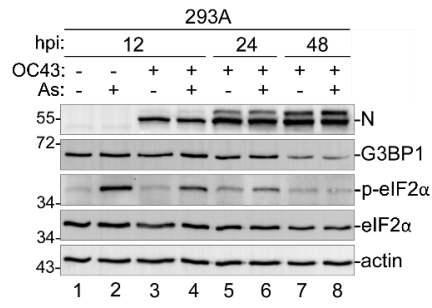
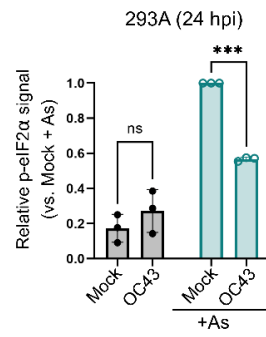
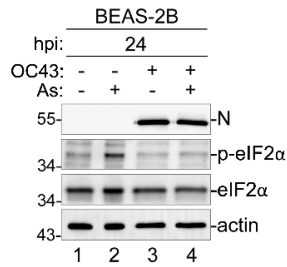
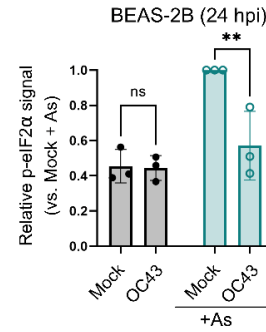
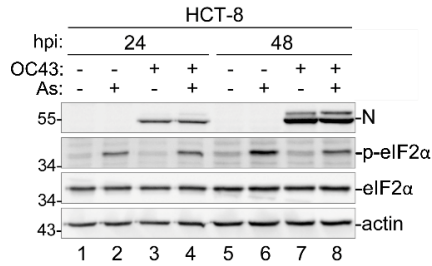
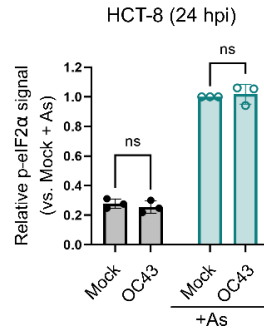
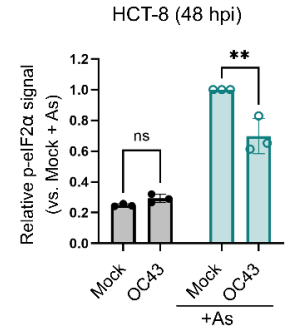
A**B****C****D****E****F****G**

Figure 3.2 Coronavirus OC43 limits eIF2 α phosphorylation. Cells were infected with OC43 at multiplicity of infection (MOI) = 1.0 and levels of N protein accumulation and phosphorylation of eIF2 α were analysed by western blot. hpi = hours post-infection. (A,C,E) Western blot analysis of As-induced eIF2 α phosphorylation and accumulation of N protein in 293A (A), BEAS-2B (C), and HCT-8 (E) cells at the indicated times post-infection. Levels of SG nucleating protein G3BP1 were also analyzed in (C). Actin was used as loading control. (B,D,F,G) Relative p-eIF2 α level (normalized to total eIF2 α or actin) was quantified in mock and OC43-infected cells at the indicated times post-infection. Two-way ANOVA and Tukey multiple comparisons tests were done to determine statistical significance (***, p -value < 0.001, **, p-value <0.01, ns = non-significant). On all plots each data point represents independent biological replicate (N \geq 3). Error bars = standard deviation.

3.3 Coronavirus OC43 limits eIF2 α phosphorylation irrespective of the activated eIF2 α kinase.

Previous results suggest that OC43 limits eIF2 α phosphorylation caused by HRI activation (Figure 3.2); however, there are three additional eIF2 α kinases that are able to phosphorylate eIF2 α (N. Kedersha et al., 2002, 2013). To investigate if the limited levels of phosphorylated eIF2 α observed in infected cells were dependent on the activation of a specific eIF2 α kinase, I analyzed the level of eIF2 α phosphorylation in infected cells treated with various agents that cause phosphorylation of eIF2 α through the activation of the other three eIF2 α kinases. Specifically, 293A cells were infected with OC43 at an MOI of 1 and were left untreated, or were treated with thapsigargin (Tg) which causes ER stress through disruption of calcium homeostasis and activates PERK (Harding et al., 1999), transfected with Polyinosinic:polycytidylic acid (poly I:C) which is a dsRNA mimic that activates PKR (García et al., 2007b), or treated with ultraviolet (UV) light which activates GCN2 (P. Zhang et al., 2002). At 24 hpi and post-treatment or transfection, cells were lysed for western blot analysis. While I did not have access to a functional phospho-PERK or total PERK antibody, I was able to examine the level of activated and total GCN2 and PKR. As expected, poly I:C transfection activated PKR, shown by the increase in phosphorylated PKR (Figure 3.3 Lane 5&6), and UV light activated GCN2, shown by the increase in phosphorylated GCN2 (Figure 3.3 Lane 7&8). Interestingly, regardless of the treatment used to activate the different eIF2 α kinases, OC43 infection still decreased the level of phosphorylated eIF2 α (Figure 3.3). These results suggest that OC43 does not limit the phosphorylation of eIF2 α through interfering with the activation of eIF2 α kinases. Instead, OC43 may promote dephosphorylation of eIF2 α in order to limit the level of phosphorylated eIF2 α in the cell during infection.

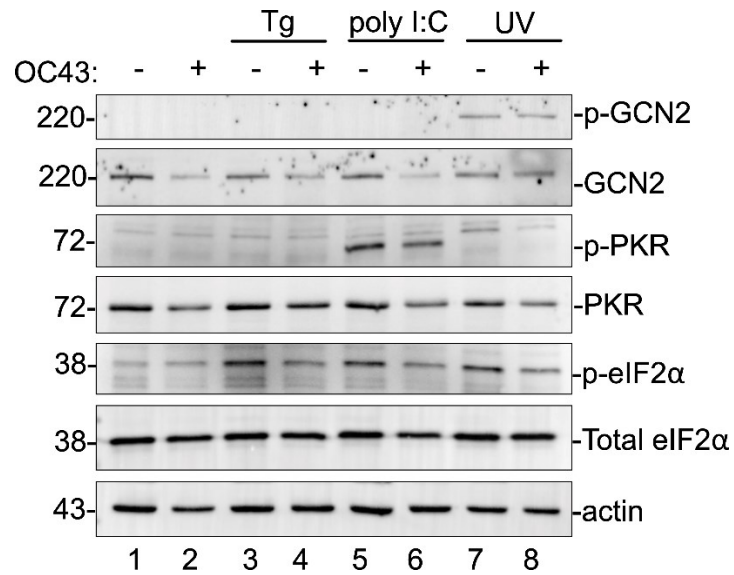


Figure 3.3 Coronavirus OC43 limits eIF2 α phosphorylation irrespective of the activated eIF2 α kinase. Cells were infected with OC43 at multiplicity of infection (MOI) = 1.0 and were left untreated (NT) or treated with thapsigargin (Tg) (1 μ M) for 1 h, transfected with Polyinosinic:polycytidylic acid (Poly I:C) (1 μ g) for 2 h, or treated with ultraviolet (UV) light (20 mJ/cm²) for 2 h. Phosphorylation of GCN2, PKR, and eIF2 α were analysed by western blot at 24 hpi. Actin was used as loading control. N = 2.

3.4 Coronavirus OC43 upregulates GADD34 RNA levels.

To test if OC43 promotes the dephosphorylation of eIF2 α , I first analyzed mRNA transcript levels of GADD34 during infection. The possible induction of GADD34 by OC43 could account for the decreased levels of phosphorylated eIF2 α observed during infection (Figure 3.2,3.3), given that GADD34 is reported to dephosphorylate eIF2 α (Harding et al., 2003). The 293A cells were infected with OC43 at an MOI of 1 and left untreated or were treated with Tg for 1 h or 4 h, and were lysed at 24 hpi for western blot or RT-qPCR analysis. Treatment of Tg for 1 h is known to phosphorylate eIF2 α , while 4 h treatment of Tg is known to induce GADD34 to a level that decreases eIF2 α phosphorylation (Novoa et al., 2003). This phenotype was confirmed by western blot analysis of Tg-treated samples. In mock cells, 1 h Tg treatment increased the level of eIF2 α phosphorylation (Figure 3.4A compare Lanes 1 & 3), while 4 h Tg treatment had low levels of phosphorylated eIF2 α similar to mock untreated cells (Figure 3.4A compare Lanes 1 & 5). Additionally, OC43 infection was again shown to limit eIF2 α phosphorylation in 1 h Tg-treated cells (Figure 3.4A compare Lanes 3 & 4). At this time, I did not have access to a functional GADD34 antibody to examine GADD34 protein levels during infection. Thus, I analyzed GADD34 RNA levels during infection. As expected, the RT-qPCR analysis showed a mild increase in GADD34 RNA levels in mock cells treated with Tg for 1 h while 4 h treatment revealed an over four-fold increase in GADD34 RNA levels relative to untreated mock cells (Figure 3.4A). In infected cells, I observed an even greater increase in GADD34 RNA levels (Figure 3.4A). RNA levels of ACTB (β -Actin) and GAPDH were also measured as a control. In fact, ACTB and GAPDH RNA levels were generally decreased in infected cells (Figure 3.4B,C). Given that RNA levels of household genes are generally decreased during infection, while GADD34 RNA levels are significantly increased, it is possible that OC43 upregulates GADD34 to dephosphorylate eIF2 α , resume translation, and promote viral protein production.

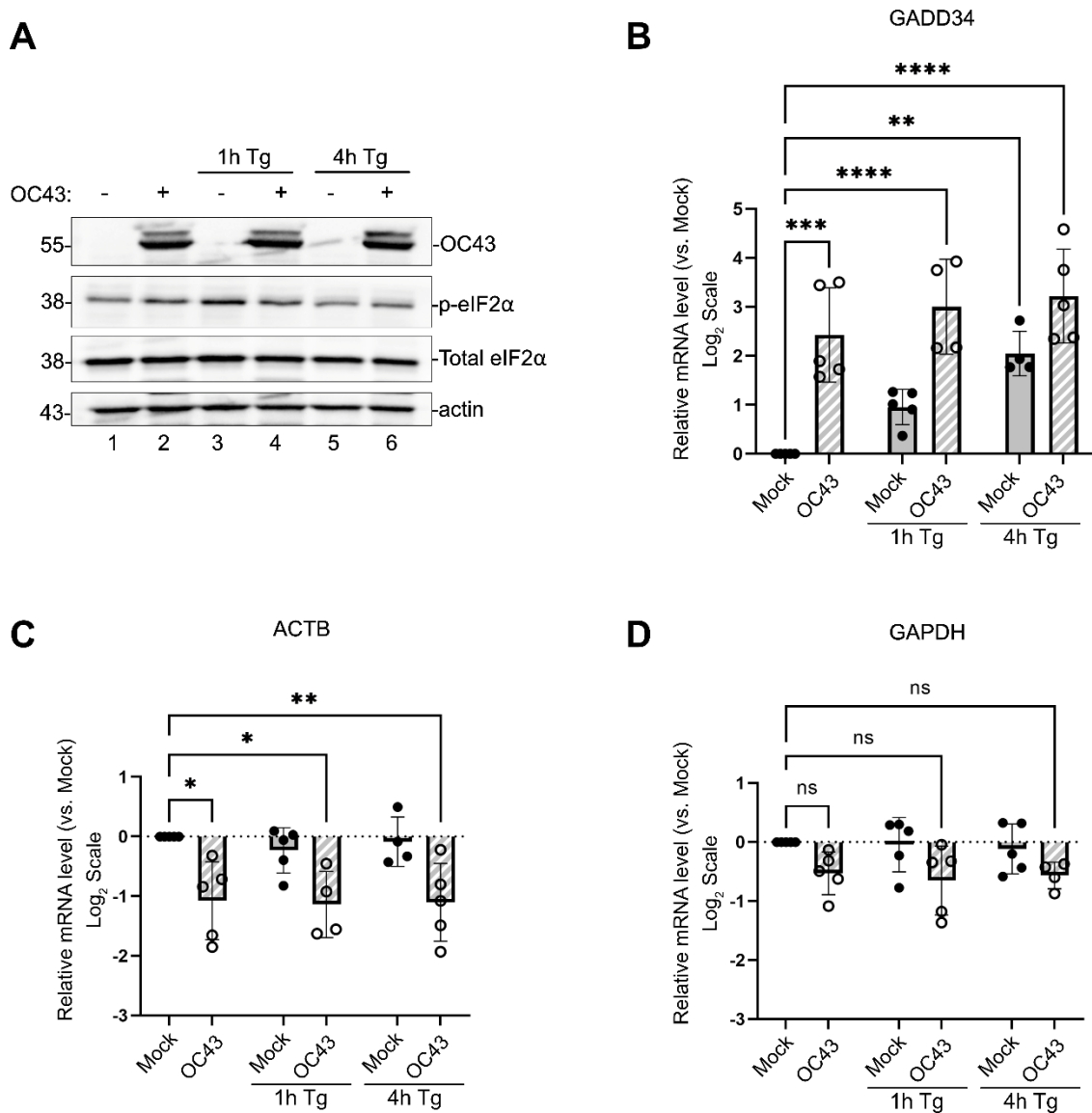


Figure 3.4 Coronavirus OC43 upregulates GADD34 RNA levels. The 293A cells infected with OC43 at MOI = 1.0 and untreated (NT) or treated with thapsigargin (Tg) (1 μ M) for 1 h or 4 h and mRNA levels were determined by RT-qPCR and level of eIF2 α phosphorylation was determined by western blot. (A) Western blot analysis of mock or infected cells untreated or treated with Tg for 1 h or 4 h (N = 1). Relative (B) GADD34, (C) ACTB (β -Actin), and (D) GAPDH mRNA levels. Values were normalized to 18S. Each data point represents independent biological replicate (N \geq 3). Error bars = standard deviation. Two-way ANOVA and Dunnett's multiple comparisons tests were done to determine statistical significance (****, p-value < 0.0001, ***, p-value < 0.001; **, p-value < 0.01; *, p-value < 0.05).

3.5 Coronavirus OC43 upregulates GADD34 independently from downstream activation of the integrated stress response.

Given that OC43 significantly upregulated GADD34 RNA levels, I next tested if OC43 could promote uORF skipping independently from prior phosphorylation of eIF2 α . To test this, I used a small molecule inhibitor of the integrated stress response (ISR), ISRIB (Rabouw et al., 2019; Sidrauski et al., 2015). During the ISR when eIF2 α is phosphorylated, it prevents eIF2B from exchanging GDP for GTP which limits the recycling of the ternary complex, inhibiting translation initiation (Jackson et al., 2010). The lack of active ternary complexes increases leaky scanning, or uORF bypass, of the 48S ribosomal subunit which in turn promotes translation of downstream ORFs (Jackson et al., 2010). ISRIB prevents translation shutdown by eIF2 α phosphorylation through binding to eIF2B and increasing the guanine exchange factor activity of eIF2B, allowing translation to continue despite the presence of phosphorylated eIF2 α (Rabouw et al., 2019; Zyryanova et al., 2018). This in turn prevents synthesis of transcription factor ATF4, because translation of this downstream ORF increases when global translation initiation is inhibited (Rabouw et al., 2019; Sidrauski et al., 2015). ATF4 is the main transcriptional inducer of GADD34, thus GADD34 is not induced during ISRIB treatment (Sidrauski et al., 2015). To confirm ISRIB treatment works in this experimental system, 293A cells were treated with Tg and ISRIB for 1 h or 4 h. Tg treatment for 1 h increased eIF2 α phosphorylation and this increase was unaffected by ISRIB treatment (see Appendix). However, ISRIB treatment did inhibit induction of GADD34 by 4 h Tg treatment which correlated with sustained eIF2 α phosphorylation, confirming that ISRIB works as expected in this experimental system (see Appendix).

After the initial testing of ISRIB, I wanted to analyze if ISRIB treatment would affect upregulation of GADD34 by OC43. The 293A cells were infected with OC43 at an MOI of 1. At 1 hpi, cells were treated with ISRIB and 50 m prior to lysis at 24 hpi (23 h post ISRIB treatment), cells were also treated with As to induce eIF2 α phosphorylation and SG formation. Because ISRIB treatment resumes translation, SG formation is also limited because many translation initiation factors are depleted from SGs as they are redirected to active sites of translation. Immunofluorescence analysis of As-treated cells

treated with ISRIB showed a significant decrease in SG formation (Figure 3.5A/B compare NT v. ISRIB of Mock + As cells). For OC43 infected cells, I again observed a significant decrease in the level of SG formation compared to mock cells treated with As (Figure 3.5A/B compare NT of Mock + As v. NT of OC43 + As cells). In fact, the level of SG formation was similar between As-treated cells treated with ISRIB and As-treated infected cells (Figure 3.5A/B compare ISRIB of Mock + As v. NT of OC43 + As cells). When infected cells were treated with ISRIB and As, there was an even further decrease in the fraction of infected cells forming SGs (Figure 3.5A/B compare NT of Mock + As v. ISRIB of OC43 + As cells). These observations suggest that ISRIB treatment does not affect OC43's ability to limit SG formation. To uncover if ISRIB treatment affects OC43-mediated dephosphorylation of eIF2 α and upregulation of GADD34, samples were also analyzed by western blot and RT-qPCR. As observed previously, OC43 significantly limited As-induced eIF2 α phosphorylation at 24 hpi (Figure 3.5C/D compare Lanes 3 & 4). With ISRIB treatment, OC43 still limited eIF2 α phosphorylation (Figure 3.5C compare lanes 7 & 8); comparisons of NT and ISRIB -treated infected cells treated with As showed nearly an identical level of phosphorylated eIF2 α (Figure 3.5D). Further, and observed previously, OC43 significantly upregulated GADD34 RNA levels, and ISRIB treatment did not affect this upregulation (Figure 3.5E). Also, ISRIB treatment did not significantly affect OC43 RNA levels, as detected by the transcript levels of N. (Figure 3.5F). These results indicate that OC43 does not require activation of the ISR to upregulate GADD34 and promote eIF2 α dephosphorylation, suggesting that OC43 can promote GADD34 expression through another mechanism.

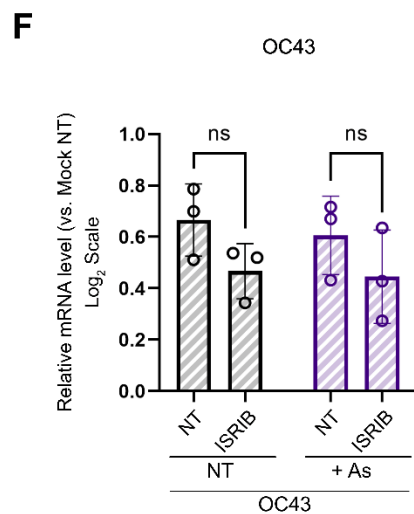
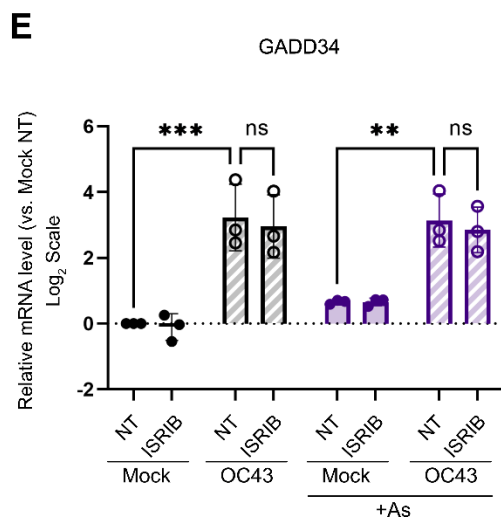
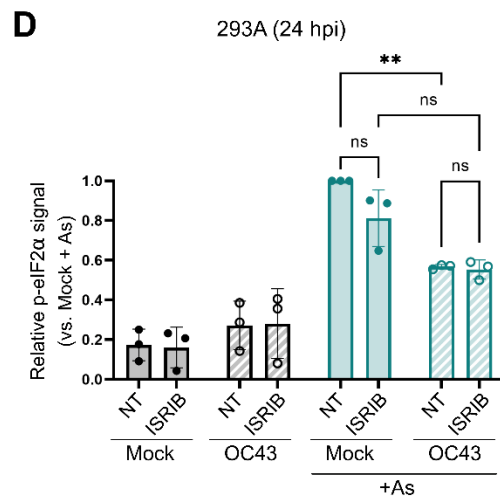
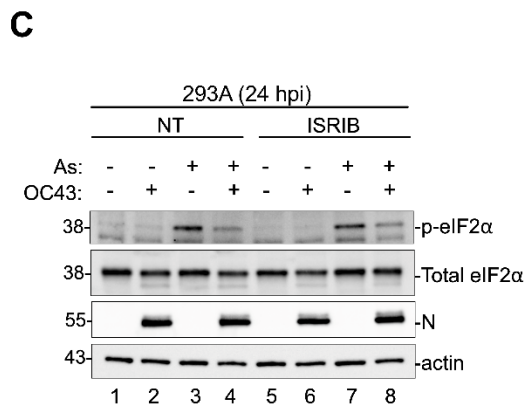
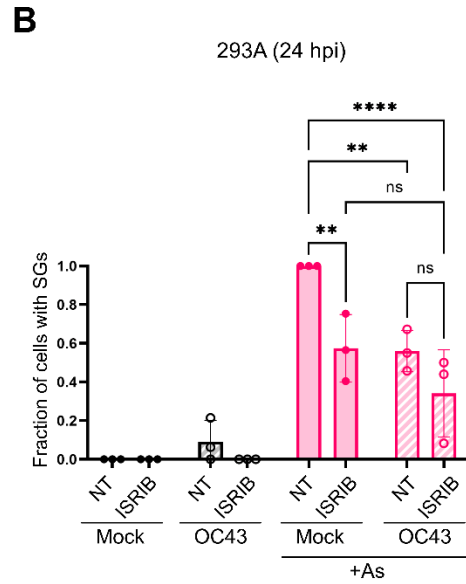
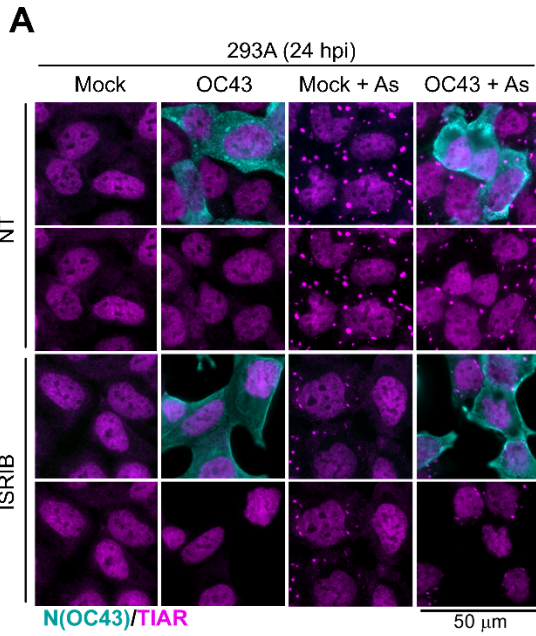


Figure 3.5 Coronavirus OC43 upregulates GADD34 independently from downstream activation of the integrated stress response. The 293A cells were infected with OC43 at MOI = 1.0, untreated (NT) or treated with ISRIB for 23h, and untreated (NT) or treated with Arsenite (As) for 50 min. SG formation in infected cells was analyzed using immunofluorescence staining for nucleoprotein (N(OC43), teal) and SG marker TIAR (magenta). Phosphorylation of eIF2 α was analysed by western blot and transcript levels were measured by RT-QPCR. (A) Immunofluorescence analysis of SG formation in mock infected and OC43-infected cells treated with ISRIB and/or sodium arsenite (+ As) or untreated infected cells. (B) Fraction of cells with SGs was quantified in mock and OC43-infected cells. (C) Western blot analysis of As-induced eIF2 α phosphorylation and accumulation of N protein in 293A cells. Actin was used as a loading control. (D) Relative level of eIF2 α phosphorylation (normalized to total eIF2 α), quantified from C. (E) RT-QPCR of GADD34 and ACTB (β -Actin). For all plots, each data point represents independent biological replicate (N=3). Error bars = standard deviation. Two-way ANOVA and Tukey multiple comparisons tests were done to determine statistical significance (**, p -value < 0.01, ***, p -value < 0.001, ****, p -value < 0.0001, ns, non-significant).

3.6 Upregulation of GADD34 by OC43 is not required for dephosphorylation of eIF2 α .

Next, I aimed to confirm if this upregulation of GADD34 by OC43 was required for the diminished levels of eIF2 α phosphorylation observed during infection. To test this, I transfected 293A cells with one of two distinct siRNAs targeting GADD34 (siGADD34#1 or siGADD34#2) as well as a non-targeting (siNT) siRNA as a control. Then, 24 h post transfection (hpt), I infected these cells with OC43 at an MOI of 1 and treated with As for 50 m prior to lysis at 24 hpi/48 hpt. Western blot analysis confirmed knockdown of GADD34 as there was little to no GADD34 protein expression in siGADD34#1 or siGADD34#2 -transfected samples (Figure 3.6A, compare upper and lower panels Lanes 5-8). In addition, I detected an increase in GADD34 protein expression in infected samples that were transfected with siNT control compared to mock samples (Figure 3.6A, compare upper and lower panels Lanes 2 & 4). This observation directly reflects the increase of GADD34 RNA levels previously observed during OC43 infection at 24 hpi (Figure 3.4A, 3.5E). As for the level of eIF2 α phosphorylation, I observed that OC43 limits the level of As-induced eIF2 α phosphorylation in siNT-transfected cells (Figure 3.6A, compare upper and lower panels Lanes 3 & 4; Figure 3.5B). In GADD34 knockdown samples, the level of eIF2 α phosphorylation in OC43-infected and As-treated cells was still significantly decreased compared to mock and As-treated cells (Figure 3.6A, compare upper and lower panels Lanes 7 & 8; Figure 3.6B). In fact, there was no significant difference between the level of phosphorylated eIF2 α in infected, As-treated cells transfected with siNT or either siGADD34 (Figure 3.6B). This result suggests that the upregulation of GADD34 by OC43 is not required for the diminished level of eIF2 α phosphorylation observed during infection. Additionally, RT-qPCR analysis of these samples confirmed knockdown of GADD34 at the RNA level (Figure 3.6C GADD34) and there was no significant change to OC43 RNA levels, as detected by the transcript levels of N (Figure 3.6C OC43). Further, there was a significant decrease in viral titers with knockdown of GADD34 compared to siNT control (Figure 3.6D), suggesting that while upregulation of GADD34 is not required for OC43-mediated decrease of eIF2 α phosphorylation, it may be required for other viral processes during infection.

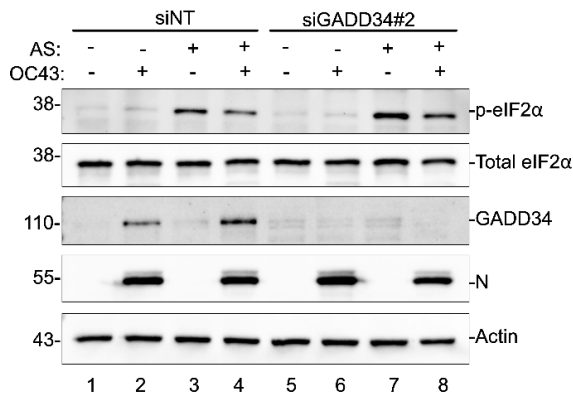
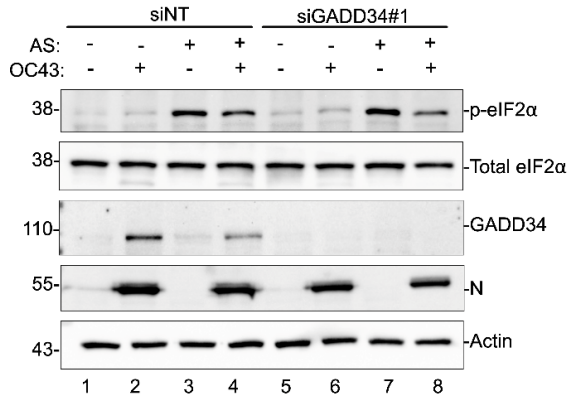
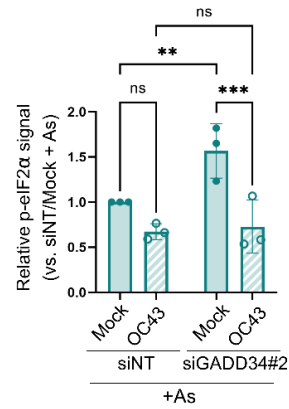
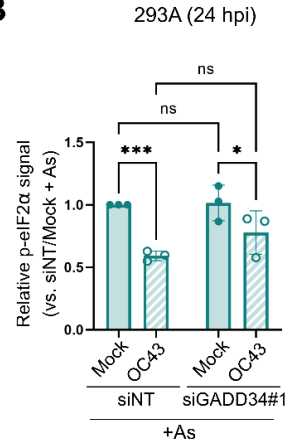
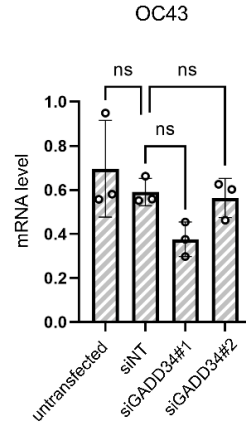
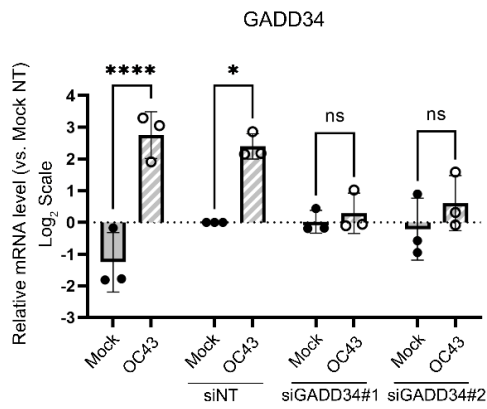
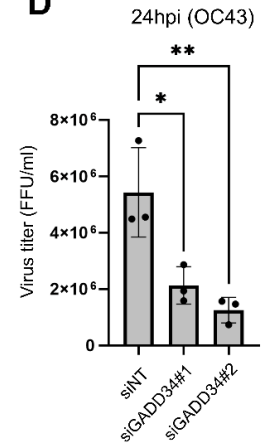
A**B****C****D**

Figure 3.6 Upregulation of GADD34 by OC43 is not required for dephosphorylation of eIF2 α . The 293A cells were infected with OC43 at MOI = 1.0 and phosphorylation of eIF2 α was analysed by western blot. Levels of GADD34 and N were analysed by western blot and RT-qPCR. Viral titers were measured by FFU/ml. hpi = hours post-infection.

(A) Western blot analysis of 293A cells transfected with siRNAs against GADD34, mock or infected with OC43, and untreated (NT) or treated with arsenite (As) at 48 hpt and 24 hpi for 50 min. (B) Relative level of eIF2 α phosphorylation compared to siNT/Mock + As (normalized to total eIF2 α), quantified from A. (C) RT-QPCR of GADD34 and OC43-N. For GADD34 RNA, two-way ANOVA and Tukey's multiple comparisons tests were done to determine statistical significance. For OC43 RNA, one-way ANOVA and Tukey's multiple comparisons test were completed to determine statistical significance. (D) Foci-forming units (FFU) calculated using immunofluorescence microscopy of OC43-N in 293As infected with harvested supernatants collected at the same time as (A-C). For virus titers, one-way ANOVA and Dunnett's multiple comparisons tests were done to determine statistical significance. For all plots, each data point represents independent biological replicate (N=3), (****, p -value < 0.0001, ***, p -value < 0.001; **, p-value <0.01; *, p-value < 0.05, ns, non-significant).

3.7 OC43 inhibits stress granule formation in the presence of 6-Thioguanine.

Previously, I observed that OC43 limits SG formation induced through As treatment and in the presence of ISRIB. In collaboration with other researchers, my lab recently identified 6-Thioguanine (6-TG) as a selective inducer of SG formation in IAV-infected cells, resulting in limited IAV replication (Slaine et al., 2021). Our corresponding preprint suggests 6-TG also limits OC43 infection, but it has yet to be confirmed if limited OC43 infection is related to SG induction, like IAV. Thus, I questioned if OC43 would still be able to limit SG formation in the presence of 6-TG or if 6-TG may induce SG formation in OC43-infected cells. The 293A cells were infected with OC43 at an MOI of 1 and were left untreated or were treated with 6-TG for 20 h, treated with 6-TG for 4 h, or treated with As for 50 m. At 24 hpi, cells were fixed for immunofluorescent microscopy and western blot. As previously observed, there was a significant decrease in As-induced SG formation and limited eIF2 α phosphorylation in infected cells (Figure 3.7A,B,D). Further, there was no significant induction of SG formation in infected cells treated with 6-TG (Figure 3.7A,B); however, longer 6-TG treatment for 20 h resulted in reduced number of infected cells (Figure 3.7A,C). Further research in this area revealed that 6-TG limits accumulation of CoV spike protein (Pringle et al., 2022), similar to how this compound affects IAV glycoprotein accumulation (Slaine et al., 2021). Notably, because there was no concurrent induction of SG formation in OC43-infected cells (Figure 3.7A), these results suggest that OC43 is still able to limit SG formation despite disruption of viral protein accumulation and activation of the ER stress response.

Figure 3.7 OC43 inhibits stress granule formation in the presence of 6-Thioguanine.

The 293A cells were infected with OC43 at MOI = 1.0, untreated (NT) or treated with 6-thioguanine (6-TG) for 20h, 6-TG for 4h, or Arsenite (As) for 50 min. SG formation in infected cells was analyzed using immunofluorescence staining for nucleoprotein (N(OC43), teal) and SG marker TIAR (magenta). Phosphorylation of eIF2 α was analysed by western blot. (A) Immunofluorescence analysis of SG formation in mock infected and OC43-infected cells treated with 6-TG and/or sodium arsenite (+ As) or untreated infected cells. (B) Fraction of cells with SGs was quantified in mock and OC43-infected cells. (C) Fraction of infected cells was quantified in infected cells treated with 6-TG (20h and 4h) and As. (D) Western blot analysis of As-induced eIF2 α phosphorylation, accumulation of N protein, and expression of endoplasmic reticulum stress marker Bip, and transcription factor ATF4. Actin was used as a loading control. For all plots, each data point represents independent biological replicate (N=3). Error bars = standard deviation. One-way ANOVA and Tukey (B) or Dunnett's (C) multiple comparisons tests were done to determine statistical significance (*, p -value < 0.05, ****, p -value < 0.0001, ns, non-significant).

3.8 Coronavirus OC43 inhibits stress granules independently of eIF2 α phosphorylation.

Thus far, I have uncovered that OC43 limits SG formation and eIF2 α phosphorylation, although I have yet to determine how OC43 limits eIF2 α phosphorylation. Instead of further investigating the mechanism of how OC43 limits eIF2 α phosphorylation during infection, I decided to focus on if limited eIF2 α phosphorylation is the only method for how OC43 suppresses SG formation. Specifically, I tested if OC43 could limit the formation of SGs that form independently from the phosphorylation of eIF2 α . Silvestrol (Sil.) is another SG-inducing agent which is reported to interfere with the function of translation initiation factor eIF4A (Mazroui et al., 2006; Slaine et al., 2017); eIF4A is an RNA helicase which promotes unwinding of the 5'UTR in order for the 48S subunit to scan along the RNA sequence (Jackson et al., 2010). Interference with eIF4A prevents translation initiation, irrespective of the phosphorylation status of eIF2 α , and leads to the aggregation of untranslated mRNPs and subsequent SG formation (Mazroui et al., 2006). Therefore, 293A cells were infected with OC43 at an MOI of 1 and at 23 hpi, cells were treated with Sil. for 1 h. At 24 hpi, cells were fixed for immunofluorescence microscopy to visualize SG formation by SG marker TIAR and cells were lysed for western blot analysis to measure the level of phosphorylated eIF2 α . Similar to the level of SG formation in As-treated mock cells (Figure 3.1B), nearly 100% of mock cells treated with Sil. formed SGs as expected (Figure 3.8A,B). However, only approximately 50% of infected cells treated with Sil. formed SGs (Figure 3.8A,B), suggesting that OC43 inhibits SGs that form independently from the phosphorylation of eIF2 α . This results also indicates that OC43 utilizes additional mechanisms, other than limiting levels of eIF2 α phosphorylation, to suppress SG formation. To confirm that Sil. treatment did not affect eIF2 α phosphorylation, I completed a western blot to analyze the level of phosphorylated eIF2 α . As observed previously, OC43 infection decreases the level of As-induced eIF2 α phosphorylation, but there was no increase in the level of phosphorylated eIF2 α in Sil. treated cells compared to mock untreated cells as expected (Figure 3.8C).

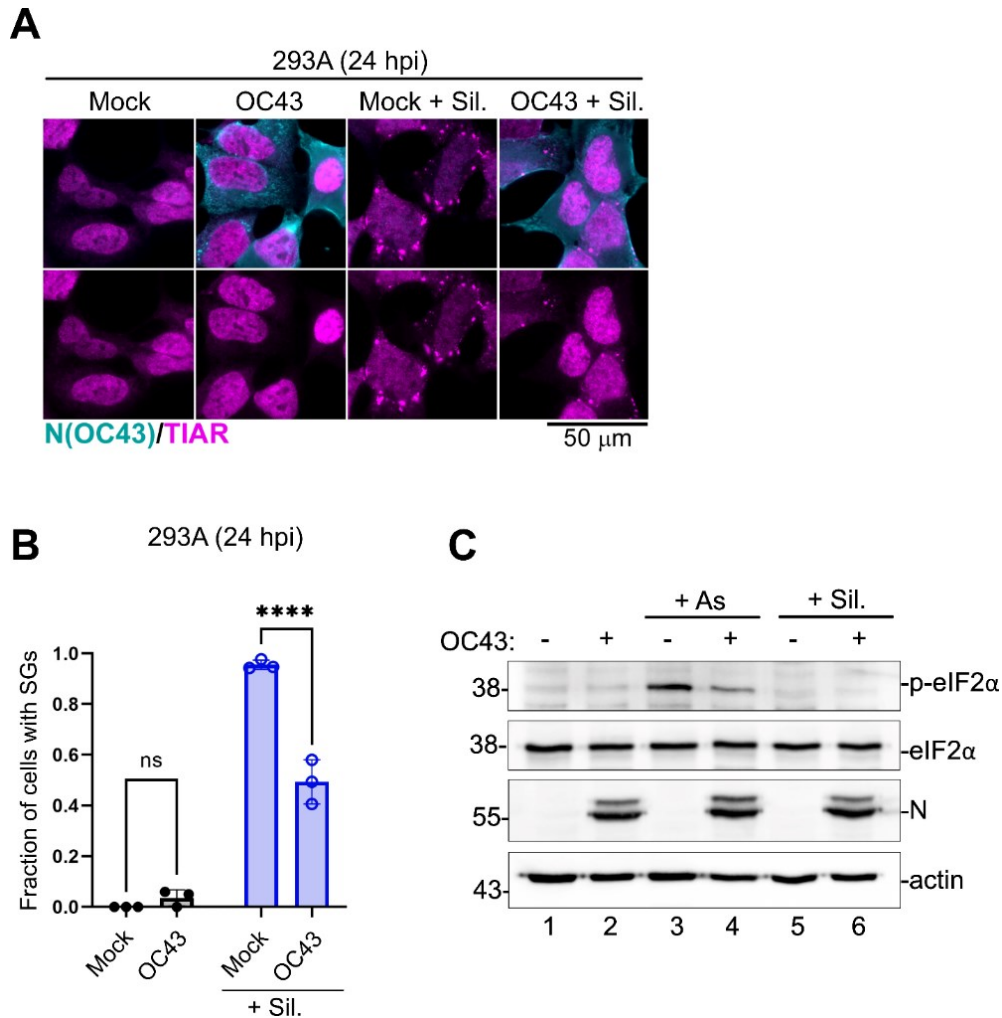


Figure 3.8 Coronavirus OC43 inhibits stress granules independently of eIF2 α phosphorylation. The 293A cells were infected with OC43 at MOI = 1.0 and treated with silvestrol (+ Sil.) for 1 h to induce SG formation. Cells were analyzed at 24 hours post-infection (hpi) using immunofluorescence staining for nucleoprotein and SG marker TIAR and western blotting to measure eIF2 α phosphorylation. (A) Immunofluorescence analysis of SG formation in mock infected and OC43-infected cells treated with silvestrol (+ Sil.) or untreated infected cells. (B) Phosphorylation of eIF2 α was analysed by western blot. (C) Fraction of cells with SGs was quantified in mock and OC43-infected 293A cells treated and stained as in panel (A). Each data point represents independent biological replicate (N=3). Error bars = standard deviation. Two-way ANOVA and Tukey multiple comparisons tests were done to determine statistical significance (****, p-value upper case or lo < 0.0001, ns = non-significant).

3.9 Coronavirus OC43 inhibits canonical stress granule formation.

An important consideration when examining SG formation is to confirm that the foci observed are canonical SGs. Thus far, the only SG marker that has been used is TIAR and during OC43 infection, I have observed an increased in nuclear localization of TIAR (Figure 3.1A,B, 3.7A, 3.8A). To confirm that OC43 infection was limiting SG formation and not redistributing TIAR away from SGs so they could not be visualized, I investigated SG formation in response to As or Sil. treatment through the use of five additional SG markers. These markers include eIF4G, G3BP1, TIA-1, G3BP2, and eIF3B; these are common SG components previously reported to localize to SGs induced by various stressors (Aulas et al., 2017). The 293A cells were infected with OC43 at an MOI of 1 and prior to fixation at 24 hpi, cells were treated with As for 50 m or Sil. for 1 h. Immunofluorescence microscopy revealed that irrespective of the SG marker used, there was an observable decrease in SG formation in OC43-infected cells compared to mock cells (Figure 3.9). Notably, this immunofluorescence analysis highlights the morphological differences in SGs formed by different stressors; in an As-treated cell, SGs are larger and less numerous while in a Sil-treated cell, the SGs appear smaller and are more numerous (Figure 3.9).

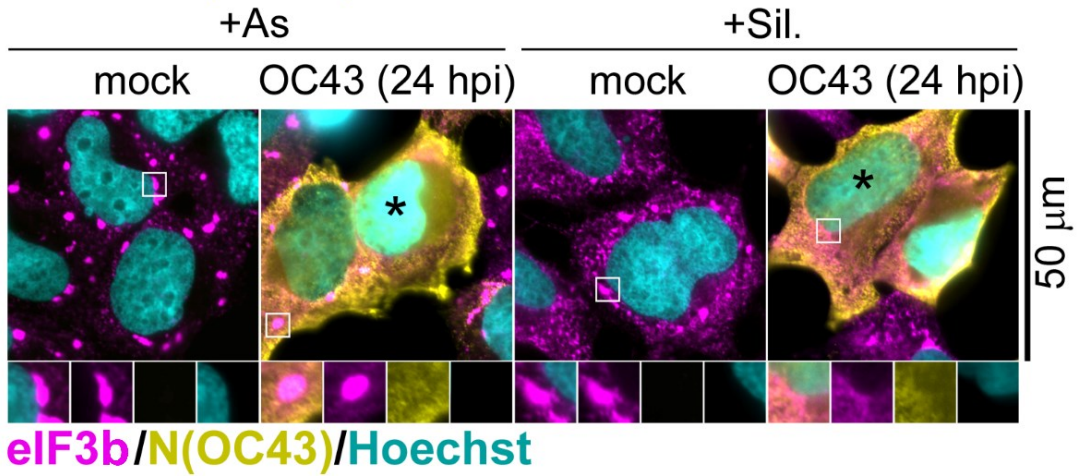
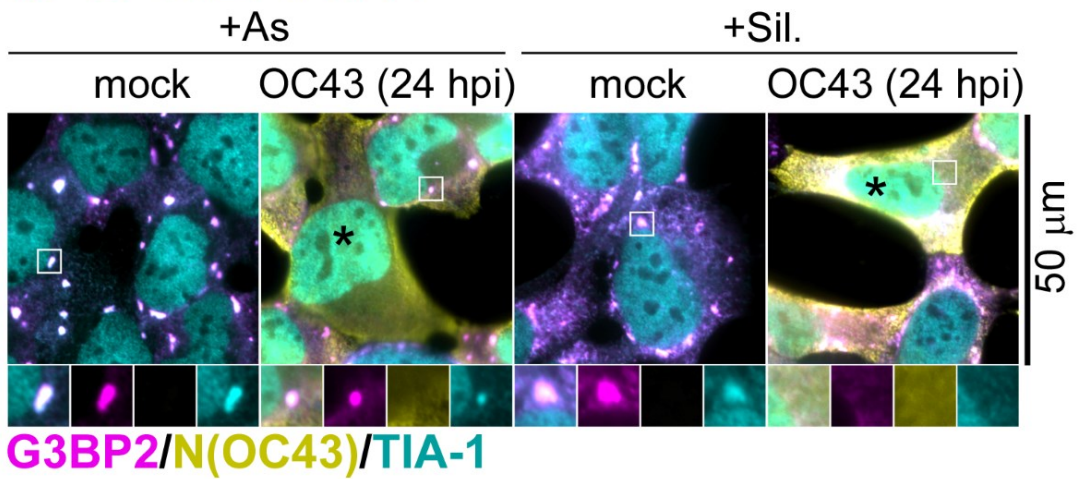
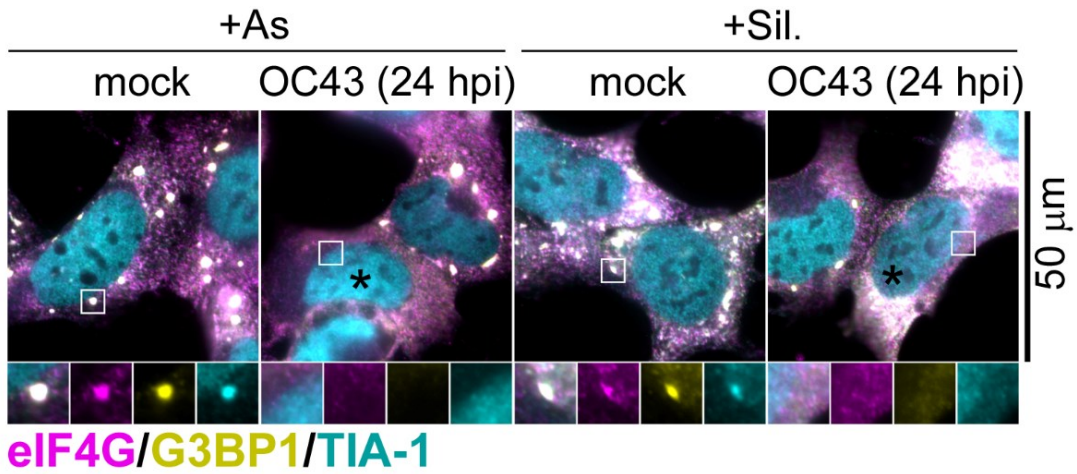


Figure 3.9 Coronavirus OC43 inhibits canonical stress granule formation. The 293A cells were infected with OC43 at MOI = 1.0 and SG formation in arsenite (+ As), Silvestrol (+ Sil.), and untreated mock and OC43 infected cells was analyzed at 24 hours post-infection (hpi) using immunofluorescence staining for nucleoprotein and the indicated SG markers. (D) Representative images of mock infected and OC43 infected cells immunostained for SG markers eIF4G (magenta), G3BP1 (yellow), TIA-1 (teal), G3BP2 (magenta), and eIF3b (magenta) as indicated. Subcellular distribution of nucleoprotein (N(OC43), yellow) was visualised by immunostaining and nuclear DNA was visualised with Hoechst dye (teal) where indicated. Black asterisks indicate infected cells that did not form SGs. Outsets show enlarged areas of cytoplasm, indicated by white squares, with separation of channels to better visualize co-localization of SGs markers. Scale bars = 50 μ m.

3.10 Coronavirus N proteins inhibit stress granule formation downstream of eIF2 α phosphorylation.

Having confirmed that OC43 inhibits the formation of canonical SGs induced through either As or Sil. treatment, I next analyzed which viral proteins potentially mediate this SG suppression. The nucleoprotein (N) was the first viral protein to examine, because it is a known RNA-binding protein and CoV2-N has recently been reported to bind G3BP1 (Gordon et al., 2020; Kruse et al., 2021; J. Li et al., 2021), a key SG protein. I generated EGFP-tagged N constructs for both OC43 and CoV2 to test if N contributes to SG suppression during OC43 infection and if this potential function of N is conserved in more pathogenic CoVs like CoV2. Then, 293A cells were transfected with either EGFP-N construct or EGFP control and 50 m prior to lysis or fixation at 24 hpt, transfected cells were treated with As. Western blot analysis revealed that ectopic overexpression of either EGFP-OC43-N or EGFP-CoV2-N did not significantly alter levels of eIF2 α phosphorylation, suggesting that N is not involved in the decreased level of eIF2 α phosphorylation observed during OC43 infection (Figure 3.10A,B). In contrast, overexpression of either EGFP-N construct resulted in a significant decrease in As-induced SGs (Figure 3.10C); however, the magnitude of SG inhibition differed between the two EGFP-N constructs. Specifically, EGFP-CoV2-N was a more potent SG inhibitor compared to EGFP-OC43-N, where 35% and 80% of transfected cells formed SGs, respectively (Figure 3.10D). While overexpression of EGFP-OC43-N only poorly limited As-induced SG formation, EGFP-OC43-N was more efficient at limiting the formation of SGs induced by Sil (Figure 3.10E,F). The 293A cells were transfected with EGFP-OC43-N, EGFP-CoV2-N, or EGFP control, treated with Sil for 1 h at 23 hpt, and at 24 hpt, cells were fixed for immunofluorescence microscopy. Only 40% of cells overexpressing EGFP-OC43-N formed SGs while 25% of cells overexpressing EGFP-CoV2-N formed SGs, relative to EGFP-expressing cells treated with Sil (Figure 3.10F). Thus, OC43-N is involved in the SG suppression observed during infection and this function of N is even more efficient for other CoVs, like CoV2.

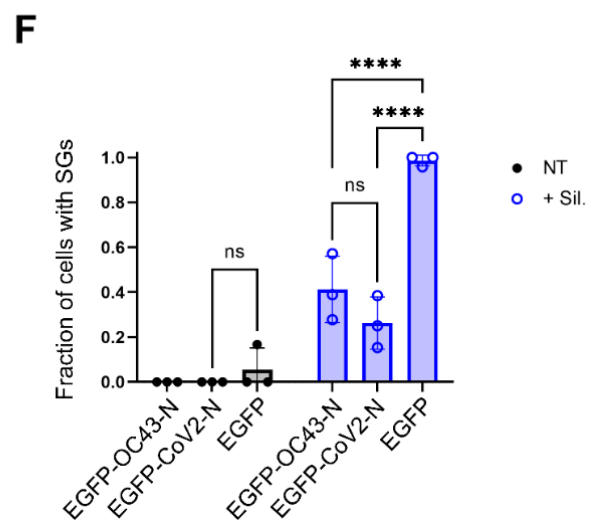
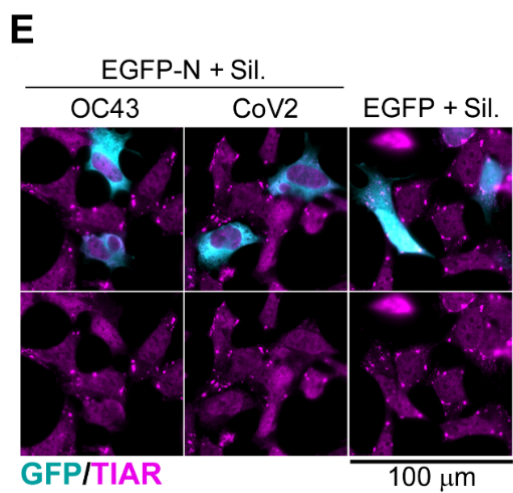
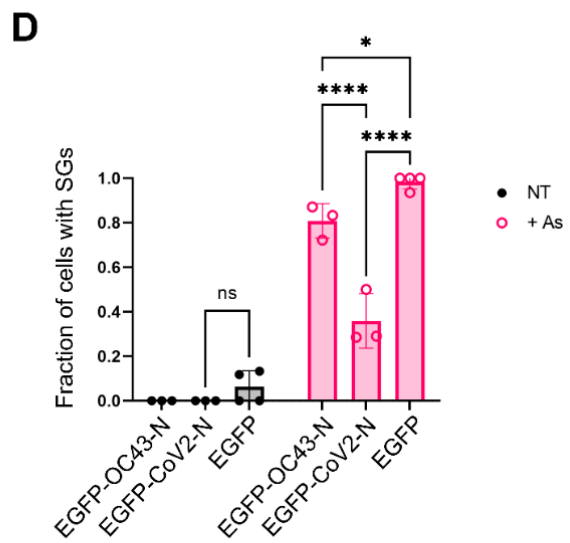
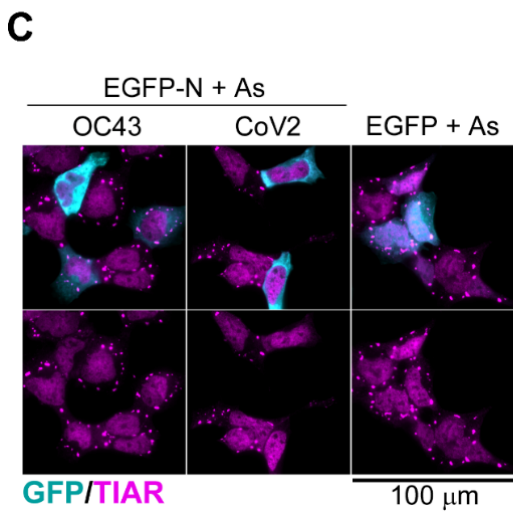
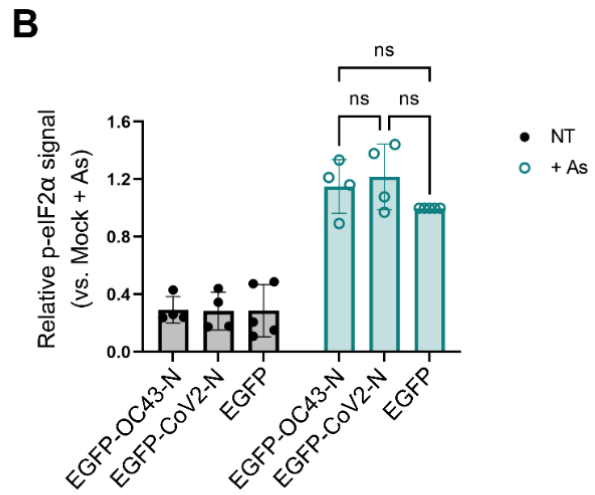
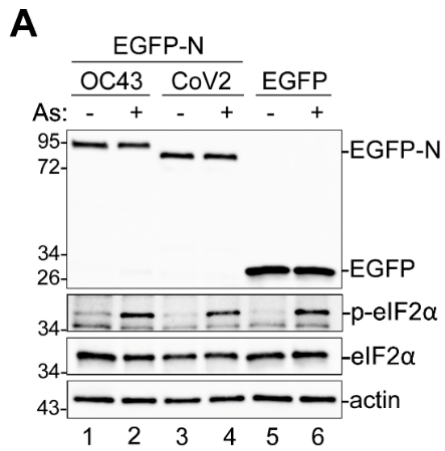


Figure 3.10 Coronavirus N proteins inhibit stress granule formation downstream of eIF2 α phosphorylation. The 293A cells were transiently transfected with the indicated EGFP-tagged viral protein expression constructs or EGFP control. At 24 h post-transfection cells were treated with sodium arsenite (+ As) or silvestrol (+ Sil.), as indicated, or left untreated. SG formation was analyzed by immunofluorescence microscopy with staining for SG marker TIAR (magenta). EGFP expression is shown in teal. Scale bars = 100 μ m. Levels of EGFP-tagged proteins and the As-induced phosphorylation of eIF2 α were analyzed by western blot. (A) Western blot analysis of cells transfected with EGFP-tagged OC43 or CoV2 nucleoprotein (EGFP-N) expression vectors or control EGFP-transfected cells. EGFP-positive cells were isolated using live cell sorting on BD FACSAria III instrument 24 hpt and were used for experiment 48h post sorting. (B) Relative level of eIF2 α phosphorylation (normalized to total eIF2 α), quantified from A. (C) Immunofluorescence microscopy of EGFP-N transfected, or control EGFP-transfected cells treated with As. (D) Fraction of transfected cells with As-induced SGs quantified from B. (E) Immunofluorescence microscopy of EGFP-N transfected or control EGFP-transfected cells treated with silvestrol. (F) Fraction of transfected cells with silvestrol-induced SGs quantified from D. On all plots each data point represents independent biological replicate ($N \geq 3$). Error bars = standard deviation. Two-way ANOVA and Tukey multiple comparisons tests were done to determine statistical significance (****, p -value < 0.0001, *, p-value < 0.05, ns, non-significant).

3.11 Coronavirus OC43 Nsp15 does not inhibit stress granule formation.

Next, I evaluated if viral protein Nsp15 would limit SG formation. Nsp15 is an endoribonuclease previously reported to limit activation of antiviral signalling pathways (Boodhoo et al., 2022). In addition, recent publications have shown that overexpression of Nsp15 from different CoVs, including IBV, TGEV, SARS, and CoV2, limited SG formation induced through As treatment (Gao et al., 2021). Thus, I speculated that Nsp15 from OC43 may also contribute to the limited SG formation observed during OC43 infection. I transfected 293A cells with EGFP-tagged OC43-Nsp15 (EGFP-Nsp15) or EGFP control and 50 m prior to lysis or fixation at 24 hpt, cells were treated with As for 50 m. Overexpression of EGFP-Nsp15 did not affect SG formation (Figure 3.11A); there was a slight, but non-significant, decrease in the level of SG formation in EGFP-Nsp15-expressing cells compared to EGFP control (Figure 3.11B). Lastly, I used western blotting to uncover if Nsp15 could limit the level of eIF2 α phosphorylation in transfected cells. There was no observable difference in the level of phosphorylated eIF2 α in cells overexpressing EGFP-Nsp15 compared to cells overexpressing EGFP (Figure 3.11C). While Nsp15 from other CoVs may limit As-induced SG formation, herein I conclude that OC43-Nsp15 does not inhibit SG formation.

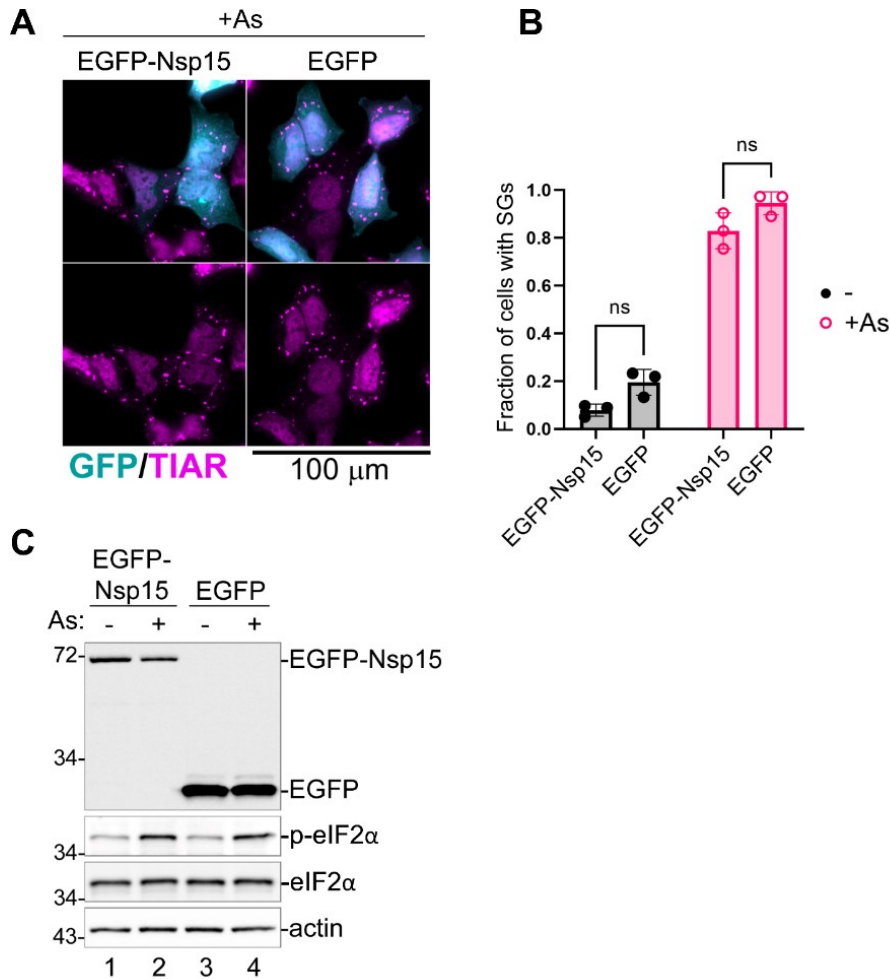


Figure 3.11 Coronavirus OC43 Nsp15 does not inhibit stress granule formation.

293A cells were transiently transfected with EGFP-OC43-nsp15 (EGFP-nsp15) or EGFP control. At 24 h post-transfection cells were treated with sodium arsenite (+ As) or left untreated. SG formation was analyzed by immunofluorescence microscopy with staining for SG marker TIAR (magenta). EGFP expression is shown in teal. Scale bars = 100 μ m. Levels of EGFP-tagged proteins and the As-induced phosphorylation of eIF2 α were analyzed by western blot. (A) Immunofluorescence microscopy of EGFP-Nsp15 transfected, or control EGFP-transfected cells treated with As. (B) Fraction of transfected cells with As-induced SGs quantified from G. Each data point represents independent biological replicate (N=3). Error bars = standard deviation. Two-way ANOVA and Tukey multiple comparisons tests were done to determine statistical significance (ns, non-significant). (C) Western blot of OC43 EGFP-Nsp15 transfected or control EGFP transfected cells treated with As.

3.12 Coronavirus Nsp1 inhibits stress granules and limits eIF2 α phosphorylation.

Thus far, I have shown that N of both OC43 and CoV2, but not Nsp15 of OC43, are partially responsible for inhibition of SG condensation downstream of translation arrest, independent from changes to the level of eIF2 α phosphorylation. Comparisons between the level of SG inhibition in OC43-N-transfected cells and OC43-infected cells highlight discrepancies between the magnitude of SG suppression, suggesting that OC43 virus utilizes additional mechanisms to limit SG formation. I next wanted to test if host shutoff protein non-structural protein 1 (Nsp1) would limit SG formation. Recent literature about Nsp1 of CoV2 has shown that Nsp1 halts host translation by physically blocking the mRNA entry channel of the 40S ribosomal complex as well as promoting the degradation of host mRNAs through the use of an unknown host nuclease (Schubert et al., 2020; Thoms et al., 2020). Importantly, OC43-Nsp1 is also reported to limit host translation, but it is incapable of promoting host RNA degradation like CoV2-Nsp1 (Mendez et al., 2021). So, I co-transfected 293A cells with HA-tagged Nsp1 constructs for OC43 or CoV2, which were previously generated in my lab, with an EGFP construct and treated with As for 50 m. Co-transfection of the Nsp1 constructs with EGFP has previously been reported to illustrate the host shutoff and RNA degradation function of Nsp1 and confirm that these constructs behave as expected (Mendez et al., 2021). At 24 hpt, transfected cells were lysed for western blot analysis. Examination of the GFP protein expression confirmed that Nsp1 was functioning as expected (Figure 3.12A). Specifically, there was a decrease in GFP expression in OC43-Nsp1-expressing cells compared to cells only transfected with GFP (Figure 3.12A, empty vec.), likely due to the host shutoff function of OC43-Nsp1. In CoV2-Nsp1-expressing cells, there was an even stronger decrease in GFP expression compared to OC43-Nsp1-transfected cells or the empty vector control; this observation is likely attributed to the dual functions of CoV2-Nsp1 in host shutoff and stimulating RNA degradation. Notably, overexpression of either OC43-Nsp1 or CoV2-Nsp1 resulted in a significant decrease in the level of eIF2 α phosphorylation in As-treated and Nsp1-transfected cells compared to EGFP control (Figure 3.12A,B). Importantly, the transfection efficiencies of these experiments range from 40-60%, so the level of eIF2 α phosphorylation in transfected cells may be even lower than observed here. Given that both Nsp1s limited eIF2 α phosphorylation, we

predicted that OC43-Nsp1 and CoV2-Nsp1 would also limit As-induced SG formation. I transfected 293A cells with HA-tagged Nsp1 constructs or an EGFP control and treated with As 50 m-prior to fixation at 24 hpt. SG formation in transfected cells was analyzed using immunofluorescence microscopy using TIAR as a SG marker. In either OC43-Nsp1- or CoV2-Nsp1-transfected cells, there was little SG formation compared to As-treated and EGFP-transfected cells (Figure 3.12C). Interestingly, overexpression of CoV2-Nsp1 resulted in an increase in TIAR nuclear localization, which may contribute to the limited SG formation in CoV2-Nsp1-expressing cells (Figure 3.12C). Alternatively, nuclear localization of TIAR may misrepresent the level of SG formation in CoV2-Nsp1-transfected cells, where TIAR is redistributed away from SGs but they still form within the cytoplasm. To test this, I also analyzed SG formation using G3BP1 as a SG marker. I transfected 293A cells with EGFP-tagged Nsp1 constructs or EGFP control and treated with As 50 m-prior to fixation at 24 hpt. Similar to using TIAR as a SG marker, overexpression of OC43-Nsp1 limited SG formation indicated by G3BP1-positive foci (Figure 3.12B). Analysis of SG formation in CoV2-Nsp1-expressing cells revealed low G3BP1 expression (Figure 3.12D), resulting in inconclusive observations about the level of SG formation in transfected cells. Using a third SG marker, G3BP2, I transfected 293A cells with HA-tagged Nsp1 constructs or EGFP control and treated with As 50 m-prior to fixation at 24 hpt. Again, overexpression of OC43-Nsp1 limited SG formation while in CoV2-Nsp1-expressing cells, small G3BP2-positive aggregates formed in the cytoplasm of the transfected cells (Figure 3.12E). Quantification of the number of SGs per cell showed no significant difference between cells expressing CoV2-Nsp1 (HA-Nsp1) or cells expressing EGFP (Figure 3.12F), but there was a significant decrease in the size of SGs in the presence of CoV2-Nsp1 compared to EGFP (Figure 3.12F). Together, Nsp1 of OC43 repeatedly inhibits SG formation, likely due to limited eIF2 α phosphorylation, and along with OC43-N, contributes to the significant SG suppression observed during OC43 infection. While CoV2-Nsp1 remodels SG composition through stimulating redistribution of TIAR to the nucleus and degradation of G3BP1.

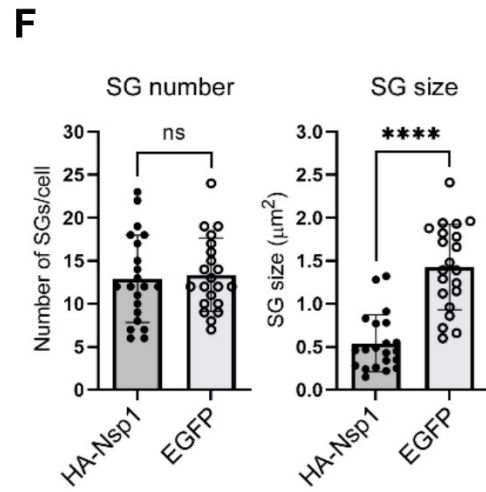
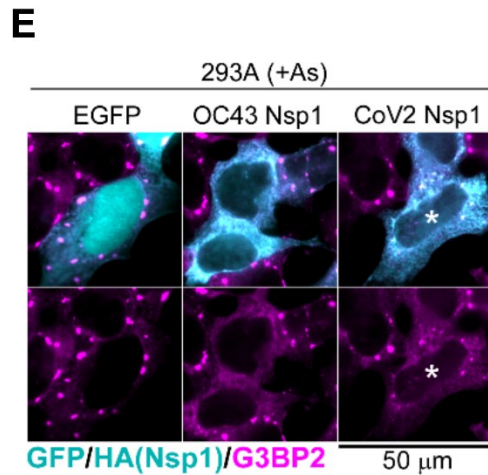
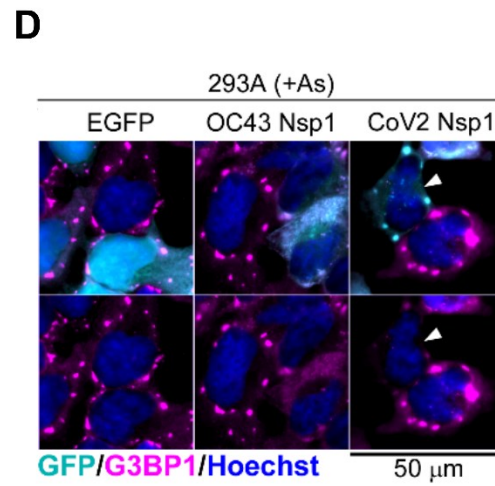
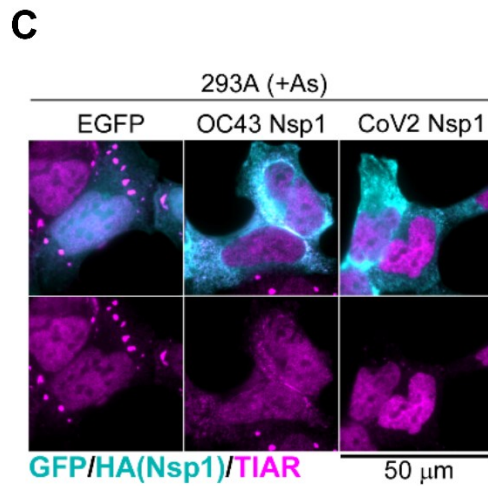
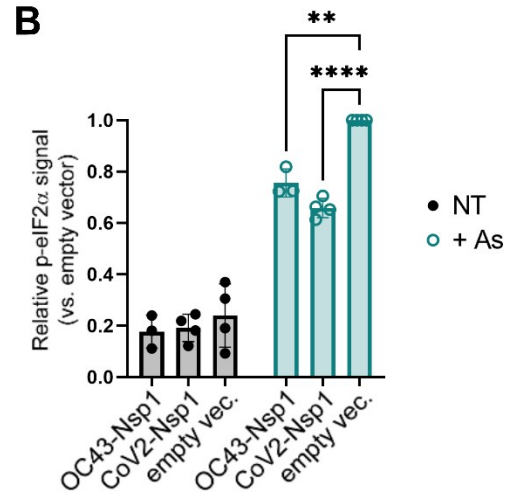
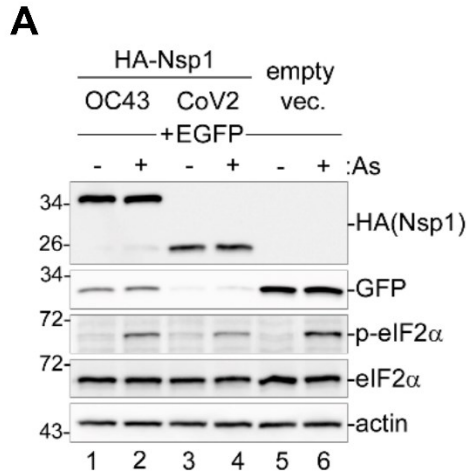


Figure 3.12 Coronavirus Nsp1 inhibits stress granules and limits eIF2 α

phosphorylation. The 293A cells were transiently transfected with the indicated HA-tagged or EGFP-tagged Nsp1 expression constructs or EGFP control. At 24h post-transfection cells were treated with sodium arsenite (+ As). SG formation was visualized by immunofluorescence microscopy and eIF2 α phosphorylation was analysed by western blot. (A) Whole cell lysates from transfected cells with or without As were analysed by western blot. (B) Relative level of eIF2 α phosphorylation (normalized to total eIF2 α), quantified from A. Each data point represents independent biological replicate (N \geq 3). Error bars = standard deviation. Two-way ANOVA and Tukey multiple comparisons tests were done to determine statistical significance (****, p -value < 0.0001, **, p -value < 0.01). (C) Immunofluorescence microscopy staining for TIAR (magenta). GFP signal in control cells and HA-tagged Nsp1 signal are shown in teal. Scale bar = 50 μ m. (D) Immunofluorescence microscopy analysis of cells expressing the indicated EGFP-tagged Nsp1 constructs or EGFP control. SG formation was visualized by staining for G3BP1 (magenta). GFP signal is shown in teal. Nuclear DNA was visualized with Hoechst (Blue). Arrowhead indicates a representative cell with low G3BP1 signal. Scale bar = 50 μ m. (E) Immunofluorescence microscopy analysis of cells expressing the indicated HA-tagged Nsp1 constructs or EGFP control. SG formation was visualized by staining for G3BP2 (magenta). GFP signal in control cells and HA-tagged Nsp1 signal are shown in teal. Asterisks indicates a representative CoV2 Nsp1 expressing cell with small SGs. Scale bar = 50 μ m. (F) G3BP2-positive SG number per cell and average SG size per cell were quantified in CoV2 HA-Nsp1-transfected cells and control EGFP-transfected cells from E. Each data point represents individual cell analysed from 3 independent biological replicates (21 cells per condition). Error bars = standard deviation. Two-tailed Students t-Test was done to determine statistical significance. (****, p -value < 0.0001, ns, non-significant).

3.13 The RNA degradation function of CoV2-Nsp1 is required for TIAR redistribution and G3BP1 depletion from stress granules.

The distinct changes to SG formation in the presence of OC43-Nsp1 compared to CoV2-Nsp1 may be related to the differential functions of these two viral proteins. As previously mentioned, both Nsp1 proteins interfere with host protein synthesis, however only CoV2-Nsp1, not OC43-Nsp1, has been shown to promote RNA degradation (Mendez et al., 2021). Thus, I questioned if the RNA degradation function of CoV2-Nsp1 was responsible for the remodeling of SGs previously observed (Figure 3.12). I utilized two CoV2 Nsp1 amino acid substitution mutants that are defective for mRNA degradation function but are still able to inhibit host protein synthesis: R99A N-terminal domain mutant (99A) and R124A,K125A linker region double mutant (125A). To confirm the function of these mutants, EGFP expression was analyzed in 293A cells co-transfected with one of the four HA-tagged Nsp1 constructs and EGFP. Western blotting analysis showed a decrease in GFP expression in OC43-Nsp1-transfected cells and even less GFP expression in WT CoV2-Nsp1-expressing cells compared to EGFP only-transfected cells (Figure 3.13A). GFP expression in cells expressing either CoV2-Nsp1 (99A) or CoV2-Nsp1 (125A) only showed a slight decrease in GFP expression (Figure 3.13A), suggesting these mutants cannot decrease GFP expression to the same degree as WT CoV2-Nsp1 and that they are deficient in mRNA degradation function. Further, only WT CoV2-Nsp1 decreased expression of G3BP1, while expression of additional SG markers G3BP2 and TIAR were unaffected by Nsp1 (Figure 3.13A). To examine if the mRNA degradation function of Nsp1 affects SG formation, 293A cells were transfected with HA-tagged Nsp1 constructs or EGFP control, treated with As for 50 m, and SG formation was visualized using TIAR (Figure 3.13B) or G3BP2 and TIA-1 (Figure 3.13C). All Nsp1s limited SG formation to various degrees (Figure 3.13D). Using TIAR as a SG marker, WT CoV2-Nsp1 was most efficient at limiting SG formation, with less than 30% of transfected cells forming SGs (Figure 3.13B,D). Although, the level of SG formation significantly increased in the presence of either CoV2-Nsp1 mutant compared to WT CoV2-Nsp1 (Figure 3.13B,D). Strikingly, nuclear localization of TIAR was only increased during overexpression of WT CoV2-Nsp1 and not overexpression of either CoV2 Nsp1 mutant (Figure 3.13B). This observation indicates that the level of SG

inhibition by WT CoV2-Nsp1 is inflated when using TIAR as a marker of SG formation. In contrast, the level of SG formation was significantly higher in WT CoV2-Nsp1-expressing cells when G3BP2 was used as the SG marker, compared to TIAR, while there was little change to the magnitude of SG formation in the presence of the two mutant CoV2-Nsp1s or OC43-Nsp1 between SG markers (Figure 3.13C,D). Further, TIA-1 staining resembled similar localization patterning as TIAR; overexpression of WT CoV2-Nsp1 promoted nuclear localization of TIA-1. TIAR and TIA-1 are related SG proteins and similar re-distribution to the nucleus by WT CoV2-Nsp1 suggests that a common aspect of these proteins is targeted by WT CoV2-Nsp1. Additionally, I examined the RNA levels of multiple SG proteins as well as housekeeping gene ACTB (β -Actin) using RT-qPCR. WT CoV2-Nsp1 significantly degraded G3BP1, G3BP2, and ACTB RNA levels, while TIAR RNA levels were significantly increased (Figure 3.13E). The degradation of G3BP1 RNA by WT CoV2-Nsp1 also explains the decrease in G3BP1 protein expression, and the lack of SGs, previously observed in EGFP-CoV2-Nsp1-expressing cells (Figure 3.12D). Together, these observations implicate the mRNA degradation function of CoV2-Nsp1 in both the degradation of G3BP1 and the localization of TIAR to the nucleus. These functions of CoV2-Nsp1 specifically target key SG proteins and highlight additional mechanisms of how CoVs proteins interfere with SG formation.

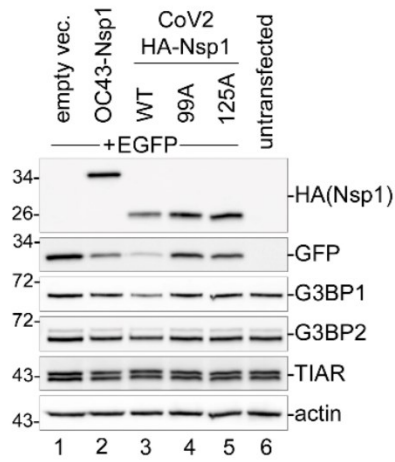
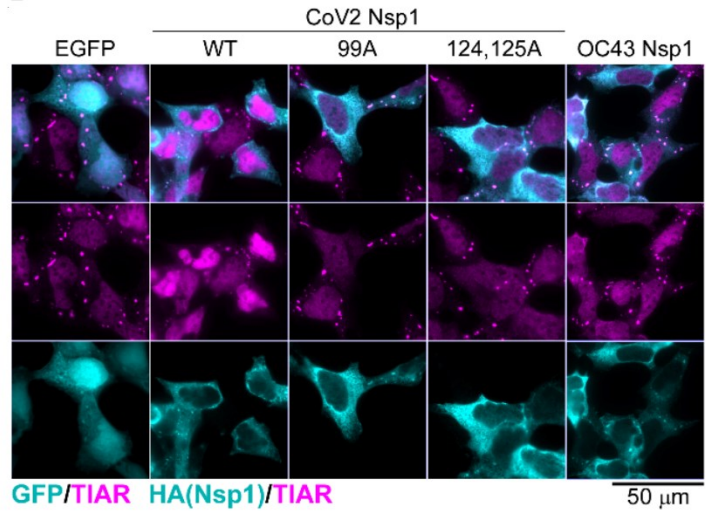
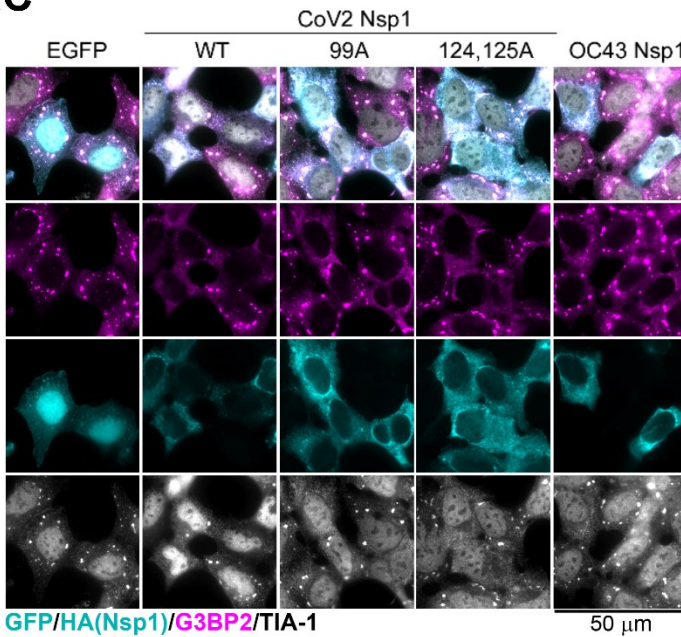
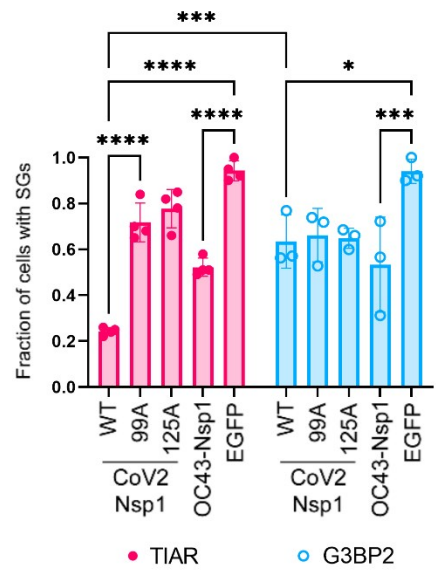
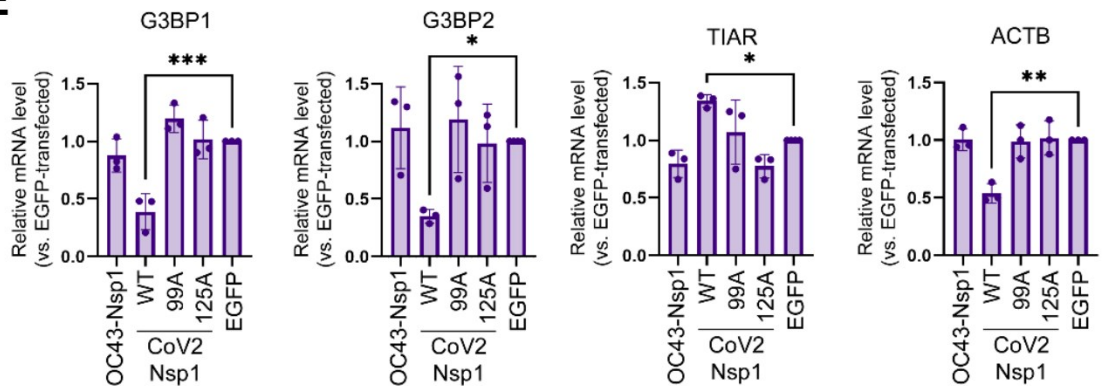
A**B****C****D****E**

Figure 3.13 The RNA degradation function of CoV2-Nsp1 is required for TIAR redistribution and G3BP1 depletion from stress granules. 293A cells were transiently transfected with the indicated HA-tagged Nsp1 expression constructs or EGFP control. At 24h post-transfection cells were left untreated or were treated with sodium arsenite (+ As) to induce SG formation. SG formation was visualized by immunofluorescent microscopy and SG protein expression was analysed by western blot. (A) Western blot analysis of cells co-transfected with the indicated HA-tagged Nsp1 constructs and EGFP. (B) Immunofluorescence microscopy analysis of cells expressing the indicated wild type and mutant Nsp1 constructs treated with As. SG formation was visualized by staining for TIAR (magenta). GFP signal in control cells and HA-tagged Nsp1 signal is shown in teal. WT = wild type; 99A = R99A mutant; 125A = R124A,K125A mutant. Scale bar = 50 μ m. (C) Immunofluorescence microscopy analysis of cells expressing the indicated wild type and mutant Nsp1 constructs treated with As. SG formation was visualized by staining for G3BP2 (magenta) and TIA-1 (greyscale). GFP signal in control cells and HA-tagged Nsp1 signal is shown in teal. WT = wild type; 99A = R99A mutant; 125A = R124A,K125A mutant. Scale bar = 50 μ m. (D) Fraction of transfected cells with As-induced SGs quantified from B (TIAR) and C (G3BP2). Each data point represents independent biological replicate (N \geq 3). Error bars = standard deviation. Two-way ANOVA and Tukey multiple comparisons tests were done to determine statistical significance (****, p-value < 0.0001; ***, p-value < 0.001; *, p-value < 0.05, ns, non-significant). Relative G3BP1, G3BP2, TIAR, and ACTB mRNA levels were determined using RT-QPCR in cells transfected with the indicated expression constructs at 24 h post-transfections. Values were normalized to 18S. Each data point represents independent biological replicate (N=3). Error bars = standard deviation. One-way ANOVA and Dunnett's multiple comparisons tests were done to determine statistical significance (***, p-value < 0.001; **, p-value < 0.01; *, p-value < 0.05).

3.14 Nsp1 of OC43 primarily inhibits stress granules through limiting eIF2 α phosphorylation.

Previous results illustrated that Nsp1 of OC43 limits As-induced eIF2 α phosphorylation (Figure 3.12A) and repeatedly suppressed SG formation (Figure 3.12C,D,E, 3.13B,C). To examine if inhibition of eIF2 α phosphorylation is the main mechanism of SG suppression by OC43 Nsp1, I treated OC43 Nsp1, CoV2 Nsp1, and EGFP expressing cells with Sil.. To visualize SGs, G3BP2 and TIA-1 were used as SG markers. Bright SG foci formed in the cytoplasm of EGFP-expressing cells as well as in cells expressing OC43 Nsp1 (Figure 3.14A), whereas most CoV2 Nsp1 expressing cells had either smaller dispersed SG foci or no discernable SGs (Figure 3.14B).

Quantification of the fraction of cells with Sil.-induced SGs demonstrated that only CoV2 Nsp1 decreased SG formation (Figure 3.14B). This indicates that the previously observed mRNA and G3BP1 depletion (Figure 3.13A,E), as well as nuclear retention of TIAR by CoV2 Nsp1 (Figure 3.12C, 3.13B), contribute to impaired SG condensation independent of eIF2 α phosphorylation inhibition, with roughly 25% of transfected cells not forming SGs and the remaining cells forming smaller SGs. In contrast, OC43 Nsp1 did not significantly inhibit SG formation when induced by a mechanism that is independent of eIF2 α phosphorylation, concluding that OC43 Nsp1 limits eIF2 α phosphorylation resulting in diminished SG formation.

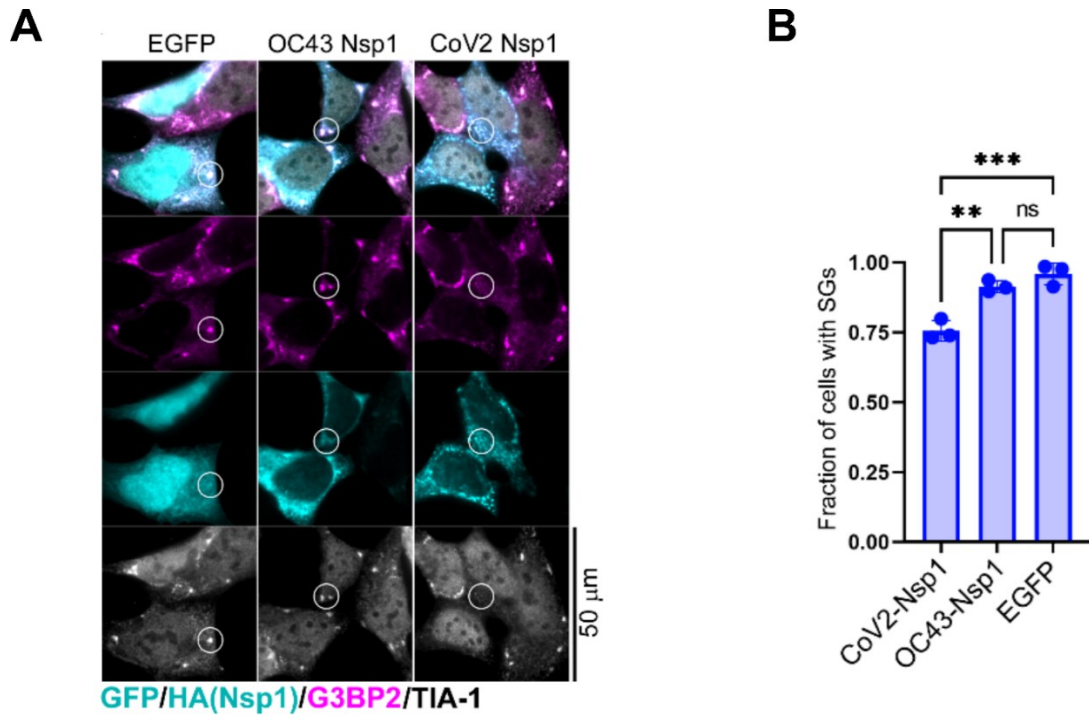


Figure 14. Nsp1 of OC43 primarily inhibits stress granules through limiting eIF2 α phosphorylation. The 293A cells were transiently transfected with the indicated HA-tagged Nsp1 expression constructs or EGFP control. At 24h post-transfection cells were treated with silvestrol (+ Sil) to induce SG formation. (A) Immunofluorescence microscopy analysis of cells expressing the indicated HA-tagged Nsp1 constructs or EGFP control and treated with Sil. SG formation was visualized by staining for G3BP2 (magenta) and TIA-1 (greyscale). GFP signal in control cells and HA-tagged Nsp1 signal are shown in teal. Circles highlight areas of cytoplasm with and without bright SG foci. Scale bar = 50 μ m. (B) Fraction of transfected cells with Sil.-induced SGs quantified from A (based on G3BP2 staining). Each data point represents independent biological replicate (N=3). Error bars = standard deviation. One-way ANOVA and Tukey multiple comparisons tests were done to determine statistical significance (***, p-value < 0.001; **, p-value < 0.01; ns, non-significant).

3.15 G3BP1 overexpression inhibits OC43 infection.

Lastly, because I observed efficient SG suppression by OC43 and CoV2, and CoV2 host shutoff causes G3BP1 depletion, I tested if G3BP1 overexpression would impair virus replication. My lab generated 293A cells stably transduced with lentivirus vectors encoding EGFP-tagged G3BP1 (293A[EGFP-G3BP1]) and control cells expressing EGFP (293A[EGFP]). Overexpression of G3BP1 has been reported to trigger SG formation in some cells (Tourrière et al., 2003). Therefore, early passage cells were sorted to generate stable cell lines with minimal spontaneous SG formation and to ensure similar levels of EGFP expression. Initial testing of these cell lines revealed no major differences in cell morphology or SG formation following As treatment (Figure 3.15A). I infected 293A[EGFP], 293A[EGFP-G3BP1], and parental untransduced 293A cells with OC43 and analyzed infection rates using immunofluorescence microscopy staining at 24 hpi. I observed that infection was limited in 293A[EGFP-G3BP1] cells, where approx. 38% of cells were infected relative to parental 293As (Figure 3.15C). Importantly, this was not due to lentiviral integration or non-specific effect of EGFP overexpression as infection rates were similar between 293A[EGFP] and parental untransduced cells (Figure 3.15B,C). Western blot analysis confirmed that the accumulation of viral N protein was decreased as well (Figure 3.15D). To examine whether the increased resistance of 293A[EGFP-G3BP1] cells to CoV infection was due to increased SG formation, I analyzed infected cells using immunofluorescence microscopy with staining for G3BP2 and viral N protein. I observed a significant increase in the level of SG formation in infected 293A[EGFP-G3BP1] cells compared to infected 293A[EGFP] cells (Figure 3.15E,F). These results suggest that OC43 is limited by heightened levels of G3BP1 and SG formation.

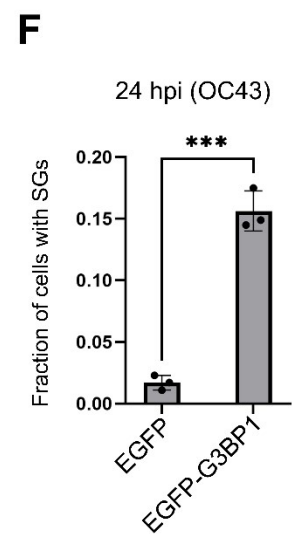
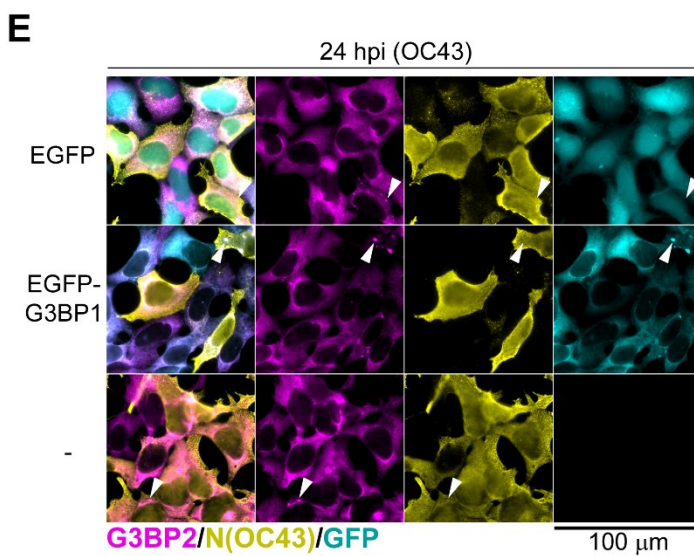
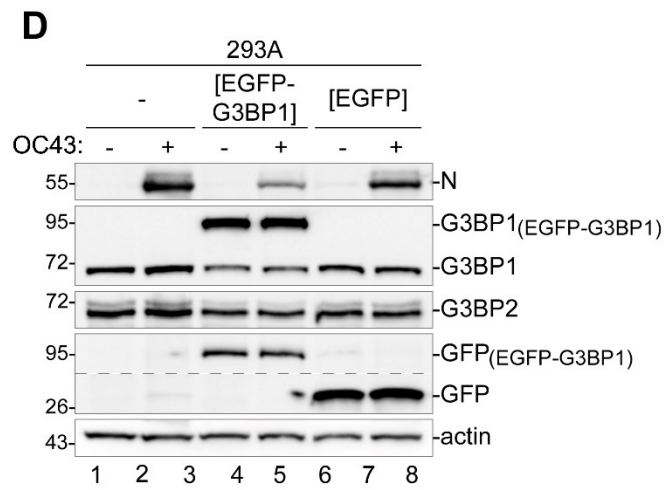
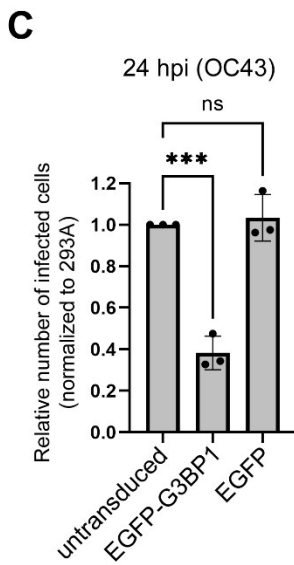
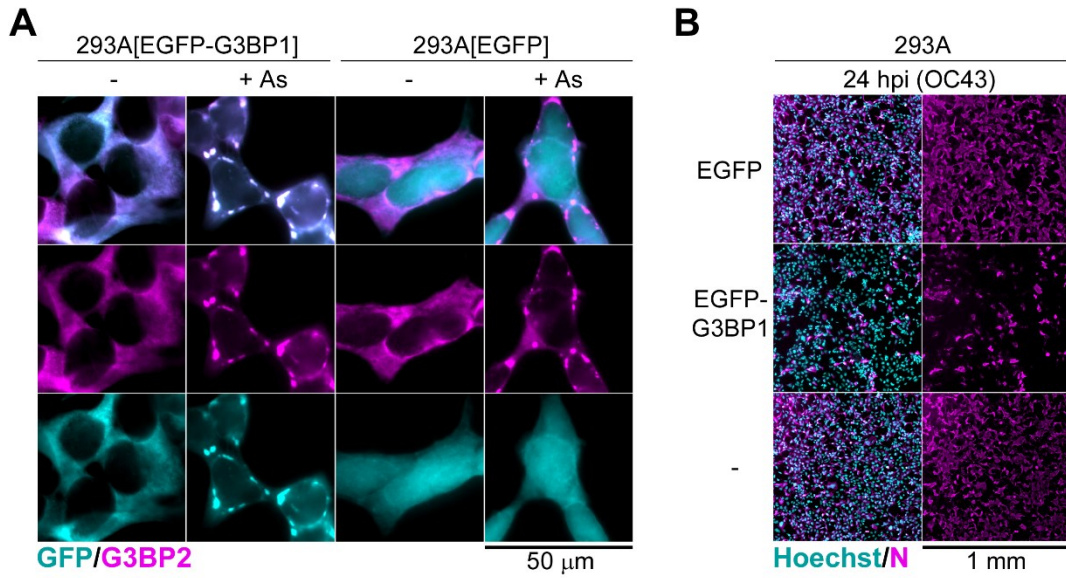


Figure 3.15 G3BP1 overexpression inhibits OC43 infection. (A) Immunofluorescence microscopy analysis of 293A[EGFP] and 293A[EGFP-G3BP1] cells untreated (-) or treated with arsenite (+ As) and stained for G3BP2 (magenta). GFP signal is shown in teal. Scale bar = 50 μ m. (B) Immunofluorescence microscopy analysis of parental 293A cells (-), 293A[EGFP], and 293A[EGFP-G3BP1] cells infected with OC43 at MOI = 1.0 and stained for OC43 N protein (magenta) at 24 hpi. Nuclei were stained with Hoechst dye (teal). Scale bar = 1 mm. (C) Relative number of infected cells (normalized to 293A) in 293A[EGFP] and 293A[EGFP-G3BP1] cells at 24 hpi, quantified from E. Each data point represents independent biological replicate (N=3). Error bars = standard deviation. One-way ANOVA and Dunnett's multiple comparisons tests were done to determine statistical significance (***, p -value < 0.001, ns, non-significant). (D) Western blot analysis of 293A, 293A[EGFP], and 293A[EGFP-G3BP1] cells infected with OC43 at 24 hpi. (E) Immunofluorescence microscopy of cells infected as in B and immunostained for G3BP2 (magenta) and OC43 N (yellow). GFP signal is shown in teal. Arrowheads indicate infected cells that formed SGs. Scale bar = 100 μ m. (F) Fraction of infected cells with SGs in 293A[EGFP] and 293A[EGFP-G3BP1] at 24 hpi, quantified from three independent experiments represented in panel E. Each data point represents independent biological replicate (N=3). Error bars = standard deviation. Unpaired T-test was done to determine statistical significance (***, p -value < 0.001).

CHAPTER 4 DISCUSSION

4.1 Overview

Herein, I have shown that CoVs encode multiple strategies to limit SG formation. Not only are these strategies utilized by common cold CoV OC43, but these mechanisms are conserved in the more recently identified CoV2. This project revealed that OC43 infection limits SG formation and eIF2 α phosphorylation. Further investigation into how OC43 limits eIF2 α phosphorylation highlighted that OC43 upregulates GADD34, but neither prior activation of the ISR nor expression of GADD34 is required for OC43-mediated inhibition of eIF2 α phosphorylation. Additional analyses into how OC43 inhibits SG formation revealed that viral proteins N and Nsp1 target multiple steps of SG formation to limit SGs. The SG inhibition function of these viral proteins was also shown for CoV2 N and Nsp1, and CoV2-Nsp1 targets SG proteins G3BP1 and TIAR to limit SG formation. Lastly, overexpression of SG protein G3BP1 limited OC43 infection.

4.2 Inhibition of eIF2 α phosphorylation by OC43

This work showed that the inhibition of SGs coincided with a decrease in the level of eIF2 α phosphorylation in infected cells (Figure 3.1,3.2). Further, I found that the inhibition of eIF2 α phosphorylation by OC43 was not specific to the activation of any one eIF2 α kinase (Figure 3.3). This is in contrast to previous research in the area of CoVs and SGs, which have reported that other CoVs limit eIF2 α phosphorylation through a PKR-specific mechanism. During MERS infection, there are low levels of phosphorylated eIF2 α and this was attributed to the function of the viral 4a protein which is thought to mask dsRNA to prevent activation of PKR (Nakagawa et al., 2018; Rabouw et al., 2016). A similar mechanism is utilized during IBV infection through the Nsp15 protein; Nsp15 limits accumulation of dsRNA and attenuates PKR activation (Brownsword et al., 2020; Gao et al., 2021). The Nsp15 protein of OC43 was tested herein and was found to be unable to limit As-induced eIF2 α phosphorylation and SG formation (Figure 3.11). These mechanisms are likely to play important roles in limiting the ISR and SG induction in MERS- and IBV-infected cells, but they do not explain the general inhibition of SG formation by OC43 in response to exogenous stressors.

Because OC43 limited eIF2 α phosphorylation irrespective of the activated kinase, I looked at how OC43 may interfere with the dephosphorylation of eIF2 α . I first found that OC43 upregulated GADD34 RNA levels (Figure 3.5). This has been observed previously with IBV infection and pseudorabies virus (PRV) infection and this function was tied to the need for these viruses to resume translation and viral protein production (X. Wang et al., 2009; Zhu et al., 2021). In fact, shRNA knockdown of GADD34 increased eIF2 α phosphorylation levels in the presence of PRV and significantly limited PRV infection (Zhu et al., 2021). Here, I showed that knockdown of GADD34 significantly decreased viral titers, however, this was not due to increased levels of eIF2 α phosphorylation (Figure 3.6). This result suggests that the upregulation of GADD34 by OC43 is not responsible for the low levels of phosphorylated eIF2 α observed during infection, but instead that GADD34 is important for other viral processes. The cellular function of GADD34 may not be limited to the dephosphorylation of eIF2 α . One publication suggested that GADD34 can reverse Golgi fragmentation during hyperosmotic stress as well as facilitate protein trafficking through the Golgi (Krokowski et al., 2017). In addition, it has been established that CoVs traverse the ER-Golgi network during replication (Hartenian et al., 2020; V'kovski et al., 2021), so it is possible that GADD34 promotes viral replication through its function in these organelles.

Additionally, I found that OC43 could upregulate GADD34 even in the presence of ISRIB (Figure 3.5). This result suggests that OC43 does not require prior activation of the ISR to induce GADD34 expression. This prompts the question of how OC43 upregulates GADD34. One possibility is that this virus encodes a factor that promotes uORF skipping. During stress conditions when cellular translation is inhibited, the increase in uORF skipping promotes expression of ATF4 (Jackson et al., 2010) and OC43 infection increased ATF4 protein levels (Figure 3.7D). ATF4 is the main transcriptional activator of GADD34 and this increase in ATF4 expression during infection could explain the increase in GADD34 expression during infection. However, it is still unclear how OC43 can increase expression of these proteins and what role both ATF4 and GADD34 play in OC43 infection.

Another alternative is that OC43 utilizes transcription factor EB (TFEB); TFEB plays a major role in the transcriptional response to amino acid starvation and mTORC1 inhibition and it was recently shown to activate both ATF4 and GADD34 expression (Gambardella et al., 2020; Martina et al., 2016; Napolitano & Ballabio, 2016). Under normal conditions, mTORC1 phosphorylates TFEB keeping TFEB at the lysosomal membrane, but during nutrient starvation, mTORC1 is dephosphorylated, inactivated, and released from the cytoplasm. In turn, TFEB is dephosphorylated which promotes its nuclear translocation where it can transcriptionally activate genes involved in lysosomal biogenesis and autophagy (Napolitano & Ballabio, 2016). TFEB is thought to activate ATF4 and GADD34 expression to permit translation of mRNAs encoding proteins involved in these pathways (Gambardella et al., 2020; Martina et al., 2016). CoVs have been reported to dysregulate autophagy (Gassen et al., 2021; Miller et al., n.d.), and perhaps this dysregulation involves activation of TFEB, resulting in ATF4 and GADD34 induction. Future research into this phenotype should examine TFEB as a potential target of CoVs.

4.3 Nsp1-mediated inhibition of eIF2 α phosphorylation

While GADD34 may not be required for reduced levels of eIF2 α phosphorylation during OC43 infection, I did identify that overexpression of either OC43 or CoV2 Nsp1 limited eIF2 α phosphorylation induced by As (Figure 3.12). Nsp1 is a known host shutoff factor; both SARS-Nsp1 and CoV2-Nsp1 have been reported to associate with the 43S ribosomal subunit, blocking the mRNA entry channel, and stalling host translation (Narayanan et al., 2008; Schubert et al., 2020; Thoms et al., 2020). It has been assumed that Nsp1 of OC43 also limits host translation and this idea was confirmed with this project, where using our EGFP reporter system, overexpression of OC43-Nsp1 reduced EGFP expression (Figure 3.12A, 3.13A). Although, OC43-Nsp1 could not reduce EGFP protein expression as strongly as CoV2-Nsp1 (Figure 3.12A, 3.13A), nor could OC43-Nsp1 degrade cellular mRNAs (Figure 3.13E). The differences between the host shutoff function of OC43-Nsp1 and CoV2-Nsp1 additionally support the idea that CoV2-Nsp1 induces mRNA degradation (Mendez et al., 2021), through an unidentified mechanism, and that OC43-Nsp1 does not have this mRNA degradation function. Future studies

should evaluate the host shutoff differences between these viruses and how their host shutoff functions may be involved in SG inhibition.

Prior to this work, Nsp1 of either OC43 or CoV2 has not been shown to interfere with eIF2 α phosphorylation and how Nsp1 maintains low levels of phosphorylated eIF2 α is still yet to be uncovered. Nsp1-mediated upregulation of GADD34 was not examined herein, yet there is another host protein capable of mediating eIF2 α dephosphorylation. CReP, the constitutive repressor of eIF2 α phosphorylation, is constantly expressed at low levels in order to regulate basal levels of eIF2 α phosphorylation and maintain host translation (Jousse et al., 2003). Both GADD34 and CReP are controlled by their uORFs and can therefore be upregulated if uORF skipping is increased by the ISR or a viral factor. In fact, this viral factor could be Nsp1 and future work should evaluate if Nsp1 can promote uORF skipping, resulting in increased expression of host proteins regulated by uORFs (i.e. GADD34, CReP).

In addition, CReP is a short-lived protein which requires constant translation of its mRNA to maintain steady protein levels (Jousse et al., 2003). If translation of CReP is unaffected by the virus, it is possible that the virus interferes with degradation of this protein. If degradation of CReP was attenuated, then CReP protein levels could increase and may account for decreased levels of eIF2 α phosphorylation in the cell. In this work, CReP was not investigated, but future projects should examine CReP expression during infection and if Nsp1 can antagonize CReP degradation.

Other viruses facilitate eIF2 α dephosphorylation by encoding viral proteins closely related to GADD34. For example, HSV γ 34.5 has high homology with GADD34, and this viral protein bridges PP1 and phosphorylated eIF2 α to dephosphorylate eIF2 α during HSV infection (Y. Li et al., 2011). HSV is not alone, other viruses encode similar proteins in order to limit eIF2 α phosphorylation and maintain steady translation rates (Rojas et al., 2015). These viral and host proteins all share a conserved RVxF motif important for binding to PP1 as well as a highly conserved C-terminal region important for binding eIF2 α (Rojas et al., 2015). While Nsp1 does not contain this conserved RVxF motif, other proteins of OC43 and CoV2 do. Specifically, analysis of primary protein sequences using BLAST (NCBI) revealed that Nsp2 of OC43 contains RVTF motif and

Nsp3 (PLPro) and Nsp4 of CoV2 contain RVVF motifs. In the future, it would be important to examine the function of these proteins in the context of eIF2 α phosphorylation to uncover if additional viral proteins promote eIF2 α dephosphorylation.

4.4 Stress granule inhibition by Nsp1

Limiting eIF2 α phosphorylation was not the only function of Nsp1 uncovered in this project. I found that CoV2-Nsp1 specifically causes nuclear retention of TIAR and that this function was dependent on the RNA degradation function of CoV2-Nsp1 (Figure 3.13). TIAR, and its closely related homolog TIA-1, are predominantly nuclear proteins that, during cellular stress, will re-localize to the cytoplasm to nucleate SGs (N. L. Kedersha et al., 1999). The precise mechanisms of TIAR/TIA-1 nuclear import and export have yet to be determined; however, the RRM2 domain, an important RNA-binding domain of TIAR and TIA-1, was shown to be required for nuclear accumulation of these proteins while the RRM3 domain is important for nuclear export (T. Zhang et al., 2005). Further, Zhang et al. (2005) showed that Actinomycin D treatment, a transcriptional inhibitor which decreases the level of cellular mRNAs, actually increased cytoplasmic localization of TIAR. Thus, general mRNA depletion is likely not the cause of TIAR nuclear retention by CoV2-Nsp1. Instead, there is likely specific dysregulation of the nuclear import and export of TIAR and TIA-1 by this viral protein.

Previously, SARS-Nsp1 was reported to interact with Nup93 and disrupt its localization to the nuclear envelope where it normally functions in the nuclear pore complex (Gomez et al., 2019). This interaction was also attenuated with mutant Nsp1 (K164A/H165A), which is deficient in mRNA degradation function and unable to block host protein synthesis (Gomez et al., 2019; Shen et al., 2020). Recent literature has also implicated CoV2-Nsp1 in the disruption of mRNA export during infection. CoV2-Nsp1 interacted with host mRNA export factors NXF1-NXT1 (K. Zhang et al., 2021); this heterodimer facilitates the translocation of mRNAs through the nuclear pore complex (K. Zhang et al., 2021). Specifically, CoV2-Nsp1 prevented proper docking of NXF1 to the nuclear pore complex. Given that Nsp1 has been shown to interact and interfere with nuclear export machinery, it is possible that these interactions limit TIAR export during Nsp1 overexpression. Future analysis of the function of these nuclear export factors in the

context of TIAR export during Nsp1 overexpression could elucidate both the mechanisms of TIAR export and how Nsp1 interferes with it.

Despite how Nsp1 limits TIAR nuclear export, the lack of cytoplasmic TIAR contributes to the SG inhibition by Nsp1 and the significant decrease in the size of SGs that do form during Nsp1 overexpression (Figure 3.12, 3.13). This decrease in SG size by CoV2-Nsp1 was also shown to be tied to a decrease in G3BP1 expression (Figure 3.12, 3.13). Only WT CoV2-Nsp1, and not OC43-Nsp1 or CoV2-Nsp1 mutants, could decrease both G3BP1 mRNA and protein expression (Figure 3.13), but how Nsp1 degrades G3BP1 is still unknown. The current understanding of CoV2-Nsp1 is that it recruits an unknown host nuclease to degrade cellular mRNAs (Hartenian et al., 2020), and it is possible that G3BP1 is a target of CoV2-Nsp1-induced mRNA degradation. Interestingly, G3BP1 protein expression was also shown to be decreased in response to Actinomycin D treatment, suggesting that global cellular decreases in mRNA levels may trigger G3BP1 degradation (Dolliver et al., 2022). These results imply that Nsp1 may trigger G3BP1 degradation through an intrinsic host pathway as opposed to recruitment of a host or viral protease.

Curiously, TIAR mRNA levels were not degraded during CoV2-Nsp1 overexpression and were instead significantly increased (Figure 3.13E). Secondary structures or specific nucleotide composition of TIAR mRNA sequences may account for its protection against Nsp1-mediated degradation. SL1 of the 5'UTR of the CoV2 RNA genome is required to protect against Nsp1 (Banerjee et al., 2020; Vora et al., 2022). Proteomic analysis of host proteins that bind that 5'UTR of the CoV2 genome identified top binders as La-related protein 1 (LARP1) and cellular nucleic acid binding protein (CNBP) (Schmidt et al., 2021) – two proteins significantly involved in the regulation and translation of terminal oligopyrimidine (TOP) mRNAs (Cockman et al., 2020). TOP mRNAs are classified as containing a m7G capped C nucleotide followed by an oligopyrimidine stretch of 7-12 nucleotides long which is often followed by a G-rich region (Cockman et al., 2020; Philippe et al., 2020). This TOP motif is found in the mRNA sequence of all ribosomal proteins as well as other RNA-binding proteins and is important for the translation of these proteins during cellular stress (Cockman et al.,

2020). TIAR and TIA-1 are not classified as TOP mRNAs, however they contain an extended oligopyrimidine stretch in their 5'UTR and they are involved in TOP mRNA translation (Cockman et al., 2020). Thus, if protection from Nsp1 degradation involves TOP mRNA machinery, this could explain why TIAR mRNA is not a target of Nsp1 degradation and is instead increased during Nsp1 overexpression. Future studies should examine if this is indeed true.

4.5 Stress granule inhibition by N

Nsp1 is an important mediator of SG inhibition by CoVs, but it is not the only viral protein responsible for SG inhibition. The N protein of both OC43 and CoV2 limited SG formation induced by multiple stressors (Figure 3.13). For As-induced SGs, there was a significant difference in the level of SG inhibition between OC43-N and CoV2-N (Figure 3.13C,D), and this inhibition was independent from changes to eIF2 α phosphorylation (Figure 3.13A), suggesting that N cannot manipulate the level of phosphorylated eIF2 α to limit SG formation like Nsp1. This is further supported by the results that N was better at inhibiting SG formation induced by Sil. treatment (Figure 3.13E,F), which induces SGs independently from eIF2 α phosphorylation (Slaine et al., 2017). The difference in the magnitude of SG inhibition by OC43-N between As-induced SGs and Sil.-induced SGs could be attributed to differences in the post-translational modifications of N in these environments. A recent publication highlighted that methylation of CoV2 N promotes inhibition of SGs induced by As treatment and this methylation is mediated by protein arginine methyltransferase 1 (PRMT1) (Cai et al., 2021). G3BP1 is another substrate of PRMT1 and when G3BP1 is methylated, SG assembly is limited (Tsai et al., 2016). During As treatment, methylation of G3BP1 was reduced and this was shown to promote SG assembly (Tsai et al., 2016). If As treatment affects methylation of PRMT1 substrates, then N methylation and the SG inhibition function of N may be attenuated during As treatment.

Further, N of CoV2 has also been reported to be phosphorylated at multiple residues within its serine/arginine (SR)-rich domain (Savastano et al., 2020). This phosphorylation can be facilitated by serine/arginine protein kinase 1 (SRPK1) and phosphorylation of CoV2-N was shown to interfere with its ability to phase separate in

the presence of RNA (Savastano et al., 2020). This is in line with previous work focusing on SARS-N that showed phosphorylation of the SR-rich domain also interfered with its multimerization activity (Peng et al., 2008). The phosphorylation of N may also affect its ability to suppress SG formation and the phosphorylation state of N may differ between As and Sil. conditions. Not only are these post-translation modifications relevant to the function of these viral protein in SG suppression, they may also explain the multiple banding patterns observed in OC43-infected western blot samples when probing for OC43-N. In multiple instances and cell lines, I observed an upper band above the 55 kda band assumed to be OC43-N (Figures 3.2, 3.4, 3.5, 3.6). This upper band could likely be modified OC43-N that is only produced during infection, as I did not observe additional bands in the N-overexpression experiments. Future studies should focus on the post-translation modifications of OC43 viral proteins, like N, and the effect these modifications have on SG inhibition.

Despite how N is modified during cellular stress, both OC43-N and CoV2-N were shown to inhibit SGs downstream of eIF2 α phosphorylation. Instead, N may limit SG formation by re-localizing or sequestering key SG proteins. In multiple proteomics publications, it has been reported that CoV2-N directly binds G3BP1 (Gordon et al., 2020; J. Li et al., 2021; Nabeel-Shah et al., 2022), and during the completion of this work, it was reported that CoV2-N inhibits SGs by altering the RNA and protein binding profile of G3BP1 during N overexpression (Nabeel-Shah et al., 2022). This was further supported by another recent publication regarding N and SGs that showed that overexpression of CoV2-N or highly homologous SARS-N limited As-induced SG formation through binding of G3BP1 (Zheng et al., 2021). This project highlighted that OC43-N shares this SG inhibition function with the N protein of more pathogenic CoVs, like CoV2, but it is yet to be determined if this is through binding with G3BP1 or disruption of G3BP1 binding to other proteins.

4.6 The antiviral role of G3BP1 during OC43 infection

Given that N is reported to bind G3BP1, Nsp1 degrades G3BP1, and the central role of G3BP1 as an SG-nucleating protein, I examined the function of G3BP1 during CoV infection. Herein, I have shown that G3BP1 overexpression limited OC43 infection,

and this coincided with an increase in SG formation in infected cells (Figure 3.15). This result suggests that G3BP1 is antiviral towards OC43 and the antiviral function of G3BP1 may be tied to its role in SG formation. Importantly, G3BP1 has SG-independent functions so the antiviral role of G3BP1 may not be exclusively tied to its role in SG nucleation. While determination of the exact mechanisms of how G3BP1 limits OC43 infection is beyond the scope of this work, there are multiple possibilities for how this occurs. One possibility is that G3BP1 overexpression alters cellular functions important for OC43 entry; our current understanding of OC43 entry surmises that OC43 binds sialic acids on the surface of the cell which then results in endocytosis of the virus into the cytoplasm (Hartenian et al., 2020; V'kovski et al., 2021). G3BP1 has not been reported to interact with cell surface proteins or endocytic vesicles, therefore it is unlikely this is how G3BP1 limits OC43 infection. Instead, it is possible that G3BP1 attenuates replication of the OC43 genome. G3BP1 has been previously reported to bind the CoV2 genome (Schmidt et al., 2021) and this binding of G3BP1 to the viral genome may limit its replication or translation. Specific analysis of how G3BP1 affects OC43 infection should be addressed in future work.

4.7 Limitations

One of the major limitations to this project was our inability to perform CoV2 infections. Pairing the CoV2 viral protein overexpression data with CoV2 infection data, as has been shown for the OC43 results, would further strengthen our conclusions about the function of CoV2 proteins N and Nsp1 in regards to eIF2 α phosphorylation and SG formation. Luckily, we were able to collaborate with Dr. Jennifer Corcoran's lab at the University of Calgary who performed CoV2 infections using the same cell line and infection conditions as we used for OC43 infections. This data complimented our overexpression data and can be examined in our recent preprint (Dolliver et al., 2022).

In addition, I encountered a number of technical issues throughout this project. The most challenging technical issue I faced was a high variability in transfection efficiency when examining the function of different OC43 and CoV2 viral proteins. This complicated analysis of eIF2 α phosphorylation in N- or Nsp1- overexpressing cells by western blot, because the population of untransfected cells could mask any inhibition of

eIF2 α phosphorylation by these viral proteins. The generation of inducible cell lines that could be used to induce expression of the viral protein in all cells would more clearly show the effects these viral proteins have on eIF2 α phosphorylation and other host processes. As an alternative, single cell analysis could also be used to assess changes within either an infected or a N- or Nsp1- overexpressing cell. The use of flow cytometry to gauge the level of eIF2 α phosphorylation as well as the expression of other SG proteins within these cells would be informative to the role of N and Nsp1 during infection.

4.8 Future directions

Lastly, there are a number of ideas that should be examined in the future in relation to this project. The initial steps of this project was to establish that OC43 infection suppressed SG formation and this was completed with infection of OC43 at an MOI of 1 in three separate cell lines. However, analysis of how increasing the MOI would affect SG suppression by OC43 was never analysed. Future work could assess how varying the level of virus in different cell lines affects the SG inhibition function of OC43. Further, one of the biggest unanswered questions herein is how does OC43 limit eIF2 α phosphorylation. I have shown that overexpression of Nsp1 can limit As-induced eIF2 α phosphorylation, but it is still unclear how Nsp1 accomplishes this. It would be important to analyze if Nsp1 utilizes host factors such as GADD34 and CREP and if there are other viral proteins that contribute to the significant decrease in eIF2 α phosphorylation levels during infection. In addition, CoV2 Nsp1 was responsible for nuclear retention of TIAR and this phenotype was dependent on the RNA degradation function of Nsp1. The mechanism of how CoV2 Nsp1 can limit nuclear export of TIAR and how this is related to RNA degradation by Nsp1 would be important to elucidate in future studies. Lastly, I identified that overexpression of G3BP1 limits OC43 infection. However, the stage of viral infection that G3BP1 targets is not fully understood. Investigation into how G3BP1 limits OC43 infection, if G3BP1 is antiviral towards other CoVs, and if the antiviral function of G3BP1 is tied to SG formation would all be important questions to address in future work.

4.9 Implications.

Based on this project, it is evident that CoVs like OC43 and CoV2 encode multiple methods to suppress SG formation and increases in SG formation, through overexpression of SG protein G3BP1, can limit viral replication. Thus, this research has identified novel targets to limit CoV infection – through the induction of SGs. The generation of new antivirals or identification of current antivirals that could inhibit the SG suppressive function of viral proteins N and Nsp1 could act as treatment options for those infected with CoVs. Further, host targeted antivirals that induce SG formation in infected cells could also be a future option for CoV treatment. Lastly, this work adds to the growing literature surrounding SGs and other biological condensates. Clarification of the SG suppression mechanisms utilized by viruses could introduce new ideas about how to dissolve persistent aggregates linked to neurodegenerative diseases and the generation of tools that could be used to support neuronal cell viability.

4.10 Conclusions and models

The aim of this project was to clarify if CoVs modulate SG responses. My early results revealed that OC43 inhibited SG formation through decreased eIF2 α phosphorylation and viral protein Nsp1. Thus, my objectives for this project include: 1) To identify the mechanism of OC43-mediated inhibition of eIF2 α phosphorylation; and 2) To characterize the functional differences of coronavirus Nsp1 proteins in modulating stress granule formation.

Herein, this data demonstrates that CoVs inhibit SG formation through multiple mechanisms. I have proposed two models to illustrate these mechanisms, one for OC43 (Figure 4.1) and one for CoV2 (Figure 4.2), that compile the results of this project. For my first objective, the mechanism of how OC43 limits eIF2 α phosphorylation was not fully elucidated in this project; however, I identified a number of important observations in relation to this viral function. Primarily, OC43-Nsp1 was found to limit eIF2 α phosphorylation and this function was conserved and more efficient for CoV2-Nsp1. Further, OC43-mediated inhibition of eIF2 α phosphorylation was not tied to the upregulation of GADD34 by OC43 and was unaffected by inhibition of the integrated stress response. How OC43 upregulates GADD34 and how Nsp1 limits eIF2 α

phosphorylation is still yet to be discovered. For my second objective, I found that Nsp1 is a potent inhibitor of SG formation. OC43-Nsp1 inhibits SG formation through decreased levels of eIF2 α phosphorylation while CoV2-Nsp1 targets both eIF2 α phosphorylation and SG proteins G3BP1 and TIAR to interfere with SG formation. Additionally, Nsp1 was not the only viral mediator of SG inhibition; both OC43-N and CoV2-N inhibited SG formation downstream of eIF2 α phosphorylation. Lastly, overexpression of SG protein G3BP1 decreased OC43 infection levels.

In conclusion, CoVs OC43 and CoV2 utilize viral proteins N and Nsp1 to inhibit SG formation. The existence of multiple SG suppression mechanisms and the conservation of these mechanisms from common cold CoV OC43 to the highly pathogenic CoV2 suggests that SG formation is an important antiviral host defense that CoVs target to ensure efficient replication.

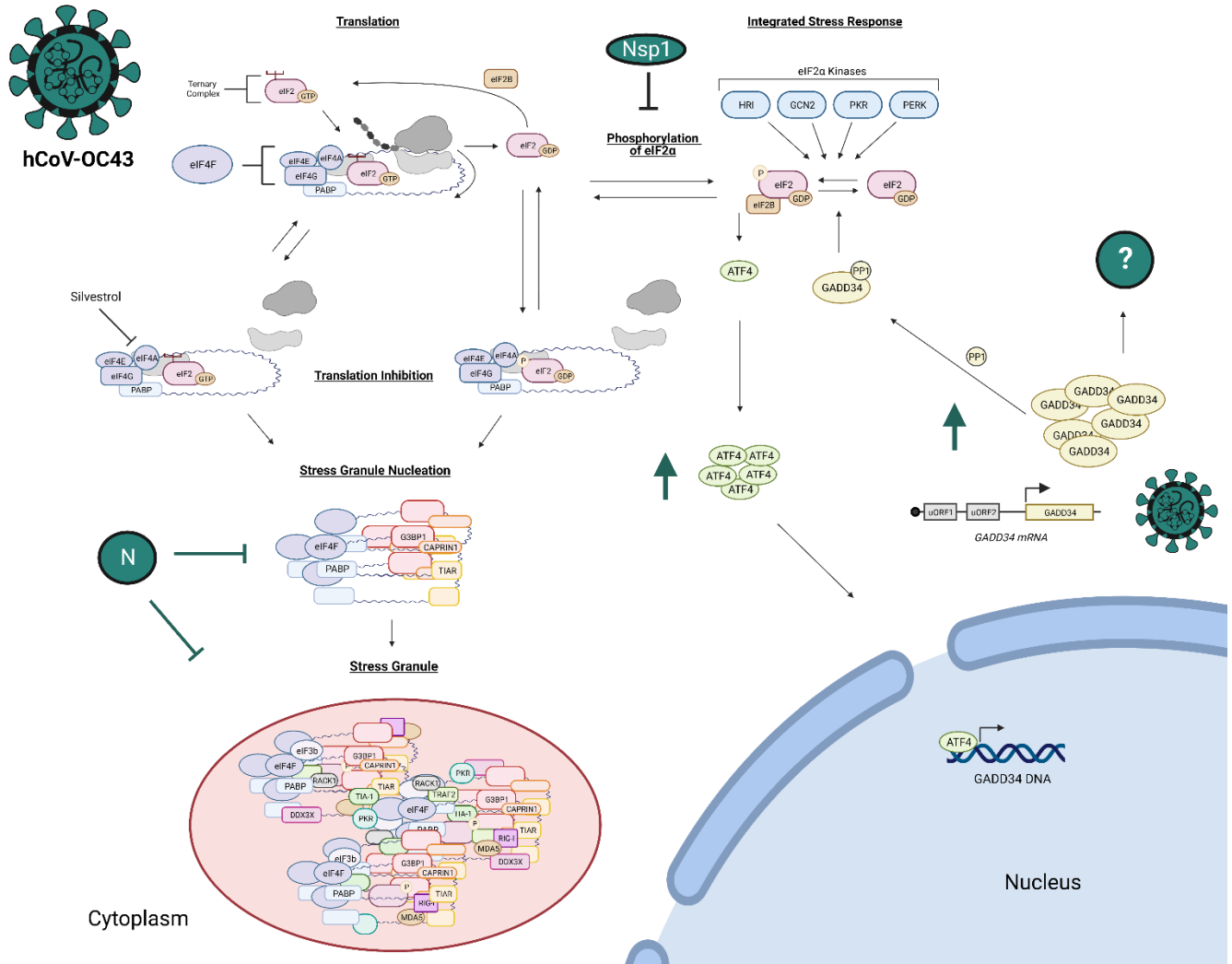


Figure 4.1. Coronavirus OC43 inhibits stress granule formation through multiple mechanisms. Figure adapted from Figure 1.1 with the following additions gathered from the results of this project. During hCoV-OC43 (OC43) infection, phosphorylation of eIF2 α is limited. This inhibition of eIF2 α phosphorylation is facilitated by OC43-Nsp1, and is how OC43-Nsp1 inhibits SG formation. OC43-N also inhibits SG formation and this occurs downstream of eIF2 α phosphorylation by limiting SG nucleation and SG formation. OC43 infection resulted in an increase in ATF4 protein expression and an increase in GADD34 mRNA and protein levels. Upregulation of GADD34 by OC43 infection was not required to limit levels of eIF2 α phosphorylation. It is currently unknown how GADD34 is upregulated during OC43 infection and what function GADD34 holds during OC43 infection.

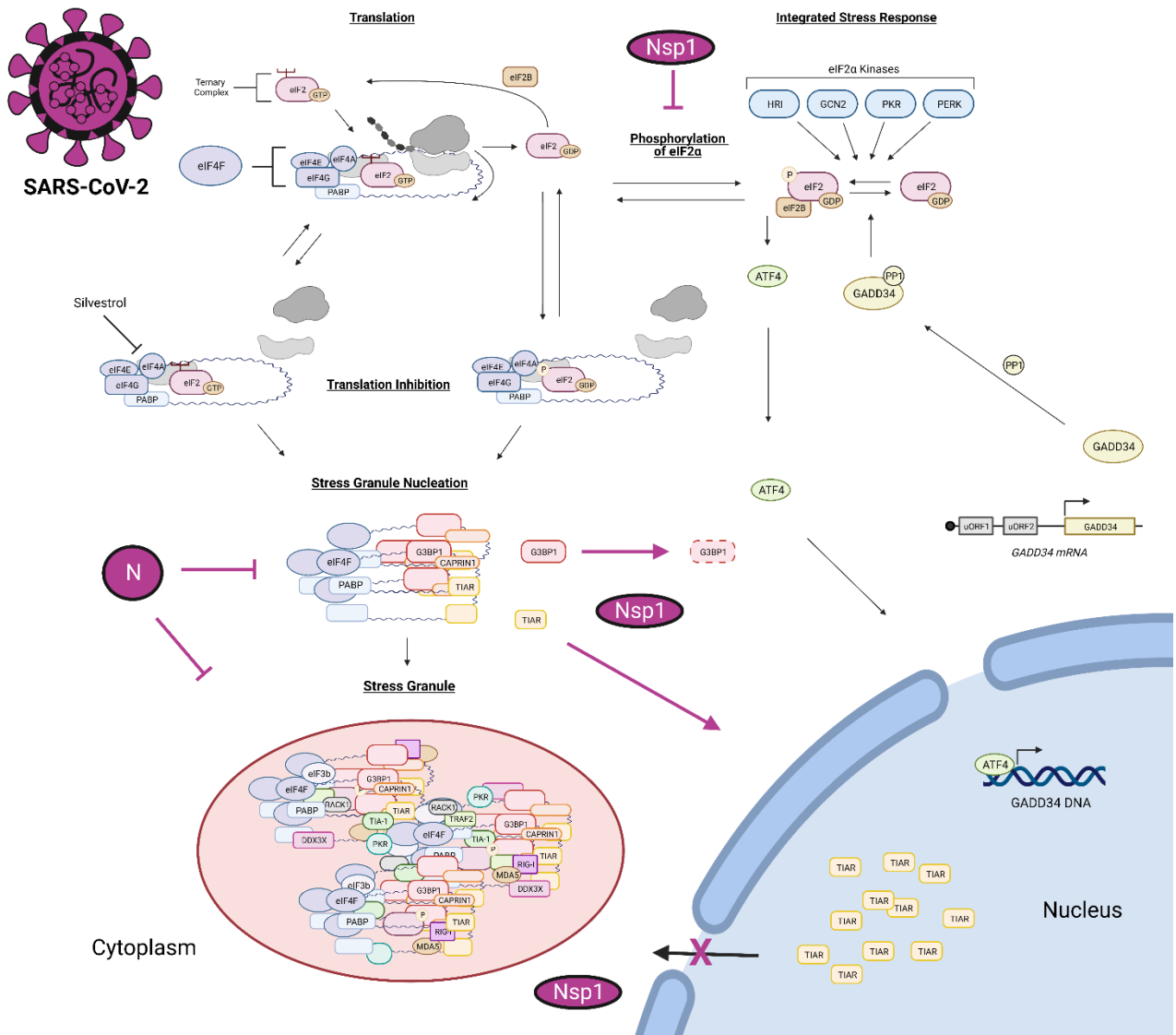


Figure 4.2 Coronavirus SARS-CoV2 inhibits SG formation through multiple mechanisms. Figure adapted from Figure 1.1 with the following additions gathered from the results of this project and in conjunction with (Dolliver et al., 2022). During SARS-CoV2 (CoV2) infection, phosphorylation of eIF2 α is limited (Dolliver et al., 2022). This inhibition of eIF2 α phosphorylation is facilitated by CoV2-Nsp1, and it is one of multiple ways CoV2-Nsp1 inhibits SGs. CoV2-Nsp1 also promotes SG inhibition through degradation of G3BP1 and retention of TIAR in the nucleus. CoV2-N also inhibits SG formation and this occurs downstream of eIF2 α phosphorylation by limiting SG nucleation and SG formation.

BIBLIOGRAPHY

- Albornoz, A., Carletti, T., Corazza, G., & Marcello, A. (2014). The Stress Granule Component TIA-1 Binds Tick-Borne Encephalitis Virus RNA and Is Recruited to Perinuclear Sites of Viral Replication To Inhibit Viral Translation. *Journal of Virology*, *88*(12), 6611–6622. <https://doi.org/10.1128/JVI.03736-13>
- Aulas, A., Fay, M. M., Lyons, S. M., Achorn, C. A., Kedersha, N., Anderson, P., & Ivanov, P. (2017). Stress-specific differences in assembly and composition of stress granules and related foci. *Journal of Cell Science*, *130*(5), 927–937. <https://doi.org/10.1242/jcs.199240>
- Banerjee, A. K., Blanco, M. R., Bruce, E. A., Honson, D. D., Chen, L. M., Chow, A., Bhat, P., Ollikainen, N., Quinodoz, S. A., Loney, C., Thai, J., Miller, Z. D., Lin, A. E., Schmidt, M. M., Stewart, D. G., Goldfarb, D., De Lorenzo, G., Rihn, S. J., Voorhees, R. M., ... Guttman, M. (2020). SARS-CoV-2 Disrupts Splicing, Translation, and Protein Trafficking to Suppress Host Defenses. *Cell*, *183*(5), 1325-1339.e21. <https://doi.org/10.1016/j.cell.2020.10.004>
- Boodhoo, N., Matsuyama-kato, A., Shojadoost, B., Behboudi, S., & Sharif, S. (2022). The severe acute respiratory syndrome coronavirus 2 non-structural proteins 1 and 15 proteins mediate antiviral immune evasion. *Current Research in Virological Science*, *3*, 100021. <https://doi.org/10.1016/j.crviro.2022.100021>
- Borišek, J., Spinello, A., & Magistrato, A. (2021). Molecular Basis of SARS-CoV-2 Nsp1-Induced Immune Translational Shutdown as Revealed by All-Atom Simulations. *The Journal of Physical Chemistry Letters*, *12*(48), 11745–11750. <https://doi.org/10.1021/acs.jpcclett.1c03441>
- Brian, D. A., & Baric, R. S. (2005). Coronavirus Genome Structure and Replication. *Coronavirus Replication and Reverse Genetics*, *287*, 1–30. https://doi.org/10.1007/3-540-26765-4_1
- Brownsword, M. J., Doyle, N., Brocard, M., Locker, N., & Maier, H. J. (2020). Infectious Bronchitis Virus Regulates Cellular Stress Granule Signaling. *Viruses*, *12*(5), 536. <https://doi.org/10.3390/v12050536>
- Buchan, J. R., Kolaitis, R.-M., Taylor, J. P., & Parker, R. (2013). Eukaryotic Stress Granules Are Cleared by Autophagy and Cdc48/VCP Function. *Cell*, *153*(7), 1461–1474. <https://doi.org/10.1016/j.cell.2013.05.037>
- Cai, T., Yu, Z., Wang, Z., Liang, C., & Richard, S. (2021). Arginine methylation of SARS-Cov-2 nucleocapsid protein regulates RNA binding, its ability to suppress stress granule formation, and viral replication. *The Journal of Biological Chemistry*, *297*(1), 100821. <https://doi.org/10.1016/j.jbc.2021.100821>

- Cascarina, S. M., & Ross, E. D. (2020). A proposed role for the SARS-CoV-2 nucleocapsid protein in the formation and regulation of biomolecular condensates. *The FASEB Journal*, *34*(8), 9832–9842. <https://doi.org/10.1096/fj.202001351>
- Choy, M. S., Yusoff, P., Lee, I. C., Newton, J. C., Goh, C. W., Page, R., Shenolikar, S., & Peti, W. (2015). Structural and Functional Analysis of the GADD34:PP1 eIF2 α Phosphatase. *Cell Reports*, *11*(12), 1885–1891. <https://doi.org/10.1016/j.celrep.2015.05.043>
- Chu, J., Galicia-Vázquez, G., Cencic, R., Mills, J. R., Katigbak, A., Porco, J. A., & Pelletier, J. (2016). CRISPR-Mediated Drug-Target Validation Reveals Selective Pharmacological Inhibition of the RNA Helicase, eIF4A. *Cell Reports*, *15*(11), 2340–2347. <https://doi.org/10.1016/j.celrep.2016.05.005>
- Cockman, E., Anderson, P., & Ivanov, P. (2020). TOP mRNPs: Molecular Mechanisms and Principles of Regulation. *Biomolecules*, *10*(7), 969. <https://doi.org/10.3390/biom10070969>
- COVID-19 Map*. (2022, July 5). Johns Hopkins Coronavirus Resource Center. <https://coronavirus.jhu.edu/map.html>
- Dauber, B., Poon, D., dos Santos, T., Duguay, B. A., Mehta, N., Saffran, H. A., & Smiley, J. R. (2016). The Herpes Simplex Virus Virion Host Shutoff Protein Enhances Translation of Viral True Late mRNAs Independently of Suppressing Protein Kinase R and Stress Granule Formation. *Journal of Virology*, *90*(13), 6049–6057. <https://doi.org/10.1128/JVI.03180-15>
- Dolliver, S. M., Kleer, M., Bui-Marinis, M. P., Ying, S., Corcoran, J. A., & Khapersky, D. A. (2022). *Nsp1 proteins of human coronaviruses HCoV-OC43 and SARS-CoV2 inhibit stress granule formation* (p. 2022.05.02.490272). bioRxiv. <https://doi.org/10.1101/2022.05.02.490272>
- Emara, M. M., & Brinton, M. A. (2007). Interaction of TIA-1/TIAR with West Nile and dengue virus products in infected cells interferes with stress granule formation and processing body assembly. *Proceedings of the National Academy of Sciences*, *104*(21), 9041–9046. <https://doi.org/10.1073/pnas.0703348104>
- Fros, J. J., Domeradzka, N. E., Baggen, J., Geertsema, C., Flipse, J., Vlak, J. M., & Pijlman, G. P. (2012). Chikungunya Virus nsP3 Blocks Stress Granule Assembly by Recruitment of G3BP into Cytoplasmic Foci. *Journal of Virology*, *86*(19), 10873–10879. <https://doi.org/10.1128/JVI.01506-12>
- Gambardella, G., Staiano, L., Moretti, M. N., De Cegli, R., Fagnocchi, L., Di Tullio, G., Polletti, S., Braccia, C., Armirotti, A., Zippo, A., Ballabio, A., De Matteis, M. A., & di Bernardo, D. (2020). GADD34 is a modulator of autophagy during starvation. *Science Advances*, *6*(39), eabb0205. <https://doi.org/10.1126/sciadv.abb0205>

- Gao, B., Gong, X., Fang, S., Weng, W., Wang, H., Chu, H., Sun, Y., Meng, C., Tan, L., Song, C., Qiu, X., Liu, W., Forlenza, M., Ding, C., & Liao, Y. (2021). Inhibition of anti-viral stress granule formation by coronavirus endoribonuclease nsp15 ensures efficient virus replication. *PLoS Pathogens*, *17*(2), e1008690. <https://doi.org/10.1371/journal.ppat.1008690>
- García, M. A., Meurs, E. F., & Esteban, M. (2007a). The dsRNA protein kinase PKR: Virus and cell control. *Biochimie*, *89*(6), 799–811. <https://doi.org/10.1016/j.biochi.2007.03.001>
- García, M. A., Meurs, E. F., & Esteban, M. (2007b). The dsRNA protein kinase PKR: Virus and cell control. *Biochimie*, *89*(6), 799–811. <https://doi.org/10.1016/j.biochi.2007.03.001>
- Gassen, N. C., Papiés, J., Bajaj, T., Emanuel, J., Dethloff, F., Chua, R. L., Trimpert, J., Heinemann, N., Niemeyer, C., Weege, F., Hönzke, K., Aschman, T., Heinz, D. E., Weckmann, K., Ebert, T., Zellner, A., Lennarz, M., Wyler, E., Schroeder, S., ... Müller, M. A. (2021). SARS-CoV-2-mediated dysregulation of metabolism and autophagy uncovers host-targeting antivirals. *Nature Communications*, *12*(1), 3818. <https://doi.org/10.1038/s41467-021-24007-w>
- Gerassimovich, Y. A., Miladinovski-Bangall, S. J., Bridges, K. M., Boateng, L., Ball, L. E., Valafar, H., & Nag, A. (2021). Proximity-dependent biotinylation detects associations between SARS coronavirus nonstructural protein 1 and stress granule-associated proteins. *Journal of Biological Chemistry*, *297*(6), 101399. <https://doi.org/10.1016/j.jbc.2021.101399>
- Gilks, N., Kedersha, N., Ayodele, M., Shen, L., Stoecklin, G., Dember, L. M., & Anderson, P. (2004). Stress Granule Assembly Is Mediated by Prion-like Aggregation of TIA-1. *Molecular Biology of the Cell*, *15*(12), 5383–5398. <https://doi.org/10.1091/mbc.e04-08-0715>
- Gomez, G. N., Abrar, F., Dodhia, M. P., Gonzalez, F. G., & Nag, A. (2019). SARS coronavirus protein nsp1 disrupts localization of Nup93 from the nuclear pore complex. *Biochemistry and Cell Biology*, *97*(6), 758–766. <https://doi.org/10.1139/bcb-2018-0394>
- Gordon, D. E., Hiatt, J., Bouhaddou, M., Rezelj, V. V., Ulferts, S., Braberg, H., Jureka, A. S., Obernier, K., Guo, J. Z., Batra, J., Kaake, R. M., Weckstein, A. R., Owens, T. W., Gupta, M., Pourmal, S., Titus, E. W., Cakir, M., Soucheray, M., McGregor, M., ... Krogan, N. J. (2020). Comparative host-coronavirus protein interaction networks reveal pan-viral disease mechanisms. *Science (New York, N.y.)*, *370*(6521), eabe9403. <https://doi.org/10.1126/science.abe9403>

- Han, A.-P., Yu, C., Lu, L., Fujiwara, Y., Browne, C., Chin, G., Fleming, M., Leboulch, P., Orkin, S. H., & Chen, J.-J. (2001). Heme-regulated eIF2 α kinase (HRI) is required for translational regulation and survival of erythroid precursors in iron deficiency. *The EMBO Journal*, 20(23), 6909–6918. <https://doi.org/10.1093/emboj/20.23.6909>
- Harding, H. P., Novoa, I., Zhang, Y., Zeng, H., Wek, R., Schapira, M., & Ron, D. (2000). Regulated translation initiation controls stress-induced gene expression in mammalian cells. *Molecular Cell*, 6(5), 1099–1108. [https://doi.org/10.1016/s1097-2765\(00\)00108-8](https://doi.org/10.1016/s1097-2765(00)00108-8)
- Harding, H. P., Zhang, Y., Bertolotti, A., Zeng, H., & Ron, D. (2000). Perk Is Essential for Translational Regulation and Cell Survival during the Unfolded Protein Response. *Molecular Cell*, 5(5), 897–904. [https://doi.org/10.1016/S1097-2765\(00\)80330-5](https://doi.org/10.1016/S1097-2765(00)80330-5)
- Harding, H. P., Zhang, Y., & Ron, D. (1999). Protein translation and folding are coupled by an endoplasmic-reticulum-resident kinase. *Nature*, 397(6716), 271–274. <https://doi.org/10.1038/16729>
- Harding, H. P., Zhang, Y., Zeng, H., Novoa, I., Lu, P. D., Calton, M., Sadri, N., Yun, C., Popko, B., Paules, R., Stojdl, D. F., Bell, J. C., Hettmann, T., Leiden, J. M., & Ron, D. (2003). An Integrated Stress Response Regulates Amino Acid Metabolism and Resistance to Oxidative Stress. *Molecular Cell*, 11(3), 619–633. [https://doi.org/10.1016/S1097-2765\(03\)00105-9](https://doi.org/10.1016/S1097-2765(03)00105-9)
- Hartenian, E., Nandakumar, D., Lari, A., Ly, M., Tucker, J. M., & Glaunsinger, B. A. (2020). The molecular virology of coronaviruses. *The Journal of Biological Chemistry*, 295(37), 12910–12934. <https://doi.org/10.1074/jbc.REV120.013930>
- Hoffmann, M., Kleine-Weber, H., Schroeder, S., Krüger, N., Herrler, T., Erichsen, S., Schiergens, T. S., Herrler, G., Wu, N.-H., Nitsche, A., Müller, M. A., Drosten, C., & Pöhlmann, S. (2020). SARS-CoV-2 Cell Entry Depends on ACE2 and TMPRSS2 and Is Blocked by a Clinically Proven Protease Inhibitor. *Cell*, 181(2), 271-280.e8. <https://doi.org/10.1016/j.cell.2020.02.052>
- Hou, S., Kumar, A., Xu, Z., Airo, A. M., Stryapunina, I., Wong, C. P., Branton, W., Tchesnokov, E., Götte, M., Power, C., & Hobman, T. C. (2017a). Zika Virus Hijacks Stress Granule Proteins and Modulates the Host Stress Response. *Journal of Virology*, 91(16), e00474-17. <https://doi.org/10.1128/JVI.00474-17>
- Hou, S., Kumar, A., Xu, Z., Airo, A. M., Stryapunina, I., Wong, C. P., Branton, W., Tchesnokov, E., Götte, M., Power, C., & Hobman, T. C. (2017b). Zika Virus Hijacks Stress Granule Proteins and Modulates the Host Stress Response. *Journal of Virology*, 91(16), e00474-17. <https://doi.org/10.1128/JVI.00474-17>

- Jackson, R. J., Hellen, C. U. T., & Pestova, T. V. (2010). THE MECHANISM OF EUKARYOTIC TRANSLATION INITIATION AND PRINCIPLES OF ITS REGULATION. *Nature Reviews. Molecular Cell Biology*, *11*(2), 113–127. <https://doi.org/10.1038/nrm2838>
- Jain, S., Wheeler, J. R., Walters, R. W., Agrawal, A., Barsic, A., & Parker, R. (2016). ATPase-Modulated Stress Granules Contain a Diverse Proteome and Substructure. *Cell*, *164*(3), 487–498. <https://doi.org/10.1016/j.cell.2015.12.038>
- Jousse, C., Oyadomari, S., Novoa, I., Lu, P., Zhang, Y., Harding, H. P., & Ron, D. (2003). Inhibition of a constitutive translation initiation factor 2alpha phosphatase, CReP, promotes survival of stressed cells. *The Journal of Cell Biology*, *163*(4), 767–775. <https://doi.org/10.1083/jcb.200308075>
- Kastan, J. P., Dobrikova, E. Y., Bryant, J. D., & Gromeier, M. (2020). CReP mediates selective translation initiation at the endoplasmic reticulum. *Science Advances*, *6*(23), eaba0745. <https://doi.org/10.1126/sciadv.aba0745>
- Katoh, H., Okamoto, T., Fukuhara, T., Kambara, H., Morita, E., Mori, Y., Kamitani, W., & Matsuura, Y. (2013). Japanese Encephalitis Virus Core Protein Inhibits Stress Granule Formation through an Interaction with Caprin-1 and Facilitates Viral Propagation. *Journal of Virology*, *87*(1), 489–502. <https://doi.org/10.1128/JVI.02186-12>
- Kedersha, N., Chen, S., Gilks, N., Li, W., Miller, I. J., Stahl, J., & Anderson, P. (2002). Evidence That Ternary Complex (eIF2-GTP-tRNA^{iMet})–Deficient Preinitiation Complexes Are Core Constituents of Mammalian Stress Granules. *Molecular Biology of the Cell*, *13*(1), 195–210. <https://doi.org/10.1091/mbc.01-05-0221>
- Kedersha, N., Ivanov, P., & Anderson, P. (2013). Stress granules and cell signaling: More than just a passing phase? *Trends in Biochemical Sciences*, *38*(10), 494–506. <https://doi.org/10.1016/j.tibs.2013.07.004>
- Kedersha, N. L., Gupta, M., Li, W., Miller, I., & Anderson, P. (1999). RNA-binding proteins TIA-1 and TIAR link the phosphorylation of eIF-2 alpha to the assembly of mammalian stress granules. *The Journal of Cell Biology*, *147*(7), 1431–1442. <https://doi.org/10.1083/jcb.147.7.1431>
- Kedersha, N., Panas, M. D., Achorn, C. A., Lyons, S., Tisdale, S., Hickman, T., Thomas, M., Lieberman, J., McInerney, G. M., Ivanov, P., & Anderson, P. (2016a). G3BP–Caprin1–USP10 complexes mediate stress granule condensation and associate with 40S subunits. *The Journal of Cell Biology*, *212*(7), 845–860. <https://doi.org/10.1083/jcb.201508028>

- Kedersha, N., Panas, M. D., Achorn, C. A., Lyons, S., Tisdale, S., Hickman, T., Thomas, M., Lieberman, J., McInerney, G. M., Ivanov, P., & Anderson, P. (2016b). G3BP–Caprin1–USP10 complexes mediate stress granule condensation and associate with 40S subunits. *Journal of Cell Biology*, *212*(7), e201508028. <https://doi.org/10.1083/jcb.201508028>
- Kesavardhana, S., Samir, P., Zheng, M., Malireddi, R. K. S., Karki, R., Sharma, B. R., Place, D. E., Briard, B., Vogel, P., & Kanneganti, T.-D. (2021). DDX3X coordinates host defense against influenza virus by activating the NLRP3 inflammasome and type I interferon response. *Journal of Biological Chemistry*, *296*, 100579. <https://doi.org/10.1016/j.jbc.2021.100579>
- Khapersky, D. A., Emara, M. M., Johnston, B. P., Anderson, P., Hatchette, T. F., & McCormick, C. (2014). Influenza A Virus Host Shutoff Disables Antiviral Stress-Induced Translation Arrest. *PLOS Pathogens*, *10*(7), e1004217. <https://doi.org/10.1371/journal.ppat.1004217>
- Khapersky, D. A., Hatchette, T. F., & McCormick, C. (2012). Influenza A virus inhibits cytoplasmic stress granule formation. *The FASEB Journal*, *26*(4), 1629–1639. <https://doi.org/10.1096/fj.11-196915>
- Khapersky, D. A., Schmaling, S., Larkins-Ford, J., McCormick, C., & Gaglia, M. M. (2016). Selective Degradation of Host RNA Polymerase II Transcripts by Influenza A Virus PA-X Host Shutoff Protein. *PLOS Pathogens*, *12*(2), e1005427. <https://doi.org/10.1371/journal.ppat.1005427>
- Kim, S. S.-Y., Sze, L., & Lam, K.-P. (2019). The stress granule protein G3BP1 binds viral dsRNA and RIG-I to enhance interferon- β response. *Journal of Biological Chemistry*, *294*(16), 6430–6438. <https://doi.org/10.1074/jbc.RA118.005868>
- Krokowski, D., Guan, B.-J., Wu, J., Zheng, Y., Pattabiraman, P. P., Jobava, R., Gao, X.-H., Di, X.-J., Snider, M. D., Mu, T.-W., Liu, S., Storrie, B., Pearlman, E., Blumental-Perry, A., & Hatzoglou, M. (2017). GADD34 function in protein trafficking promotes adaptation to hyperosmotic stress in human corneal cells. *Cell Reports*, *21*(10), 2895–2910. <https://doi.org/10.1016/j.celrep.2017.11.027>
- Kruse, T., Benz, C., Garvanska, D. H., Lindqvist, R., Mihalic, F., Coscia, F., Inturi, R., Sayadi, A., Simonetti, L., Nilsson, E., Ali, M., Kliche, J., Moliner Morro, A., Mund, A., Andersson, E., McInerney, G., Mann, M., Jemth, P., Davey, N. E., ... Ivarsson, Y. (2021). Large scale discovery of coronavirus-host factor protein interaction motifs reveals SARS-CoV-2 specific mechanisms and vulnerabilities. *Nature Communications*, *12*(1), 6761. <https://doi.org/10.1038/s41467-021-26498-z>

- Kumar, A., Ishida, R., Strilets, T., Cole, J., Lopez-Orozco, J., Fayad, N., Felix-Lopez, A., Elaish, M., Evseev, D., Magor, K. E., Mahal, L. K., Nagata, L. P., Evans, D. H., & Hobman, T. C. (2021). SARS-CoV-2 Nonstructural Protein 1 Inhibits the Interferon Response by Causing Depletion of Key Host Signaling Factors. *Journal of Virology*, *95*(13), e00266-21. <https://doi.org/10.1128/JVI.00266-21>
- Künkel, F., & Herrler, G. (1993). Structural and Functional Analysis of the Surface Protein of Human Coronavirus OC43. *Virology*, *195*(1), 195–202. <https://doi.org/10.1006/viro.1993.1360>
- Langereis, M. A., Feng, Q., & van Kuppeveld, F. J. (2013). MDA5 Localizes to Stress Granules, but This Localization Is Not Required for the Induction of Type I Interferon. *Journal of Virology*, *87*(11), 6314–6325. <https://doi.org/10.1128/JVI.03213-12>
- Li, J., Guo, M., Tian, X., Wang, X., Yang, X., Wu, P., Liu, C., Xiao, Z., Qu, Y., Yin, Y., Wang, C., Zhang, Y., Zhu, Z., Liu, Z., Peng, C., Zhu, T., & Liang, Q. (2021). Virus-Host Interactome and Proteomic Survey Reveal Potential Virulence Factors Influencing SARS-CoV-2 Pathogenesis. *Med*, *2*(1), 99-112.e7. <https://doi.org/10.1016/j.medj.2020.07.002>
- Li, W., Moore, M. J., Vasilieva, N., Sui, J., Wong, S. K., Berne, M. A., Somasundaran, M., Sullivan, J. L., Luzuriaga, K., Greenough, T. C., Choe, H., & Farzan, M. (2003). Angiotensin-converting enzyme 2 is a functional receptor for the SARS coronavirus. *Nature*, *426*(6965), 450–454. <https://doi.org/10.1038/nature02145>
- Li, Y., Zhang, C., Chen, X., Yu, J., Wang, Y., Yang, Y., Du, M., Jin, H., Ma, Y., He, B., & Cao, Y. (2011). ICP34.5 Protein of Herpes Simplex Virus Facilitates the Initiation of Protein Translation by Bridging Eukaryotic Initiation Factor 2 α (eIF2 α) and Protein Phosphatase 1. *The Journal of Biological Chemistry*, *286*(28), 24785–24792. <https://doi.org/10.1074/jbc.M111.232439>
- Manivannan, P., Siddiqui, M. A., & Malathi, K. (2020). RNase L Amplifies Interferon Signaling by Inducing Protein Kinase R-Mediated Antiviral Stress Granules. *Journal of Virology*, *94*(13), e00205-20. <https://doi.org/10.1128/JVI.00205-20>
- Martina, J. A., Diab, H. I., Brady, O. A., & Puertollano, R. (2016). TFEB and TFE3 are novel components of the integrated stress response. *The EMBO Journal*, *35*(5), 479–495. <https://doi.org/10.15252/embj.201593428>
- Matsuki, H., Takahashi, M., Higuchi, M., Makokha, G. N., Oie, M., & Fujii, M. (2013). Both G3BP1 and G3BP2 contribute to stress granule formation. *Genes to Cells*, *18*(2), 135–146. <https://doi.org/10.1111/gtc.12023>

- Mazroui, R., Sukarieh, R., Bordeleau, M.-E., Kaufman, R. J., Northcote, P., Tanaka, J., Gallouzi, I., & Pelletier, J. (2006). Inhibition of Ribosome Recruitment Induces Stress Granule Formation Independently of Eukaryotic Initiation Factor 2 α Phosphorylation. *Molecular Biology of the Cell*, 17(10), 4212–4219. <https://doi.org/10.1091/mbc.E06-04-0318>
- McCormick, C., & Khapersky, D. A. (2017). Translation inhibition and stress granules in the antiviral immune response. *Nature Reviews. Immunology*, 17(10), 647–660. <https://doi.org/10.1038/nri.2017.63>
- Mediani, L., Antoniani, F., Galli, V., Vinet, J., Carrà, A. D., Bigi, I., Tripathy, V., Tiago, T., Cimino, M., Leo, G., Amen, T., Kaganovich, D., Cereda, C., Pansarasa, O., Mandrioli, J., Tripathi, P., Troost, D., Aronica, E., Buchner, J., ... Carra, S. (2021). Hsp90-mediated regulation of DYRK3 couples stress granule disassembly and growth via mTORC1 signaling. *EMBO Reports*, 22(5), e51740. <https://doi.org/10.15252/embr.202051740>
- Mendez, A. S., Ly, M., González-Sánchez, A. M., Hartenian, E., Ingolia, N. T., Cate, J. H., & Glaunsinger, B. A. (2021). The N-terminal domain of SARS-CoV-2 nsp1 plays key roles in suppression of cellular gene expression and preservation of viral gene expression. *Cell Reports*, 37(3), 109841. <https://doi.org/10.1016/j.celrep.2021.109841>
- Miller, K., McGrath, M. E., Hu, Z., Ariannejad, S., Weston, S., Frieman, M., & Jackson, W. T. (n.d.). Coronavirus interactions with the cellular autophagy machinery. *Autophagy*, 16(12), 2131–2139. <https://doi.org/10.1080/15548627.2020.1817280>
- Nabeel-Shah, S., Lee, H., Ahmed, N., Burke, G. L., Farhangmehr, S., Ashraf, K., Pu, S., Braunschweig, U., Zhong, G., Wei, H., Tang, H., Yang, J., Marcon, E., Blencowe, B. J., Zhang, Z., & Greenblatt, J. F. (2022). SARS-CoV-2 nucleocapsid protein binds host mRNAs and attenuates stress granules to impair host stress response. *IScience*, 25(1). <https://doi.org/10.1016/j.isci.2021.103562>
- Nakagawa, K., Narayanan, K., Wada, M., & Makino, S. (2018). Inhibition of Stress Granule Formation by Middle East Respiratory Syndrome Coronavirus 4a Accessory Protein Facilitates Viral Translation, Leading to Efficient Virus Replication. *Journal of Virology*, 92(20), e00902-18. <https://doi.org/10.1128/JVI.00902-18>
- Napolitano, G., & Ballabio, A. (2016). TFEB at a glance. *Journal of Cell Science*, 129(13), 2475–2481. <https://doi.org/10.1242/jcs.146365>
- Narayanan, K., Huang, C., Lokugamage, K., Kamitani, W., Ikegami, T., Tseng, C.-T. K., & Makino, S. (2008). Severe Acute Respiratory Syndrome Coronavirus nsp1 Suppresses Host Gene Expression, Including That of Type I Interferon, in Infected Cells. *Journal of Virology*, 82(9), 4471–4479. <https://doi.org/10.1128/JVI.02472-07>

- Narayanan, K., Ramirez, S. I., Lokugamage, K. G., & Makino, S. (2015). Coronavirus nonstructural protein 1: Common and distinct functions in the regulation of host and viral gene expression. *Virus Research*, 202, 89–100. <https://doi.org/10.1016/j.virusres.2014.11.019>
- Novoa, I., Zhang, Y., Zeng, H., Jungreis, R., Harding, H. P., & Ron, D. (2003). Stress-induced gene expression requires programmed recovery from translational repression. *The EMBO Journal*, 22(5), 1180–1187. <https://doi.org/10.1093/emboj/cdg112>
- Onomoto, K., Jogi, M., Yoo, J.-S., Narita, R., Morimoto, S., Takemura, A., Sambhara, S., Kawaguchi, A., Osari, S., Nagata, K., Matsumiya, T., Namiki, H., Yoneyama, M., & Fujita, T. (2012). Critical Role of an Antiviral Stress Granule Containing RIG-I and PKR in Viral Detection and Innate Immunity. *PLOS ONE*, 7(8), e43031. <https://doi.org/10.1371/journal.pone.0043031>
- Panas, M. D., Varjak, M., Lulla, A., Er Eng, K., Merits, A., Karlsson Hedestam, G. B., & McInerney, G. M. (2012). Sequestration of G3BP coupled with efficient translation inhibits stress granules in Semliki Forest virus infection. *Molecular Biology of the Cell*, 23(24), 4701–4712. <https://doi.org/10.1091/mbc.E12-08-0619>
- Peng, T., Lee, K., & Tarn, W. (2008). Phosphorylation of the arginine/serine dipeptide-rich motif of the severe acute respiratory syndrome coronavirus nucleocapsid protein modulates its multimerization, translation inhibitory activity and cellular localization. *The Febs Journal*, 275(16), 4152–4163. <https://doi.org/10.1111/j.1742-4658.2008.06564.x>
- Philippe, L., van den Elzen, A. M. G., Watson, M. J., & Thoreen, C. C. (2020). Global analysis of LARP1 translation targets reveals tunable and dynamic features of 5' TOP motifs. *Proceedings of the National Academy of Sciences of the United States of America*, 117(10), 5319–5328. <https://doi.org/10.1073/pnas.1912864117>
- Pringle, E. S., Duguay, B. A., Bui-Marinis, M. P., Mulloy, R. P., Landreth, S. L., Desiredy, K. S., Dolliver, S. M., Ying, S., Caddell, T., Slaine, P. D., Bearne, S. L., Falzarano, D., Corcoran, J. A., Khapersky, D. A., & McCormick, C. (2022). Thiopurines inhibit coronavirus Spike protein processing and incorporation into progeny virions. *BioRxiv*, 2022.03.10.483772. <https://doi.org/10.1101/2022.03.10.483772>
- Protter, D. S. W., & Parker, R. (2016). Principles and Properties of Stress granules. *Trends in Cell Biology*, 26(9), 668–679. <https://doi.org/10.1016/j.tcb.2016.05.004>
- Rabouw, H. H., Langereis, M. A., Anand, A. A., Visser, L. J., de Groot, R. J., Walter, P., & van Kuppeveld, F. J. M. (2019). Small molecule ISRIB suppresses the integrated stress response within a defined window of activation. *Proceedings of the National Academy of Sciences*, 116(6), 2097–2102. <https://doi.org/10.1073/pnas.1815767116>

- Rabouw, H. H., Langereis, M. A., Knaap, R. C. M., Dalebout, T. J., Canton, J., Sola, I., Enjuanes, L., Bredenbeek, P. J., Kikkert, M., Groot, R. J. de, & Kuppeveld, F. J. M. van. (2016). Middle East Respiratory Coronavirus Accessory Protein 4a Inhibits PKR-Mediated Antiviral Stress Responses. *PLOS Pathogens*, *12*(10), e1005982. <https://doi.org/10.1371/journal.ppat.1005982>
- Rehwinkel, J., & Gack, M. U. (2020). RIG-I-like receptors: Their regulation and roles in RNA sensing. *Nature Reviews Immunology*, *20*(9), 537–551. <https://doi.org/10.1038/s41577-020-0288-3>
- Reineke, L. C., Kedersha, N., Langereis, M. A., van Kuppeveld, F. J. M., & Lloyd, R. E. (2015). Stress Granules Regulate Double-Stranded RNA-Dependent Protein Kinase Activation through a Complex Containing G3BP1 and Caprin1. *MBio*, *6*(2), e02486-14. <https://doi.org/10.1128/mBio.02486-14>
- Reineke, L. C., & Lloyd, R. E. (2015). The stress granule protein G3BP1 recruits protein kinase R to promote multiple innate immune antiviral responses. *Journal of Virology*, *89*(5), 2575–2589. <https://doi.org/10.1128/JVI.02791-14>
- Rojas, M., Vasconcelos, G., & Dever, T. E. (2015). An eIF2 α -binding motif in protein phosphatase 1 subunit GADD34 and its viral orthologs is required to promote dephosphorylation of eIF2 α . *Proceedings of the National Academy of Sciences of the United States of America*, *112*(27), E3466–E3475. <https://doi.org/10.1073/pnas.1501557112>
- Sánchez-Aparicio, M. T., Ayllón, J., Leo-Macias, A., Wolff, T., & García-Sastre, A. (2017). Subcellular Localizations of RIG-I, TRIM25, and MAVS Complexes. *Journal of Virology*, *91*(2), e01155-16. <https://doi.org/10.1128/JVI.01155-16>
- Savastano, A., Ibáñez de Opakua, A., Rankovic, M., & Zweckstetter, M. (2020). Nucleocapsid protein of SARS-CoV-2 phase separates into RNA-rich polymerase-containing condensates. *Nature Communications*, *11*, 6041. <https://doi.org/10.1038/s41467-020-19843-1>
- Schmidt, N., Lareau, C. A., Keshishian, H., Ganskih, S., Schneider, C., Hennig, T., Melanson, R., Werner, S., Wei, Y., Zimmer, M., Ade, J., Kirschner, L., Zielinski, S., Dölken, L., Lander, E. S., Caliskan, N., Fischer, U., Vogel, J., Carr, S. A., ... Munschauer, M. (2021). The SARS-CoV-2 RNA–protein interactome in infected human cells. *Nature Microbiology*, *6*(3), 339–353. <https://doi.org/10.1038/s41564-020-00846-z>
- Schubert, K., Karousis, E. D., Jomaa, A., Scaiola, A., Echeverria, B., Gurzeler, L.-A., Leibundgut, M., Thiel, V., Mühlemann, O., & Ban, N. (2020). SARS-CoV-2 Nsp1 binds the ribosomal mRNA channel to inhibit translation. *Nature Structural & Molecular Biology*, *27*(10), 959–966. <https://doi.org/10.1038/s41594-020-0511-8>

- Shen, Z., Zhang, G., Yang, Y., Li, M., Yang, S., & Peng, G. (2020). Lysine 164 is critical for SARS-CoV-2 Nsp1 inhibition of host gene expression. *The Journal of General Virology*, *102*(1), jgv001513. <https://doi.org/10.1099/jgv.0.001513>
- Sidrauski, C., McGeachy, A. M., Ingolia, N. T., & Walter, P. (2015). The small molecule ISRIB reverses the effects of eIF2 α phosphorylation on translation and stress granule assembly. *ELife*, *4*, e05033. <https://doi.org/10.7554/eLife.05033>
- Slaine, P. D., Kleer, M., Duguay, B. A., Pringle, E. S., Kadijk, E., Ying, S., Balgi, A., Roberge, M., McCormick, C., & Khapersky, D. A. (2021). Thiopurines Activate an Antiviral Unfolded Protein Response That Blocks Influenza A Virus Glycoprotein Accumulation. *Journal of Virology*, *95*(11), e00453-21. <https://doi.org/10.1128/JVI.00453-21>
- Slaine, P. D., Kleer, M., Smith, N. K., Khapersky, D. A., & McCormick, C. (2017). Stress Granule-Inducing Eukaryotic Translation Initiation Factor 4A Inhibitors Block Influenza A Virus Replication. *Viruses*, *9*(12), 388. <https://doi.org/10.3390/v9120388>
- Sola, I., Galán, C., Mateos-Gómez, P. A., Palacio, L., Zúñiga, S., Cruz, J. L., Almazán, F., & Enjuanes, L. (2011). The Polypyrimidine Tract-Binding Protein Affects Coronavirus RNA Accumulation Levels and Relocalizes Viral RNAs to Novel Cytoplasmic Domains Different from Replication-Transcription Sites ∇ . *Journal of Virology*, *85*(10), 5136–5149. <https://doi.org/10.1128/JVI.00195-11>
- Thoms, M., Buschauer, R., Ameisemeier, M., Koepke, L., Denk, T., Hirschenberger, M., Kratzat, H., Hayn, M., Mackens-Kiani, T., Cheng, J., Straub, J. H., Stürzel, C. M., Fröhlich, T., Berninghausen, O., Becker, T., Kirchhoff, F., Sparrer, K. M. J., & Beckmann, R. (2020). Structural basis for translational shutdown and immune evasion by the Nsp1 protein of SARS-CoV-2. *Science*, *369*(6508), 1249–1255. <https://doi.org/10.1126/science.abc8665>
- Thulasi Raman, S. N., Liu, G., Pyo, H. M., Cui, Y. C., Xu, F., Ayalew, L. E., Tikoo, S. K., & Zhou, Y. (2016). DDX3 Interacts with Influenza A Virus NS1 and NP Proteins and Exerts Antiviral Function through Regulation of Stress Granule Formation. *Journal of Virology*, *90*(7), 3661–3675. <https://doi.org/10.1128/JVI.03010-15>
- Tourrière, H., Chebli, K., Zekri, L., Courselaud, B., Blanchard, J. M., Bertrand, E., & Tazi, J. (2003). The RasGAP-associated endoribonuclease G3BP assembles stress granules. *The Journal of Cell Biology*, *160*(6), 823–831. <https://doi.org/10.1083/jcb.200212128>
- Tsai, W.-C., Gayatri, S., Reineke, L. C., Sbardella, G., Bedford, M. T., & Lloyd, R. E. (2016). Arginine Demethylation of G3BP1 Promotes Stress Granule Assembly. *The Journal of Biological Chemistry*, *291*(43), 22671–22685. <https://doi.org/10.1074/jbc.M116.739573>

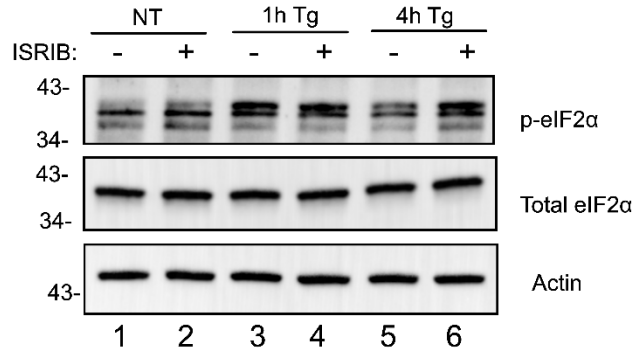
- Visser, L. J., Medina, G. N., Rabouw, H. H., de Groot, R. J., Langereis, M. A., de los Santos, T., & van Kuppeveld, F. J. M. (2019). Foot-and-Mouth Disease Virus Leader Protease Cleaves G3BP1 and G3BP2 and Inhibits Stress Granule Formation. *Journal of Virology*, *93*(2), e00922-18. <https://doi.org/10.1128/JVI.00922-18>
- V'kovski, P., Kratzel, A., Steiner, S., Stalder, H., & Thiel, V. (2021). Coronavirus biology and replication: Implications for SARS-CoV-2. *Nature Reviews Microbiology*, *19*(3), 155–170. <https://doi.org/10.1038/s41579-020-00468-6>
- Vora, S. M., Fontana, P., Mao, T., Leger, V., Zhang, Y., Fu, T.-M., Lieberman, J., Gehrke, L., Shi, M., Wang, L., Iwasaki, A., & Wu, H. (2022). Targeting stem-loop 1 of the SARS-CoV-2 5' UTR to suppress viral translation and Nsp1 evasion. *Proceedings of the National Academy of Sciences of the United States of America*, *119*(9), e2117198119. <https://doi.org/10.1073/pnas.2117198119>
- Wang, J., Shi, C., Xu, Q., & Yin, H. (2021). SARS-CoV-2 nucleocapsid protein undergoes liquid–liquid phase separation into stress granules through its N-terminal intrinsically disordered region. *Cell Discovery*, *7*, 5. <https://doi.org/10.1038/s41421-020-00240-3>
- Wang, X., Liao, Y., Yap, P. L., Png, K. J., Tam, J. P., & Liu, D. X. (2009). Inhibition of Protein Kinase R Activation and Upregulation of GADD34 Expression Play a Synergistic Role in Facilitating Coronavirus Replication by Maintaining De Novo Protein Synthesis in Virus-Infected Cells. *Journal of Virology*, *83*(23), 12462–12472. <https://doi.org/10.1128/JVI.01546-09>
- White, J. P., Cardenas, A. M., Marissen, W. E., & Lloyd, R. E. (2007). Inhibition of Cytoplasmic mRNA Stress Granule Formation by a Viral Proteinase. *Cell Host & Microbe*, *2*(5), 295–305. <https://doi.org/10.1016/j.chom.2007.08.006>
- Wippich, F., Bodenmiller, B., Trajkovska, M. G., Wanka, S., Aebersold, R., & Pelkmans, L. (2013). Dual Specificity Kinase DYRK3 Couples Stress Granule Condensation/Dissolution to mTORC1 Signaling. *Cell*, *152*(4), 791–805. <https://doi.org/10.1016/j.cell.2013.01.033>
- Yang, P., Mathieu, C., Kolaitis, R.-M., Zhang, P., Messing, J., Yurtsever, U., Yang, Z., Wu, J., Li, Y., Pan, Q., Yu, J., Martin, E. W., Mittag, T., Kim, H. J., & Taylor, J. P. (2020). G3BP1 Is a Tunable Switch that Triggers Phase Separation to Assemble Stress Granules. *Cell*, *181*(2), 325-345.e28. <https://doi.org/10.1016/j.cell.2020.03.046>
- Yang, W., Ru, Y., Ren, J., Bai, J., Wei, J., Fu, S., Liu, X., Li, D., & Zheng, H. (2019). G3BP1 inhibits RNA virus replication by positively regulating RIG-I-mediated cellular antiviral response. *Cell Death & Disease*, *10*(12), 1–15. <https://doi.org/10.1038/s41419-019-2178-9>

- Ying, S., & Khapersky, D. A. (2020). UV damage induces G3BP1-dependent stress granule formation that is not driven by mTOR inhibition-mediated translation arrest. *Journal of Cell Science*, *133*(20). <https://doi.org/10.1242/jcs.248310>
- Zhang, K., Miorin, L., Makio, T., Dehghan, I., Gao, S., Xie, Y., Zhong, H., Esparza, M., Kehrer, T., Kumar, A., Hobman, T. C., Ptak, C., Gao, B., Minna, J. D., Chen, Z., García-Sastre, A., Ren, Y., Wozniak, R. W., & Fontoura, B. M. A. (2021). Nsp1 protein of SARS-CoV-2 disrupts the mRNA export machinery to inhibit host gene expression. *Science Advances*, *7*(6), eabe7386. <https://doi.org/10.1126/sciadv.abe7386>
- Zhang, P., McGrath, B. C., Reinert, J., Olsen, D. S., Lei, L., Gill, S., Wek, S. A., Vattem, K. M., Wek, R. C., Kimball, S. R., Jefferson, L. S., & Cavener, D. R. (2002). The GCN2 eIF2 α Kinase Is Required for Adaptation to Amino Acid Deprivation in Mice. *Molecular and Cellular Biology*, *22*(19), 6681–6688. <https://doi.org/10.1128/MCB.22.19.6681-6688.2002>
- Zhang, T., Delestienne, N., Huez, G., Kruys, V., & Gueydan, C. (2005). Identification of the sequence determinants mediating the nucleo-cytoplasmic shuttling of TIAR and TIA-1 RNA-binding proteins. *Journal of Cell Science*, *118*(23), 5453–5463. <https://doi.org/10.1242/jcs.02669>
- Zheng, Z.-Q., Wang, S.-Y., Xu, Z.-S., Fu, Y.-Z., & Wang, Y.-Y. (2021). SARS-CoV-2 nucleocapsid protein impairs stress granule formation to promote viral replication. *Cell Discovery*, *7*(1), 1–11. <https://doi.org/10.1038/s41421-021-00275-0>
- Zhu, T., Jiang, X., Xin, H., Zheng, X., Xue, X., Chen, J.-L., & Qi, B. (2021). GADD34-mediated dephosphorylation of eIF2 α facilitates pseudorabies virus replication by maintaining de novo protein synthesis. *Veterinary Research*, *52*(1), 148. <https://doi.org/10.1186/s13567-021-01018-5>
- Ziebuhr, J., Snijder, E. J., & Gorbalenya, A. E. Y. 2000. (2000). Virus-encoded proteinases and proteolytic processing in the Nidovirales. *Journal of General Virology*, *81*(4), 853–879. <https://doi.org/10.1099/0022-1317-81-4-853>
- Zyryanova, A. F., Weis, F., Faille, A., Alard, A. A., Crespillo-Casado, A., Sekine, Y., Harding, H. P., Allen, F., Parts, L., Fromont, C., Fischer, P. M., Warren, A. J., & Ron, D. (2018). Binding of ISRIB reveals a regulatory site in the nucleotide exchange factor eIF2B. *Science*, *359*(6383), 1533–1536. <https://doi.org/10.1126/science.aar5129>

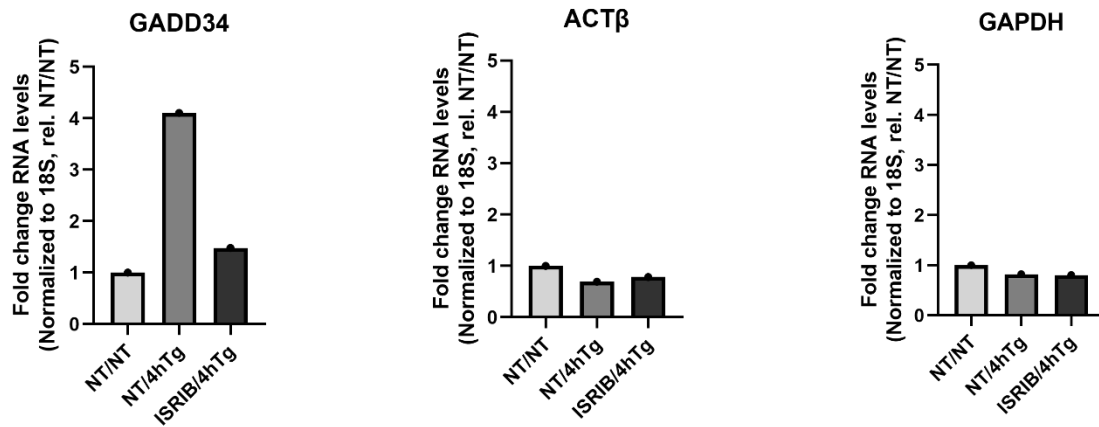
APPENDIX: ISRIB inhibits GADD34 induction and dephosphorylation of eIF2 α .

To confirm ISRIB treatment works as expected in this experimental system, 293A cells were left untreated or were treated with Tg for 1 h to induce eIF2 α phosphorylation or 4h to induce GADD34 expression. Cells were also treated with ISRIB for 1 h or 4 h to analyze if ISRIB affects Tg-induced GADD34 upregulation. As expected, 4 h Tg treatment increased eIF2 α phosphorylation and GADD34 RNA levels; however, ISRIB treatment prevented Tg-induced GADD34 upregulation and resulted in sustained eIF2 α phosphorylation (see Appendix). Thus, ISRIB treatment works as expected in this experimental system.

A



B



Appendix. ISRIB inhibits GADD34 induction and dephosphorylation of eIF2 α . The 293A cells were untreated (NT) or treated with Tg (1 μ M) for 1 h or 4 h only or treated with both TG and ISRIB (200 nM) for 1 h or 4 h. Phosphorylation of eIF2 α was analysed by western blot and transcript levels were measured by RT-QPCR. (A) Western blot analysis of Tg-induced eIF2 α phosphorylation. Actin was used as a loading control. (B) RT-QPCR of GADD34, ACTB (β -Actin), and GAPDH. For all plots, each data point represents independent biological replicate (N=1).